

Synthesis and Study of a Lithium-Selective Chelator

by

Mark A. Brutto

A thesis
presented to the University of Waterloo
in fulfilment of the
thesis requirement for the degree of
Master of Science
in
Chemistry

Waterloo, Ontario, Canada, 2024

© Mark A. Brutto 2024

Author's Declaration

I hereby declare that I am the sole author of this thesis. This is a true copy of the thesis, including any required final revisions, as accepted by my examiners.

I understand that my thesis may be made electronically available to the public.

Abstract

Lithium, the lightest metal on the periodic table, serves as a very valuable resource due to its many applications in things such as glass and ceramics, greases, and most importantly, batteries. The battery industry consumes the majority of our collected lithium, and this trend is expected to continue with increased electric vehicle usage. An increased awareness for our carbon footprint and greenhouse gas emissions, along with governmental legislation has led to an exponential increase in our lithium demand. Unfortunately, current lithium collection processes are unable to keep up with this increased demand, thus creating a need for new or improved lithium collection processes. The majority of lithium is collected from two major sources, lithium-rich brines in the ABC (Argentina, Bolivia, Chile) region and China, as well as minerals and ores typically found in China and Australia. Current techniques include expensive processes such as roasting and leaching from minerals and ores, or lengthy precipitation processes from pre-evaporated brines, both of which have proven to be unfit for future industrial demands.

This research aims to develop and study a lithium-selective ligand that will eliminate lengthy evaporation processes typically associated with lithium collection from brines. Chapter 1 begins with a literature review on lithium and its societal and economic importance. It will explore current lithium isolation processes and their drawbacks preventing more expansive and efficient collection. Chapter 2 will include the inspiration behind our ligand design, starting with a preliminary direction and a complete adjustment upon computational calculations. Chapter 3 will include the synthesis and study of our proposed motif, illustrating a cheap and efficient synthesis, and promising preliminary lithium selectivity when compared with other 1st group cations.

Acknowledgements

The decision to take on this degree caught me by surprise as I had no clue what graduate school really entailed. A simple reach out from Dr. Schipper sparked my interest in pursuing grad school and it was one of the most enlightening decisions I've ever made. Filled with more failure than I could ever imagine, this Master's experience taught me lots about chemistry, relationships, and most importantly, myself. Thank you so much to everyone who helped guide me through this journey, you are all very appreciated.

First, I would like to thank my entire family. Mom and Dad, thank you for all the support throughout undergrad and grad school. I appreciate all the sacrifices you guys have made and I hope that I have made you guys proud. My siblings, John, Alex, and Patty B, thank you for putting up with my annoyingness when I come back home and for being a nice break from the chaos of grad school. I'm looking forward to coming back to annoy some more to make up for these last two years.

Next, I would like to thank someone near and dear to my heart. Alyssa, my amazing girlfriend and best friend, thank you for everything. Thank you for being patient and pushing me to succeed in grad school. It's been a difficult transition since you moved out after you graduated, but I'm so glad to make it out the other side and I can't wait to come back and pick up where we left off. Thank you for the weekend visits and all the trips we've used as a break for both of us. And lastly, thank you for all the convincing to bring Lil Nai into our life and showing me how unreal cats are (even though I'm allergic now). I can't wait to see where the future takes us (and for the cruise hehe).

All the people in the Schipper Group, it has only been 3 total years but what a ride it

has been. Dr. Derek Schipper, thank you for being an unreal supervisor and for agreeing to let me join the lab. This experience has taught me so much and you were at the forefront of it. Thanks for all the parties and the AI-generated Chuck Norris jokes, it was fun. Jianan Wang, I don't know where you went but I hope you're enjoying your new journey in life. Thank you for teaching me the very basics in the lab during my 494 and for showing me Kabob Shack. Scott McNeil, thanks for being my very first friend in grad school. You are legitimately the smartest person I've ever met and I would not have made it through those first 2 terms without you. Thank you for all the encouragement and laughs, I still hope to make it to BC sometime soon to visit. Luke Glofcheskie and Zhaoxiang Liu, my 494 comrades, thanks for pushing through that time period with me, I wish you both the best. Mila Abaeva, the ancient, senior PhD student, thanks for all the chemistry wisdom and assurance you've given me over the years. I'm gonna miss procrastinating for entire days talking across the office, the lab woulda been a mess without you. Gigi Hu, I'm gonna miss seeing your cute face everyday, whether you were mid-nap or not. Thanks for all the logical conversations and for putting up with all my jokes, I wish you the absolute best. Eduarda Omena, thanks for the laughs and 'entertainment' you brought. I appreciate all your efforts in fixing my corrupt brain and I wish you all the best in whatever your future holds. Riley Woods, legit the most pure human in the world, thanks for showing me what I should aspire to be like. The year that we were in the lab was a blast and I appreciate you putting up with my immense amount of talking cause I 100% woulda lost it if I was in your shoes. The sky is your limit and I hope you get everything you want in life. Ryan Scott, what a silly man, thank you for the immense chemistry knowledge you would give me. You were always down to grab food and do literally anything and I greatly appreciated it. I hope you continue doing sus experiments safely and that your love for chemistry never dies, it's inspiring. Thank you to the Taylor Boys, G.K and Robbie

Brill. The year you guys were here was some of the most I've had and I'm blaming the weight I gained on all the fun nights we had at Molly's (way too many nights). I hope you make daptomycin and have unlimited successful columns.

Thank you to my committee members, Dr. Michael Chong and Dr. Adrian Schwan. Thank you for being apart of my master's journey and for all your helpful feedback in CHEM 784 and 794. Your advice has stuck with me ever since.

Finally, the OG London boys. The FOMO has been real these past 2 years but I'm glad I always had a group to rely on. The endless brainrot discussions in the group chats got me through my worst days, and all the rowdy hangout sessions whenever we were all available were some of my most anticipated days. I'm hype to head back and finally get to see everyone much more often. Thanks men <3

Table of Contents

Author's Declaration	ii
Abstract	iii
Acknowledgements	iv
List of Schemes	ix
List of Figures	x
List of Tables	xii
List of Abbreviations	xiii
Chapter 1: Lithium	1
1.1 Introduction to Lithium	1
1.2 Economical Importance	1
1.3 Current Lithium Isolation.....	4
1.3.1 Recovery from Minerals and Ores.....	5
1.3.1.1 Acid Process	7
1.3.1.2 Alkaline Process	10
1.3.1.3 Chlorination Process	12
1.3.2 Recovery from Brines.....	13
1.3.2.1 Precipitation.....	14
1.3.2.2 Adsorption	17
1.3.3 Recovery from Secondary Sources.....	19
1.4 Scope of Thesis	20
Chapter 2: Ligand Design	21
2.1 Lithium Binding Motifs.....	21
2.2 Ferrocene Building Block.....	25
2.2.1 Forming Bridged Ether on Ferrocene	25
2.2.2 Molecular Switches	30
2.3 Early Synthesis	32
2.4 Computational Experiments.....	34
2.5 Concluding Remarks	46
Chapter 3: Synthesis and Study	47
3.1 Ligand Synthesis	47
3.1.1 Manipulations of Carbonyl.....	51
3.2 Preliminary Binding Characterization.....	53

3.2.1 Mass Spectrometry	53
3.2.2 NMR Experiments	56
3.3 Qualitative NMR Experiments.....	60
3.4 Quantitative Binding Characterization.....	65
3.5 Future Work.....	68
Conclusion	70
References	72
Appendix	79
A General Considerations.....	79
Materials & Instrumentation	79
B Reaction Procedures.....	80
Synthesis of bisester (3.3).....	80
Synthesis of piperidinone (3.4).....	80
Synthesis of bispidinone (2.27)	82
C Spectral Data	83
D Quantitative NMR Data	89

List of Schemes

Scheme 2.1: Synthesis of bulky decalin side-chain crown ethers to reduce sandwich complexation	24
Scheme 2.2: Cooperative dehydration of methanol-substituted ferrocene.....	26
Scheme 2.3: Equilibrium shifts presented during cooperative dehydration process.	27
Scheme 2.4: Hydrolysis of bridged crown ethers to original alcohol substituents ...	28
Scheme 2.5: Modified ferrocene substitution for successful heteroannular macrocyclizations.....	29
Scheme 2.6: Molecular switch illustrating the photoisomerization of dithienylethene.....	31
Scheme 2.7: Proposed mechanism of action for ferrocene-based lithium chelator.	32
Scheme 2.8: Synthesis of molecule 2.16	33
Scheme 2.9: Synthesis of molecule 2.17	34
Scheme 3.1: Double conjugate addition reaction mechanism to form 3.3	46
Scheme 3.2: a) Dieckmann condensation/decarboxylation mechanism to form 3.4 ; b) Side methyl ether cleavage mechanism to form 3.5	48
Scheme 3.3: Mannich reaction mechanism to form bispidinone 2.27	50
Scheme 3.4: a) Clemmensen reduction attempt conditions; b) Wolff-Kishner reduction attempt conditions; c) Sodium borohydride reduction attempt conditions; d) Cyclic acetal protection attempt conditions: M sandwich complex formed from flat crown ethers in solution.	52
Scheme 3.5: Typical equilibrium for hydration of ketone vs. H-bonding incentivized equilibrium observed.....	57
Scheme 3.6: Synthesis of a LiCl-selective organogel 3.9 developed by Sessler	60

List of Figures

Figure 1.1: Common modern applications of lithium in a) glass and ceramics, b) greases, and c) batteries.	1
Figure 1.2: Pie charts illustrating industrial distribution of lithium resources from 2005-2020.....	3
Figure 1.3: Projected worldwide supply and demand for lithium resources.	4
Figure 1.4: Generic process for lithium recovery from minerals and ores	7
Figure 1.5: Conversion of (a) α -spodumene to (b) β -spodumene through calcination at 1100 °C.....	8
Figure 1.6: Electrochemical processes undergone by Nemaska Lithium Inc. in Quebec	9
Figure 1.7: Alkaline process for lithium carbonate recovery.....	11
Figure 1.8: Lithium-rich brine pools in ABC region in South America.....	14
Figure 1.9: Generic precipitation process for removal of industrial lithium carbonate from natural brines.	16
Figure 1.10: a) Generic Li-ion sieve mechanism of action; b) Crystal structure of Li-Mn-O molecular sieve; c) Li adsorption process; d) Li desorption process.	18
Figure 1.11: a) Toxco's method for recycling Li-ion batteries; b) Accurec's method for recycling Li-ion batteries.	20
Figure 2.1: Commonly used lithium-chelators	21
Figure 2.2: Polymeric membrane developed by Warnock et al. with three different subunits to control lithium selectivity	22
Figure 2.3: Illustration of 2:1 CE:M sandwich complex formed from flat crown ethers in solution.....	23
Figure 2.4: Proposed lithium-binding motif.....	30
Figure 2.5: a) ΔG values for complexation of Li & Na with 2.18, 2.19, and 2.20 , b) adjusted binding populations for complexation of Li & Na with 2.18, 2.19, and 2.20	37
Figure 2.6: a) ΔG values for complexation of Li & Na with 2.21 and 2.22 , b) adjusted binding populations for complexation of Li & Na with 2.21 and 2.22 , c) $\Delta\Delta G$ values for Li-Na for 2.21 and 2.22	41
Figure 2.7: a) ΔG values for complexation of Li & Na with 2.23, 2.24, and 2.25 ,	

b) adjusted binding populations for complexation of Li & Na with 2.23 , 2.24 , and 2.25 , c) $\Delta\Delta G$ values for Li-Na for 2.23 , 2.24 and 2.25	42
Figure 2.8: a) ΔG values for complexation of Li & Na with 2.26 , 2.27 , and 2.28 , b) adjusted binding populations for complexation of Li & Na with 2.26 , 2.27 , and 2.28 , c) $\Delta\Delta G$ values for Li-Na for 2.26 , 2.27 and 2.28	44
Figure 3.1: Mass spectrum produced in MeOH/H ₂ O/FA solution when introduced with lithium acetate.	54
Figure 3.2: Mass spectrum produced in MeOH/H ₂ O/FA solution when introduced with sodium acetate.	55
Figure 3.3: ¹ H NMR spectrum of 2.27 in D ₂ O illustrating the equilibrium between diol and ketone forms; see Fig. S3-5 for comparison to original ligand in CDCl ₃	56
Figure 3.4: ¹ H-NMR spectra (300 MHz, D ₂ O, 298 K) of Host, 2.27 solutions in D ₂ O and mixed with 0-20 eq LiOH.	58
Figure 3.5: ¹ H-NMR spectra (300 MHz, CD ₃ CN, 298 K) of 10 mM (Host, 2.27) solutions in CD ₃ CN and mixed with excess LiCl, NaCl, and KCl alone and in combination.	61
Figure 3.6: ¹ H-NMR spectra (300 MHz, CD ₃ CN, 298 K) of 10 mM (Host, 2.27) solutions in CD ₃ CN and mixed with excess LiTFSI and NaTFSI alone and in combination.	63
Figure 3.7: ¹ H-NMR spectra (300 MHz, CD ₃ CN, 298 K) of 2.27 (Host) recorded at a concentration of 10 mM in the presence of different concentrations of LiTFSI (Guest).....	65
Figure 3.8: Changes in the chemical shift of (proton) on 2.27 (Host) as a function of added LiTFSI (Guest)..	66
Figure S3-1: ¹ H-NMR (300 MHz, CDCl ₃) of 3.3	81
Figure S3-2: ¹³ C-NMR (75 MHz, CDCl ₃) of 3.3	82
Figure S3-3: ¹ H-NMR (300 MHz, CDCl ₃) of 3.4	83
Figure S3-4: ¹³ C-NMR (75 MHz, CDCl ₃) of 3.4	84
Figure S3-5: ¹ H-NMR (300 MHz, CDCl ₃) of 2.27	85
Figure S3-6: ¹³ C-NMR (75 MHz, CDCl ₃) of 2.27	86
Figure S4-1: (0.5 mL, CD ₃ CN, LiTFSI); (a) 0 mM; (b) 2 mM; (c) 5 mM; (d) 7 mM; (e) 9 mM; (f) 12 mM; (g) 14 mM; (h) 16 mM; (i) 18 mM; (j) 21 mM; (k) 23 mM; (l) 25 mM; (m) 28 mM; (n) 30 mM	87

List of Tables

Table 1.1: Properties of most common lithium-mined minerals	6
Table 1.2: Chlorination roasting conditions from various minerals.....	12
Table 2.1: Computationally calculated binding energies and populations for molecules 2.18, 2.19, and 2.20	36
Table 2.2: Computationally calculated binding energies and populations for molecules 2.21, 2.22, 2.23, 2.24, and 2.25	40
Table 2.3: Computationally calculated binding energies and populations for molecules 2.26, 2.27, and 2.28	43
Table 3.1: Summary of important values and their peak assignments.....	54
Table 3.2: Summary of important values and their peak assignments.	55

List of Abbreviations

ABC	Argentina, Bolivia, Chile
AcOH	acetic acid
CE:M	crown ether:metal
Cp	cyclopentadienyl
CSA	camphorsulfonic acid
DCM	dichloromethane
EDTA	ethylenediaminetetraacetic acid
FA	formic acid
HEDTA	hydroxyethylethylenediaminetriacetic acid
ICP-MS	Inductively Coupled Plasma Mass Spectrometry
LLE	Liquid-Liquid extraction
MD	Molecular dynamics
MeOH	methanol
NMR	Nuclear magnetic resonance
R&D	Research & development
SCE	Saturated calomel electrode
SLE	Solid-Liquid extraction
THF	tetrahydrofuran
TLC	Thin layer chromatography
TMEDA	tetramethylethylenediamine
UV-VIS	Ultraviolet-visible

Chapter 1: Lithium

1.1 Introduction to Lithium

Lithium is the lightest metal on the periodic table having an atomic weight of 6.941 g/mol. Lithium plays a crucial role in modern industry having major applications in glass and ceramics, greases, and most importantly, batteries (Fig 1.1).¹⁻⁴ It is used as an additive in glass and ceramics to reduce thermal expansion, increase mold strength, keep colour consistency, increase durability, and reduce glass erosion.⁵ Lithium is used in greases to improve viscosity and water/heat resistance, therefore playing a pivotal role in vehicles and heavy machinery.⁶ Most importantly, lithium's present and future lives heavily in the battery industry, as it remains the state-of-the-art material in the batteries that power our everyday lives.⁷



Figure 1.1: Common modern applications of lithium in a) glass and ceramics, b) greases, and c) batteries.

1.2 Economical Importance

In recent years, a greater emphasis has been placed on carbon footprints and

greenhouse gas emissions. It is common knowledge that the vehicles transporting us in society are an easy target when trying to reduce global emissions. Current gasoline-powered passenger vehicles emit around 4.6 metric tonnes of CO₂ a year, simultaneously producing other greenhouse gases from their tailpipes such as methane and nitrous oxide.⁸⁻¹⁰ In hopes of decreasing our global carbon footprint and slowing global warming, the automobile industry has made a drastic switch to the R&D of electric vehicles. These vehicles would have virtually no greenhouse gas emissions, greatly reducing our environmental impact as well as our annual spending on the high gasoline prices currently. Although lithium has applications in many other industries, there has been an exponential change in industrial allocation, greatly moving towards the battery industry as the majority holder. It was estimated that in 2005, the different lithium applications all shared a very similar chunk of the market with no clear outliers.¹¹ The pie charts shown below (Fig 1.2) illustrate the lithium market in 5-year increments. In just 5 years, the glass and ceramics industry grew majorly, and the battery industry showed similar appreciable growth. Fast forward to 2015, these two industries made up roughly 67% of lithium use with clear trends toward exponential growth in the battery industry. Now, post-2020, about 50% of lithium collected is used for batteries, and this trend is only expected to rise rapidly with greater developments in electric vehicles and increased environmental awareness.¹¹

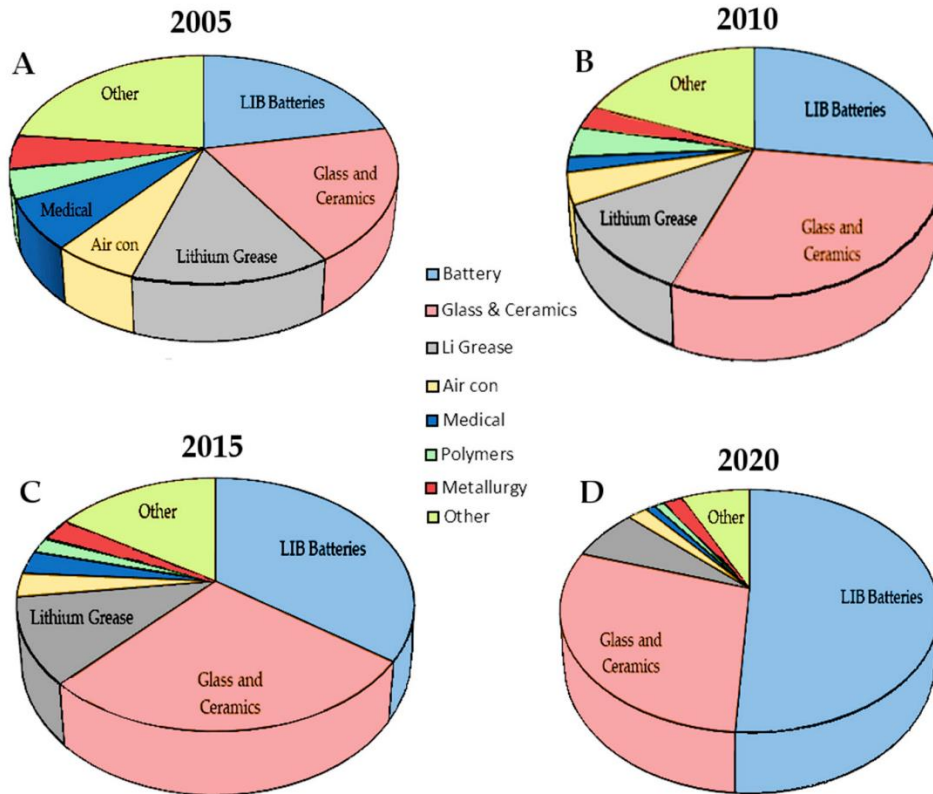


Figure 1.2: Pie charts illustrating industrial distribution of lithium resources from 2005-2020.¹¹

Visualizing this distribution of resources, it is safe to assume that lithium collection will be an important area of study. The battery industry is not only rapidly becoming the most common use of lithium, but due to the increased desire for sustainable transportation, this sector is going to expand exponentially in and of itself. Lithium demand in 2024 is estimated to be around 750 000 metric tonnes of lithium carbonate worldwide. These demands are currently being met with today’s lithium isolation practices, however the future holds many uncertainties. Lithium demands are forecasting to be 2 000 000 tonnes by 2030 and are expected to exponentially increase all the way to 5.5 million metric tonnes by 2040 (Fig 1.3).¹² With current lithium isolation methods, the supply is not expected to increase much outside of normal industrial advancement, and by 2040 the

predicted supply is estimated to be less than half of the demand.¹² More critically in Canada, a new act was passed that requires all automobile manufacturers to produce strictly zero-emission cars by the year 2035.¹³ With these projections and new governmental pressure, it is crucial to develop and improve on existing lithium collection methods to keep up with demand and ensure our carbon footprint and negative environmental impact is limited.

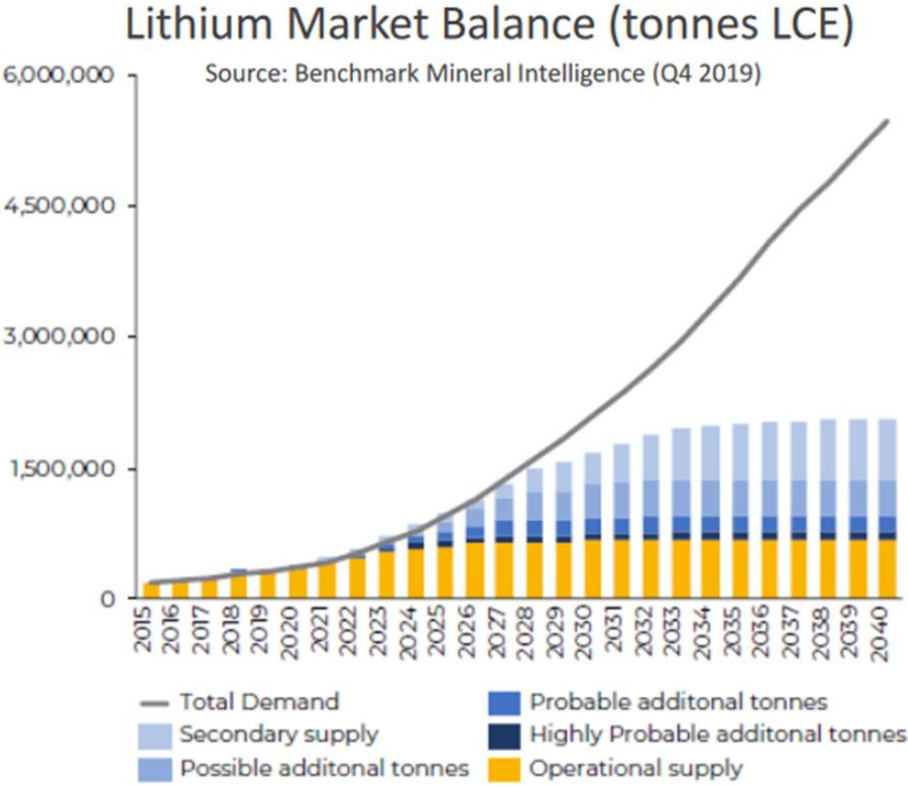


Figure 1.3: Projected worldwide supply and demand for lithium resources. Projections indicate supply will fall behind majorly with current lithium isolation practices.¹²

1.3 Current Lithium Isolation

As explained above, lithium is in increasing demand due to increased electric

vehicle usage. Lithium is currently extracted from two major sources worldwide, natural brines and minerals or ores. There is also an abundance of lithium in the earth's crust and oceans, however the relative concentrations when compared to the total crust volume as well as other contaminants leave these sources undesirable.¹⁴ Recovery of lithium from minerals and ores is an expensive and harsh process. Minerals containing lithium are commonly roasted at temperatures above 800 °C and treated with acidic or basic conditions to retrieve crude lithium.¹⁵ The lithium then undergoes a purification process to recover industrial grade Li_2CO_3 . Lithium-rich brines are the other primary source of lithium, however currently less popular than bulk mineral recovery because mineral recovery is much quicker and easier to scale-up with current technologies. Lithium-rich brines can only be used after a pre-concentration process has been done, typically through solar evaporation.^{16,17} This process is lengthy and laborious, so consequently is used less frequently, although recently explored more due to diminishing resources. To develop new and improved isolation processes, we must first understand our current technologies in detail to determine where expansion is possible.

1.3.1 Recovery from Minerals and Ores

Industrial lithium is typically in the carbonate form (Li_2CO_3) and commonly isolated from minerals and ores. Minerals containing lithium are mostly complex silicate structures and phosphates, common examples being spodumene, lepidolite, petalite, and amblygonite (Table 1.1).¹⁷ Spodumene, most commonly mined in Australia, is the most popular lithium-bearing mineral due to its high lithium content, commercial processability, and abundance. Lepidolite, due to its complex structure and difficult processing, is

typically added in ore form directly to glass and ceramics for properties listed in Section 1.1.¹⁵ Petalite, another simple silicate, is commonly mined in Africa and also used similarly to spodumene due to commercial processability. The last example, amblygonite, is a fluorophosphate that contains the highest lithium content of the bunch.

Name	Formula	Li Content (wt. %)	Majority Location
Spodumene	$\text{LiAlSi}_2\text{O}_6$	1.9-3.3	Australia
Lepidolite	$\text{K}(\text{Li},\text{Al})_3(\text{Si},\text{Al})_4\text{O}_{10}(\text{F},\text{OH})_3$	1.5-3.6	Zimbabwe
Petalite	$\text{LiAlSi}_4\text{O}_{10}$	1.6-2.1	Zimbabwe
Amblygonite	$(\text{Li},\text{Na})\text{AlPO}_4(\text{F},\text{OH})$	3.5-4.2	Canada, Brazil
Eucryptite	LiAlSiO_4	2.34	Zimbabwe
Zinnwaldite	$\text{KLiFeAl}(\text{AlSi}_3)\text{O}_{10}(\text{F},\text{OH})_2$	1.59	China

Table 1.1: Properties of most common lithium-mined minerals¹⁸⁻²⁰

The collection of lithium from each mineral all follow very similar processes. In spodumene, for example, the ores are ground up to increase the surface area for greater lithium accessibility. Spodumene is then roasted at temperatures up to 1100 °C to convert the structure to one more susceptible to attack by later chemical processes.²¹ After roasting, the lithium is prepared further using either acid, alkaline, or chlorination

processes. All other ores do not require the same pre-treatment at high temperatures and are typically prepared by roasting at temperatures closer to 800 °C with additives already implemented, then lastly leached with water (Fig 1.4).¹⁶

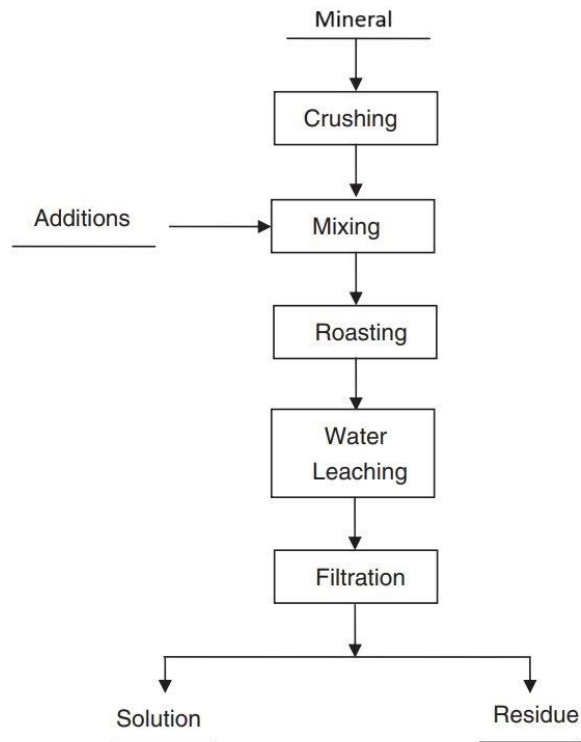


Figure 1.4: Generic process for lithium recovery from minerals and ores.²²

1.3.1.1 Acid Process

Spodumene is the most common mineral used for lithium collection due to its abundance and accessibility, so the acid process will mainly be outlined with this in mind. As mentioned earlier, spodumene is first roasted at around 1100 °C. This process converts the recovered α -spodumene to β -spodumene, a structure that is much more susceptible to chemical attack as it is more porous than its counterpart (Fig 1.5).^{23,24} β -

Spodumene is then ground again and roasted again in contact with concentrated H_2SO_4 . This process converts the lithium present into water-soluble Li_2SO_4 . Water is then used to leach the Li_2SO_4 and excess sulfuric acid out of the ground-up spodumene.^{16,21} The leftover sulfuric acid is then neutralized with CaCO_3 . Separation of solids and liquids occurs, with the leached supernatant mainly composed of Li_2SO_4 , calcium, and other metal impurities. These impurities can then be removed via sequential precipitation methods using a controlled pH, allowing each metal impurity to crash out of solution and be separated from the remaining supernatant.²³ At the end of the process, you are left with a dilute solution of Li_2SO_4 in water. This solution is then concentrated by evaporation, causing a severe lithium concentration increase and allowing an easier recrystallization process. Na_2CO_3 is added to this solution to carbonate the Li_2SO_4 and produce Li_2CO_3 . The by-products produced are excess Na_2CO_3 and Na_2SO_4 , both of which are soluble in water. Li_2CO_3 is insoluble in water and crystallizes out of solution in which it can be collected, washed, dried, then sold to major distributors.²³

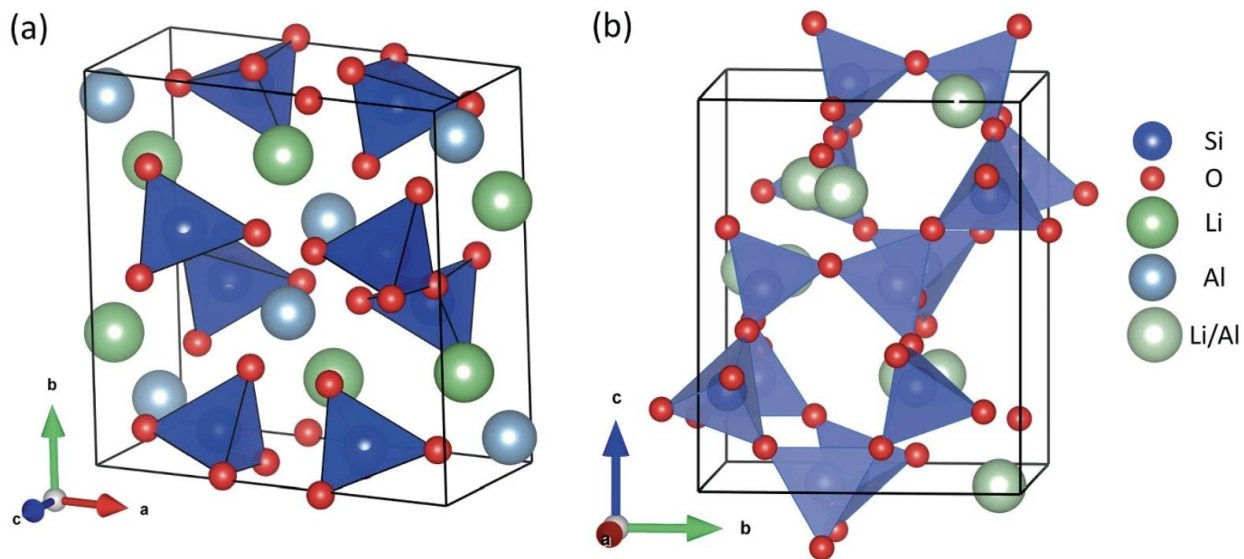


Figure 1.5: Conversion of (a) α -spodumene to (b) β -spodumene through calcination at $1100\text{ }^\circ\text{C}$.²⁵

Although Li_2CO_3 is the major form of lithium distributed, there are other forms of lithium that are important to isolate such as LiOH . This process is started similarly, with high temperature roasting and sulfuric acid leaching being the first two steps. Again, metal impurity removal is done through addition of CaCO_3 as well as sequential precipitations. Ion-exchange processes occur to leave behind a pure Li_2SO_4 and Na_2SO_4 solution.²⁶ Electrochemical processes are employed to produce LiOH from Li_2SO_4 , also supplying one of the first reported pathways to get LiOH without going through Li_2CO_3 conversion first. Upon evaporation of the LiOH solution, high purity $\text{LiOH}\cdot\text{H}_2\text{O}$ crystals are produced and ready to be distributed.²⁶ This process (Fig 1.6) developed in Quebec by Nemaska Lithium Inc. is important as they also retrieve high-quality lithium carbonate through this method by introducing CO_2 to the LiOH solution. This produces LiHCO_3 , which upon heating produces Li_2CO_3 . Using this highly useful extraction method, they are able to isolate two of the most popular forms of lithium from spodumene, serving particularly useful for us due to their location and use of Canadian resources.

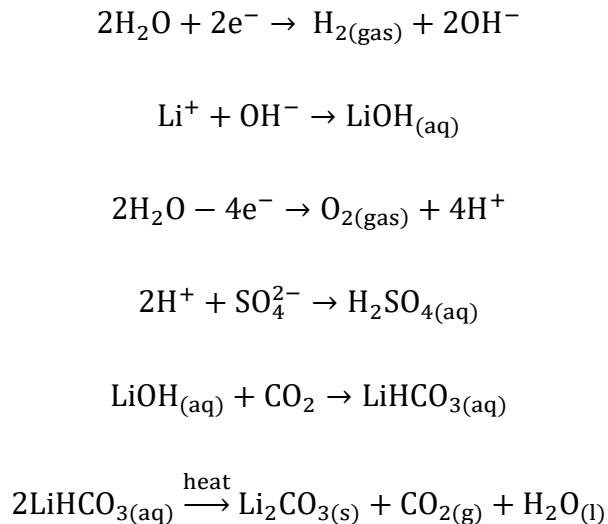


Figure 1.6: Electrochemical processes used by Nemaska Lithium Inc. in Quebec.²⁶

Another important movement in the acid-leaching process is the ability to skip the high temperature calcination needed to convert α -spodumene to β -spodumene. Guo et al. discovered that dissolving α -spodumene in diluted sulfuric acid and heating anywhere from 50-125 °C can be used as a pre-treatment.²⁷ Then hydrofluoric acid is added and stirred for 3 h to digest and leach the lithium from α -spodumene directly into water.²⁷ Precipitation using Na_2CO_3 yields Li_2CO_3 recovery at around 96% of the potential return, rendering this an effective method to avoid high temperature roasting, but generally more corrosive and harmful than sulfuric acid. Regardless, acid-leaching processes are still very common, however they do require very high concentrations of acid which could be unsafe. These processes require special machinery to deal with high amounts of acid at high temperatures, making this a costly extraction method.¹⁷

1.3.1.2 Alkaline Process

Alkaline lithium recovery processes are a cheaper, less harmful way to retrieve pure Li_2CO_3 or LiOH from ores. Again, spodumene is the most common ore used in these processes, so it will be the example used in this section to illustrate how the process operates. Similarly to the acidic process, α -spodumene is relatively ineffective for extraction of lithium due to the tight crystal structure and small pores for leaching agent to enter. Grinding and calcination at temperatures around 1100 °C are needed to convert the structure to β -spodumene, allowing for proper chemical entry to leach out the lithium.^{23,24} Na_2CO_3 or limestone solutions are used to convert the original lithium silicate structure into something more soluble, most commonly carbonates.^{28,29} Carbon dioxide is then introduced to the system in a process known as bio-carbonation, which converts

insoluble lithium carbonate to an aqueous solution filled with LiHCO_3 . The remaining solid residue is removed at this point and discarded, leaving behind an aqueous solution of LiHCO_3 .¹⁴ This solution is evaporated slowly to produce the desired lithium salt product, supplying Li_2CO_3 if Na_2CO_3 was used earlier in the process, or $\text{LiOH}\cdot\text{H}_2\text{O}$ if limestone was used at the beginning. Any liquid still retained at the end of the process is recycled back to the first step of the system, allowing for a highly efficient and low waste process (Fig 1.7).

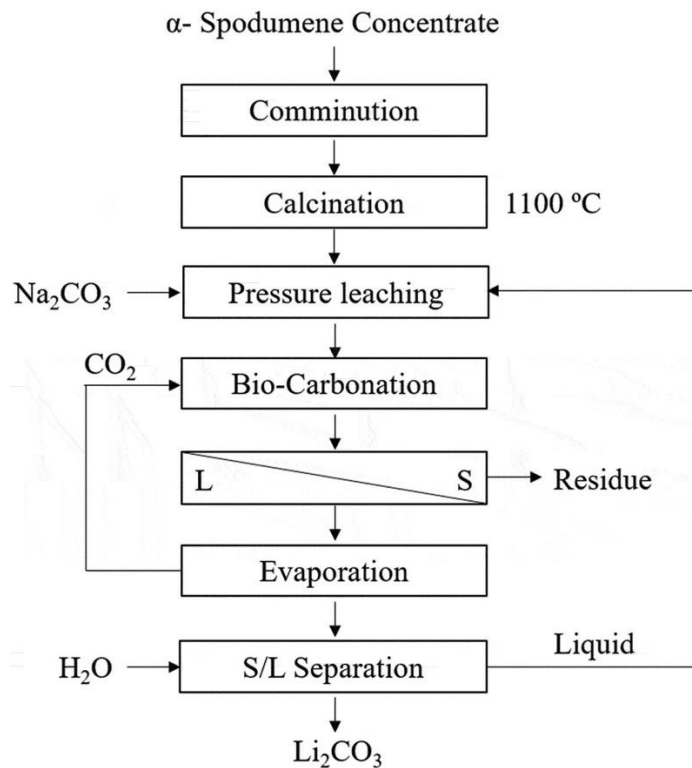


Figure 1.7: Alkaline process for lithium carbonate recovery.^{16,23}

Important to note of this process is that both the hydroxide and carbonate versions of lithium can be isolated, making it a slightly tunable process. Although the

alkaline pathway works well, LiCl, another very popular form of commercial lithium, must be achieved through another leaching process called chlorination.

1.3.1.3 Chlorination Process

Chlorination of minerals and ores requires roasting at extremely high temperatures, similar to the temperatures used for calcination of α -spodumene. This roast is in the presence of some chloride source, typically HCl or Cl_2 , all depending on the source of the lithium.^{30,31} As summarized in Table 1.2, various temperatures and reagents are needed to break down different ores. A notable example of this includes the quantitative extraction of lithium from lepidolite using HCl at only 935 °C.³¹ Lithium can be mined from spodumene quantitatively using chlorine gas at 1100 °C, however the recovery percentage drops to 58% when roasted at 1000 °C. There have also been reports using CaCl_2 or NaCl as the chloride source when extracting from lepidolite, subjecting the ore to lower temperatures (950 °C) than before.³²

Raw Material	Roasting Temp (°C)	Time (h)	%Li Extraction	Product
Lepidolite	935	13	100	LiCl
Spodumene	1000	4	58	LiCl
Spodumene	1100	2.5	100	LiCl
Lepidolite	w/ CaCO_3 & CaCl_2 , 950	5	80	LiCl

Table 1.2: Chlorination roasting conditions from various minerals.^{31–34}

Aside from similar drawbacks with acid and alkaline processes such as the high roasting temperatures, the only consequence in chlorination roasting is the corrosivity of the chlorine sources. This requires the use of highly expensive, corrosion-resistant equipment, which already adds to the large energy costs associated with mineral extraction.¹⁶ Albeit, chlorination roasting of minerals and ores provides few major drawbacks and is still used as the primary source of lithium chloride from minerals.

1.3.2 Recovery from Brines

Lithium recovery from brines is pushing to be the leading source of lithium production, trending soon towards accounting for about 65% of all lithium recovery. The majority of this fraction is taken from the lithium-rich brines in the ABC (Argentina, Bolivia, and Chile) region of South America, and smaller amounts can be found in China.²¹ Lithium is recovered from brines using three major processes, precipitation, adsorption, and ion exchange techniques. Regardless of the process, brine recovery is about 30-50% cheaper than recovery from minerals and ores due to lower energy costs and relatively natural processing.²³

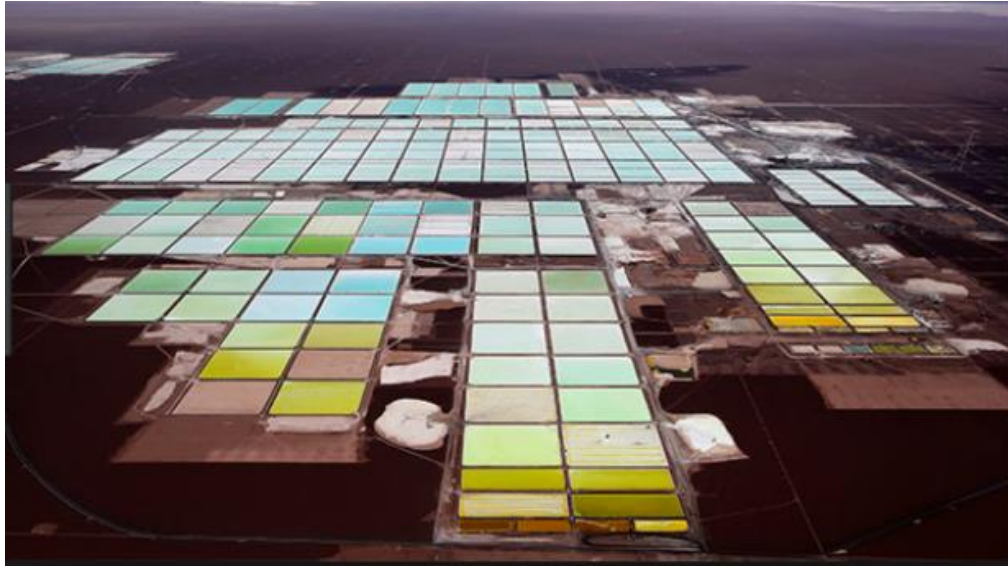


Figure 1.8: Lithium-rich brine pools in ABC region in South America.

In all three techniques, there is a lengthy pre-evaporation process that must take place before lithium recovery can occur. Although these are lithium-rich brines, they are still rich in many other cationic contaminants such as calcium, magnesium, potassium, and sodium. These contaminants heavily dilute the lithium in solution, requiring some pre-evaporation to concentrate the lithium to an appreciable amount. The brines are pooled in organized shallow ponds (Fig 1.8) in hot, humid climates that allow for the sun and wind to slowly evaporate the water for 1-2 years. This pre-concentration is required to convert the ponds to about 6% lithium, concentrated enough to begin the extraction processes.^{16,17,22}

1.3.2.1 Precipitation

Depending on the brine location, the precipitation process varies relative to the

concentration of contaminants.³⁵ As mentioned before, the precipitation process starts with a lengthy solar evaporation to slowly increase the extremely dilute lithium content. After this, boron is removed through a solvent extraction process as it is the most dissimilar of all the contaminants of interest. Upon removal of boron, $\text{Ca}(\text{OH})_2$ (lime milk) is added to precipitate out $\text{Mg}(\text{OH})_2$, leaving behind aq. CaCl_2 and the rest of the liquor. The calcium is then removed by precipitating out CaCO_3 through the addition of either Na_2CO_3 or already isolated Li_2CO_3 .¹⁴ The CaCO_3 that crashes out from this process is then roasted at very high temperatures, hydrated to produce lime milk, then used in a regenerative process to remove the magnesium from the next cycle. With any residual 2^+ cationic contaminants such as Mg^{2+} or Ca^{2+} , ion-exchange processes can be employed to further purify the solution.¹⁷ Carbonation with Na_2CO_3 occurs to precipitate out industrial grade Li_2CO_3 , which is then filtered and used, or sent off for further purification for use in batteries (Fig 1.9).

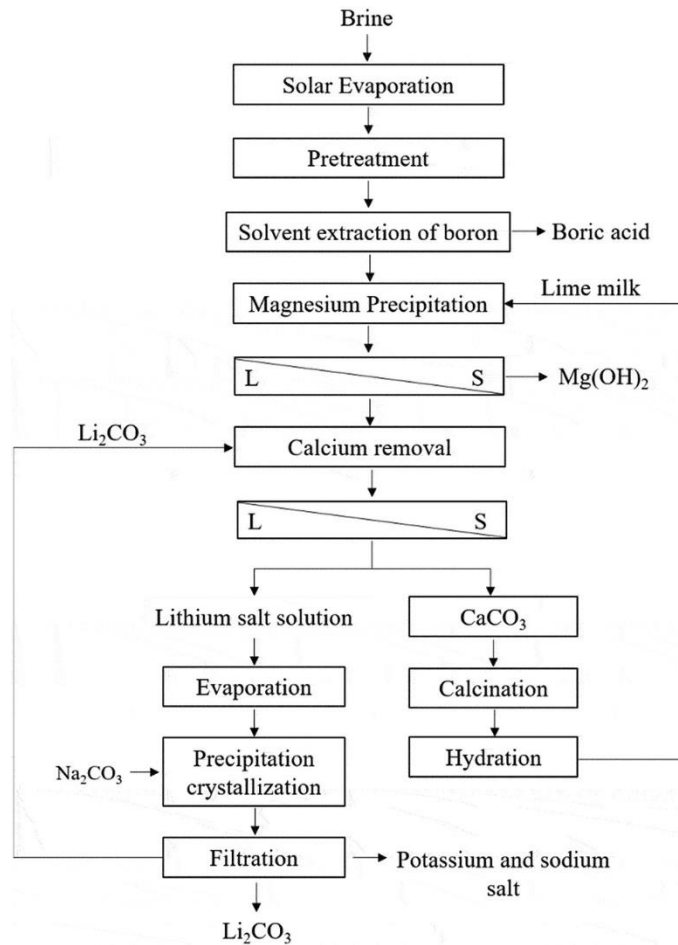


Figure 1.9: Generic precipitation process for removal of industrial lithium carbonate from natural brines.¹⁷

Other brines may alter in their precipitation steps depending on the composition. Uyuni solar brine in Bolivia has one of the highest natural lithium compositions in the world, however there are copious amounts of magnesium as well, making lithium isolation more difficult. An et al. developed a process to purify lithium from this specific brine, using excess lime milk to precipitate out $Mg(OH)_2$ and gypsum at high pH.³⁶ The next step involved the use of sodium oxalate to precipitate out any remaining calcium, leaving behind the common sodium and lithium-containing liquor seen earlier (Fig 1.7), which is then carbonated with Na_2CO_3 to produce Li_2CO_3 once again.³⁵

1.3.2.2 Adsorption

Removal of lithium using adsorbents is another process used in recovery from natural brines. The focus on this section will be mainly on inorganic adsorbents which tend to rely on a type of memory for lithium size and selectivity. A common inorganic adsorbent are aluminum salts which tend to have a high selectivity and capacity for lithium, potentially allowing easier scale-up to industry.³⁷ Aluminum salts are used by introducing LiCl with Al(OH)₃ in an integrated structure, essentially creating small cavities in between the aluminum atoms where the lithium sits.³⁸ Upon complexation and decomplexation, the size of the cavity remains the same, illustrating a memory effect that will allow lithium to continue adsorbing into the structure. Many of these aluminum adsorbents are powders, which pose fluidity issues and loss of adsorbent due to inevitable dissolution after repeated use. These salts can be implemented in resins to bypass these issues, but current production costs are too high for industrial scale-up.³⁹

A very common inorganic adsorbent is a lithium-ion sieve which implements a similar mechanism of action to the lithium aluminum salt. Essentially, an inorganic structure is formed, and lithium is introduced to the system forming custom-sized pores where the lithium can sit.^{40,41} The lithium can then be removed without disrupting the crystal structure using an acidic eluent, leaving behind a pore that is designed to fit only the Li⁺ ion. Since Li⁺ is the smallest of all alkali metals, this pore should theoretically only be able to isolate Li and any ions smaller than it, hence making them Li-selective (Fig 1.10).⁴¹

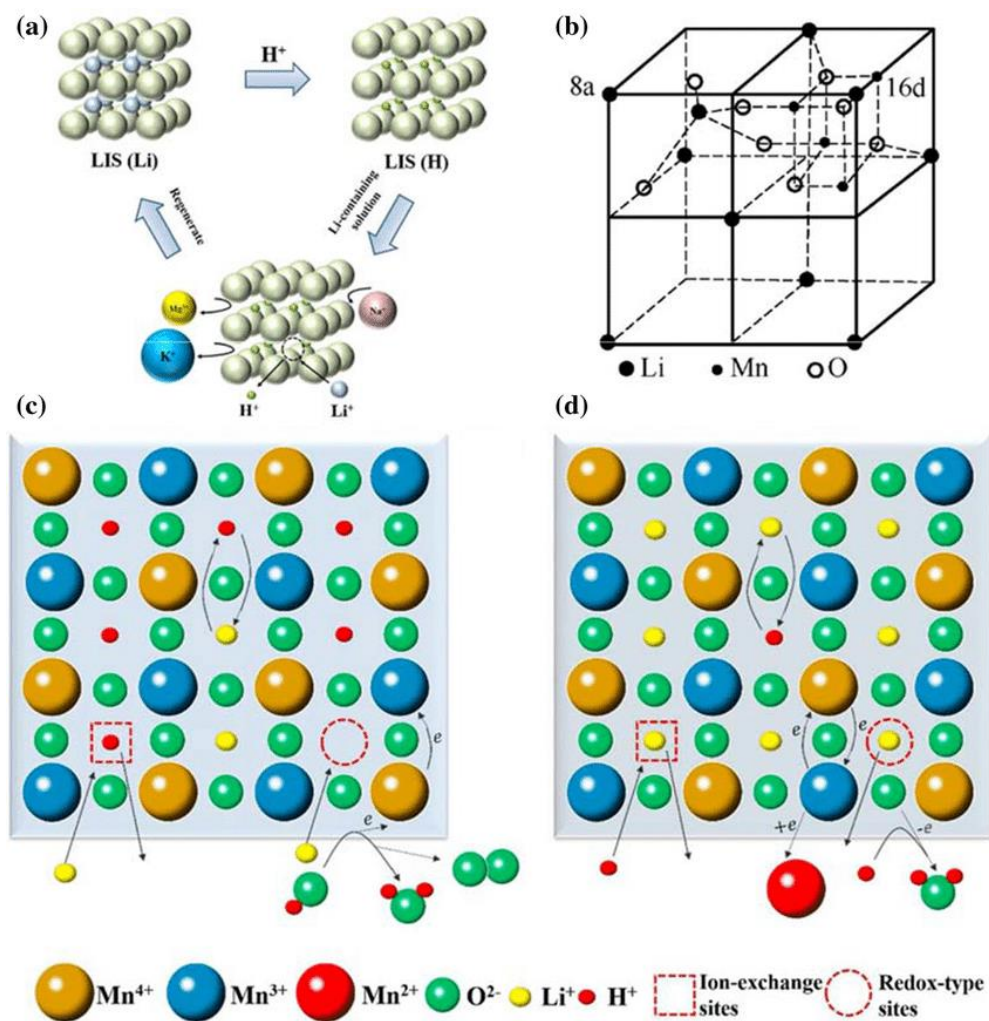


Figure 1.10: a) Generic Li-ion sieve mechanism of action; b) Crystal structure of Li-Mn-O molecular sieve; c) Li adsorption process; d) Li desorption process.^{40–42}

These sieves are typically made up of either MnO or TiO structures. MnO sieves have demonstrated greater Li-selectivity and adsorption capacity, however during desorption with acid, MnO sieves undergo non-negligible Mn dissolution into solution, polluting the water with Mn which is environmentally unfriendly.⁴² Due to this, recent attention has been focused on improving the performance of TiO sieves. These sieves also undergo Ti dissolution during the desorption process, but this is less worrisome due

to the relative environmental inertness of Ti.⁴¹

Organic adsorbents have also been explored for Li-selectivity, however the scope remains relatively limited at this time. Typically, organic adsorbents that are Li-selective are implemented in things such as polymers or resins to be used commercially.³⁷ They are also used in solvent extraction techniques, where the organic ligand is used to exploit selectivity and solubility differences to isolate lithium. Common organic binding motifs are discussed in the next chapter, however a typical one that is mentioned a lot is crown ethers.⁴³ These are used in both solid-state and solution applications as they have proven to show some Li selectivity. However, the properties of these systems must be carefully monitored, thus probing us to look at other potential candidates.

1.3.3 Recovery from Secondary Sources

Although lithium recovery from natural sources remains the clear research focus, recovery from secondary sources such as old batteries could prove important for sustainability. Old, used batteries that contain lithium also contain other important metals. Efficient recycling of the spent lithium in these batteries could be a way to better our environmental impact, while also slowing the depletion of our natural resources.¹⁷ Current methods used to recycle lithium-ion batteries are either through electrochemical processes or through similar precipitation processes described earlier. Two treatments are outlined below; Toxco essentially using repeated mixing and filtering (Fig 1.11a), Accurec using a binder to separate the electrode materials from the lithium (Fig 1.11b).

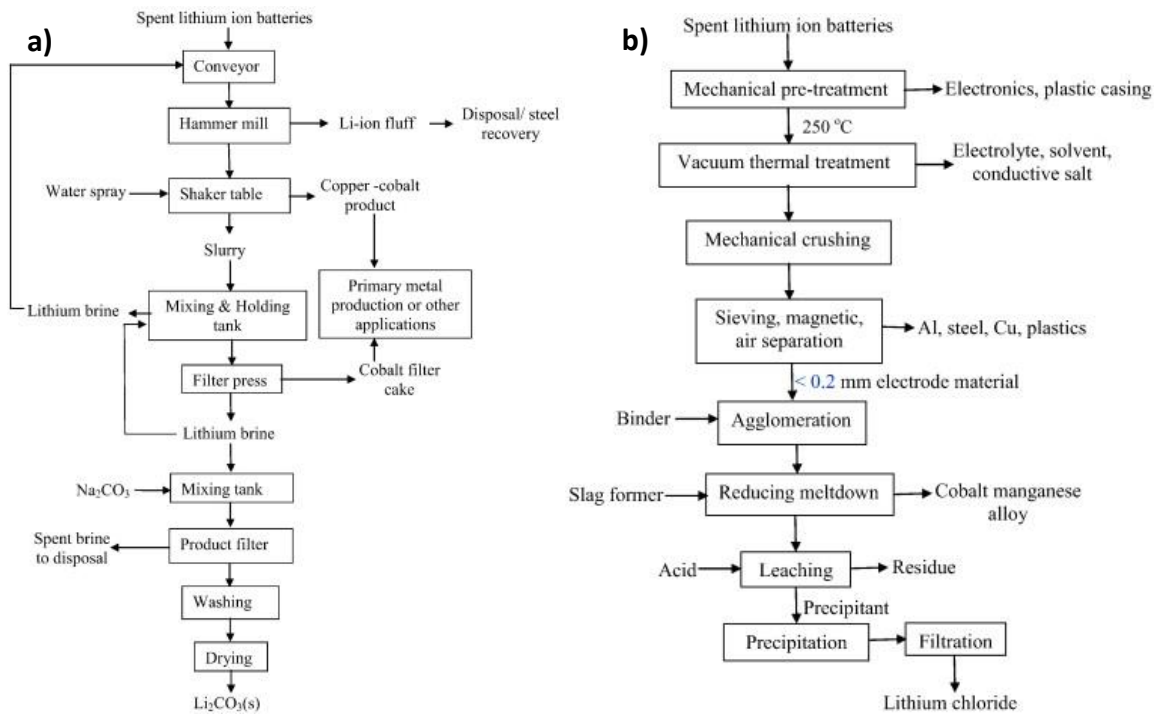


Figure 1.11: a) Toxco's method for recycling Li-ion batteries; b) Accurec's method for recycling Li-ion batteries. ^{44,45}

1.4 Scope of Thesis

The purpose of this thesis is to gain a deeper understanding on how we currently isolate a very sought-after natural resource. Knowing our current strategies has led to peaked interest in organic adsorbents, one in particular in which we have designed and explored. Chapter 2 outlines the design inspiration and how our idea came into fruition. Chapter 3 illustrates our dive into the synthesis of our proposed ligand and its selectivity towards lithium.

Chapter 2: Ligand Design

2.1 Lithium Binding Motifs

In search of inspiration for ligand design, current molecules used for lithium chelation were explored to determine their viability in our proposed research. Lithium is commonly known to have a strong affinity for heteroatoms with lone pairs available for donation, usually nitrogen or oxygen. This implies that frequently used lithium chelators should also contain these specific atoms. Some useful lithium-binding motifs that have been explored are ethylenediamines such as EDTA, HEDTA, and TMEDA, or oxygen-containing macrocycles called crown ethers (Fig 2.1).⁴⁶

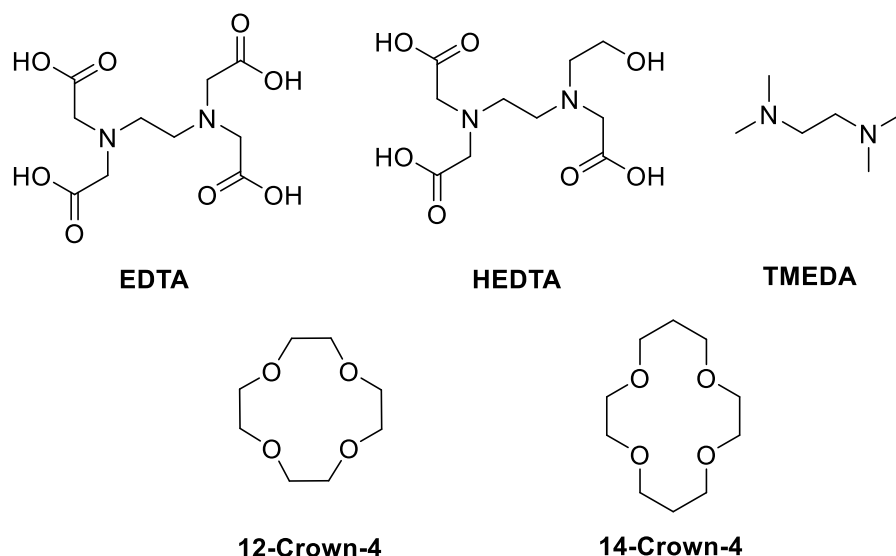


Figure 2.1: Commonly used lithium-chelators.

Although these are all used for lithium chelation, these compounds also possess the ability to bind other candidates as well. EDTA, HEDTA, and TMEDA have all shown the ability to bind some first-row transition metals such as Mn (II), Cu (II), Fe (III), and Co

(III), with EDTA also used to bind heavy metals as well.⁴⁶ Although proving useful in lithium chelation, crown ethers also possess strong affinities for other alkali and alkaline earth metals, most notably Na^+ , K^+ , Ca^{2+} , and Mg^{2+} . Cation selectivity in crown ethers is largely controlled by modifying the cavity size or the number of binding heteroatoms, increasing the size needed as you move down the periodic table. A major player in the area of applicable lithium selectivity using crown ethers is work done by Warnock et al. in which they are trying to synthesize a polymer with three different subunits to try and selectively bind lithium.⁴⁷ Their subunits involve a 12-crown-4 binding motif to try and selectively bind lithium, a simple ether subunit with various lengths was added to control water uptake, and a crosslinker subunit was added to promote formation of solids during polymerization (Fig 2.2).

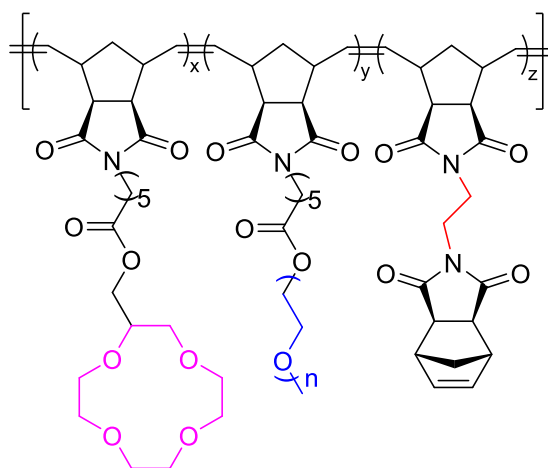


Figure 2.2: Polymeric membrane developed by Warnock et al. with three different subunits to control lithium selectivity.⁴⁷

Although targeting lithium, they determined that the 12-crown-4 subunit in their polymer had greater affinity towards sodium due to the diffusion of sodium into the

membrane occurring faster.⁴⁸ MD calculations they performed explained this deviation from their hypothesis. They found that in an aqueous medium, lithium preferred a 4-coordinate system and sodium preferred a 6-coordinate system. However, once their 12-crown-4 membrane was introduced, sodium's preferred coordination environment dropped to 4, and due to the higher diffusivity of sodium over lithium into the membrane, it selectively bound sodium. Another MD calculation aimed to measure the average coordination number of both lithium and sodium with free 12-crown-4 molecules in solution. They determined that when allowed, these alkali metals will try to form a 2:1 CE:M sandwich complex to allow even tighter binding and more coordination sites (Fig 2.3).⁴⁷

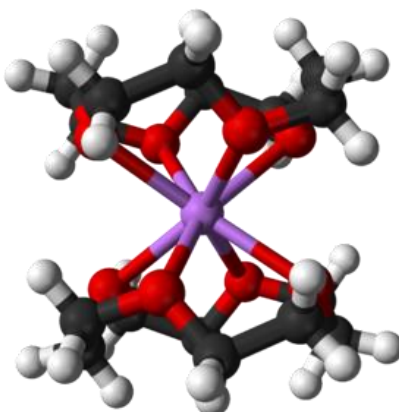
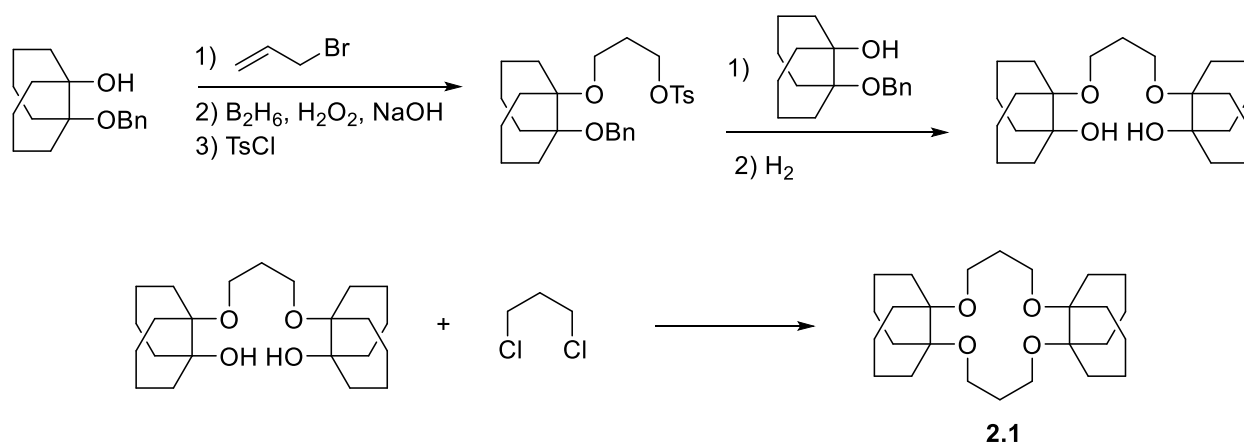


Figure 2.3: Illustration of 2:1 CE:M sandwich complex formed from flat crown ethers in solution.

This was further probed by Kobihiro and Pedersen, who also verified the tendency of crown ethers to form 2:1 CE:M complexes when using flat crown ethers such as dibenzo-18-crown-6.⁴⁹ Sandwich complexes encourage sodium selectivity due to the larger cavity size along with more coordination sites, essentially removing the use of flat

crown ethers alone for lithium collection. To combat this issue, the addition of bulky side groups to either side of the crown ether could prevent sandwich complex formation.⁵⁰ Kobiro hypothesized that 14-crown-4 should be selective towards lithium complexation due to the coordination number it offers, however it forms a sandwich complex in solution to more tightly bind sodium.⁴⁹ They sought out to incorporate bulky decalin side chains on the crown ether to impose strong steric effects and hopefully deter the formation of sandwich complex. Upon synthesis of the decalin crown ether **2.1**, they determined that the decalin side chains were almost perpendicular to the ring which provided sufficient bulkiness to prevent sandwich complex formation (Scheme 2.1).



Scheme 2.1: Synthesis of bulky decalin side-chain crown ethers to reduce sandwich complexation.⁴⁹

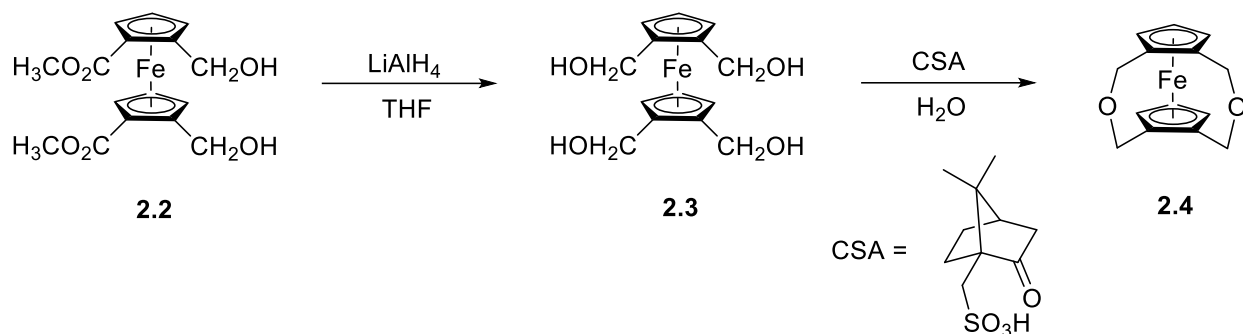
Throughout LLE studies, **2.1** was found to almost quantitatively extract lithium. Unfortunately, the lithium was so strongly bound therefore burying the cation deep into the ionophore that they encountered trouble with the latter half of the lithium isolation process, decomplexation.⁴⁹ Although bulky crown ethers appear feasible for selective

lithium isolation. The shared decomplexation problem due to the deep rooting and tight binding of the metal in sandwiched crown ethers may prove troublesome for efficient industrial lithium isolation. We sought out to design a lithium-selective ionophore that proves to be both selective towards lithium, as well as easy to remove lithium to collect once bound.

2.2 Ferrocene Building Block

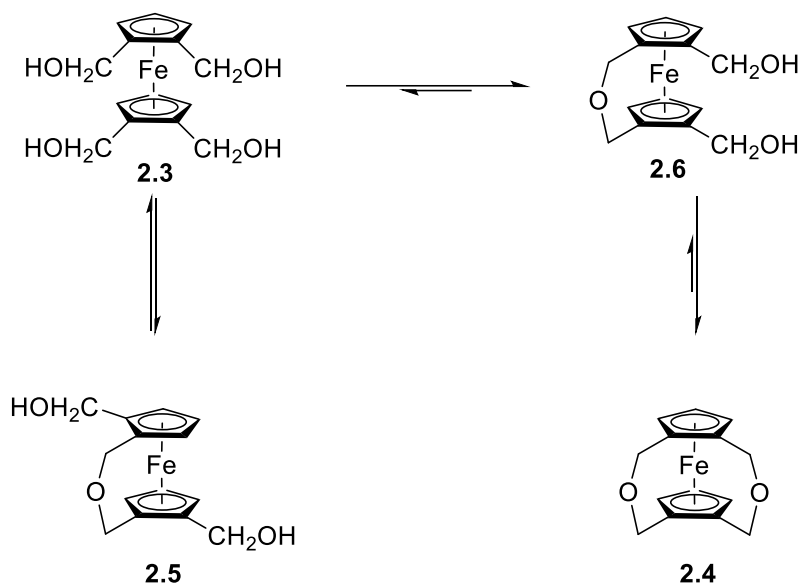
2.2.1 Forming Bridged Ether on Ferrocene

Knowing that crown ether sandwich complexes increase the binding strength around chelated metal cations, we began to search for ways to implement a pre-arranged sandwich complex into our ligand design. Intriguing work from Petter et al. in 1990 revealed that ferrocene molecules substituted at the 1,1' and 2,2' positions with methanol groups could undergo a cooperative dehydration to form two crown ether bridges in close proximity to each other.⁵¹ Substitution at these positions first entails functionalization of cyclopentadiene before formation of the ferrocene complex, typically done by adding ester groups (**2.2**). Full reduction of these groups to their corresponding alcohols gives the precursor **2.3** to the doubly-dehydrated product **2.4** that is formed through the acid-catalyzed ether formation from alcohols (Scheme 2.2).



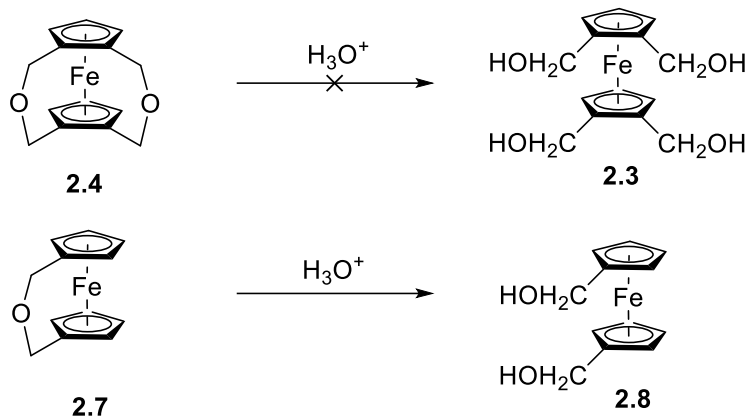
Scheme 2.2: Cooperative dehydration of methanol-substituted ferrocene.⁵¹

Important to note about this work is the label of cooperative dehydration. Acid-catalyzed formation of ethers from alcohols is a reversible process, and since Petter et al. were able to isolate **2.4**, it serves us to believe that the equilibrium leans more towards the product side. This was confirmed through kinetic studies that showed the ether formation was reversible up until the desired first ether bridge **2.6** formed. Once the 1,1' positions were linked with an ether bridge, the equilibrium shifted towards the formation of the second ether bridge **2.4**. This equilibrium shift is believed to be due to the newly imposed lack of free rotation in the Cp rings, as well as a new angular tilt of 12 °C (Scheme 2.3).⁵¹



Scheme 2.3: Equilibrium shifts presented during cooperative dehydration process.⁵¹

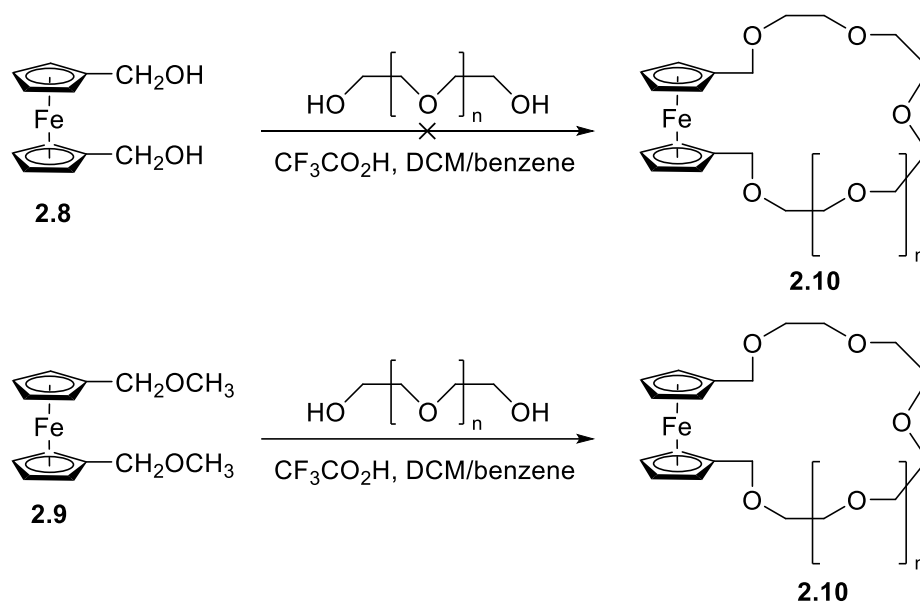
The stability of **2.4** was reaffirmed upon attempt of the reverse reaction involving the hydrolysis of the bridged ethers back to **2.3**. Upon attempt of hydrolyzing **2.4**, no reaction occurred and the starting material was left intact. However, this does differ from their findings upon attempt of hydrolyzing **2.7** in which hydrolysis readily afforded them the original alcohol **2.8** (Scheme 2.4). Petter et al. attributes this to the even greater angular tilt (16 °C) as well as a complete lock of configuration. With hydrolysis only occurring with one ether bridge, it can be deduced that our double-ether bridge design we are proposing is not only necessary to achieve selective lithium separation, but intrinsically increases the stability of the ligand as well.⁵¹



Scheme 2.4: Hydrolysis of bridged crown ethers to original alcohol substituents.⁵¹

Knowing that it is feasible to have two ether bridges on one ferrocene molecule, we then sought after increasing the ether size. Petter et al. was able to create ether bridges with one oxygen atom each, however it is known that effective lithium chelators typically require at least four Li – X coordination sites to create significant enough interactions to pull lithium out of its original medium. With this insight, we searched for ferrocene molecules with longer ether bridges connecting the Cp rings in hope of bridging this gap. Rao et al. developed a method to undergo a heteroannular macrocyclization with similarly functionalized Cp rings to Petter, reacting the alcohol or methoxy substituents with various lengths of glycols to create larger ether bridges.⁵² Rao built off work completed by Czech et al. in which their group was able to synthesize bridged Cp rings using tetraethylene glycol dithiol to afford them various thioether bridge lengths.⁵³ Instead of being limited to thioethers, it was found by Rao that with slight modification of the ferrocene, they were able to produce different lengths of the all-oxygen bridged ethers with similar efficiency. However, the caveat comes when attempts were made to produce ether bridges starting with the original hydroxy functional groups like **2.8** as they were

unsuccessful. The formed product turned out to be the dehydration product **2.7** reported by Petter et al. and mentioned above. When attempts were made with diether starting material **2.9**, all of the macrocyclizations of different lengths were successful although producing slightly low yields of **2.10** (14%-31%, Scheme 2.5).



Scheme 2.5: Modified ferrocene substitution for successful heteroannular macrocyclizations.⁵²

Rao hypothesizes that the driving force is an entropic one, and that the liberation of 2 equivalents of methanol per ether bridge might be sufficient to push the reaction. A similar macrocyclization in which the 1,1' and 2,2' positions were substituted reportedly worked more efficiently than the single ether bridge, however this was only briefly mentioned and not expanded upon.⁵²

Using a combination of logic from the work of both Rao and Petter, we hypothesized that two crown ether bridges on ferrocene could potentially serve as a

lithium-selective binding motif to pull lithium from natural sources. It has been shown that multiple ether bridges of one oxygen each can form on ferrocene and that the formation of two bridges is a major equilibrium driving force. It has also been demonstrated that ether bridges of various lengths can be formed on ferrocene, however the requirement of substituting the alcohols out for methyl ethers seems necessary. We are hopeful that the equilibrium trend will serve true for the formation of two larger ether bridges, and that although other side products may be produced in the reaction, we will eventually reach our desired isolatable lithium-binding motif (Fig 2.4).

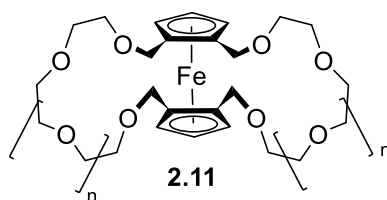
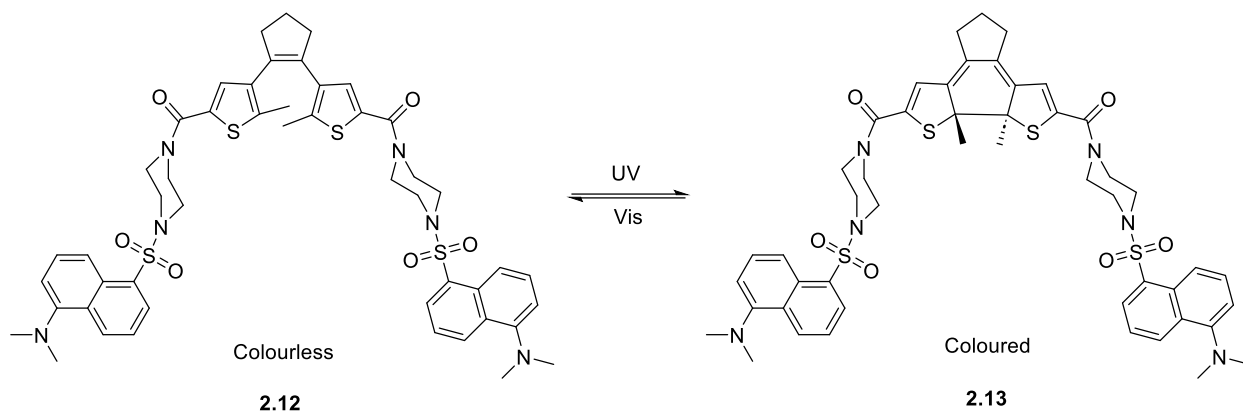


Figure 2.4: Proposed lithium-binding motif

2.2.2 Molecular Switches

Not only must we put thought about the inspiration behind the motif design and how we hypothesize that it will bind lithium, we must also begin thinking about how the lithium can be removed from the molecule and collected to regenerate the binding cycle. Although a major part of the ferrocene design was to create a rigid backbone to arrange two crown ethers close enough to each other form a sandwich complex, it also serves as a potential molecular switch for lithium retrieval post-binding. Molecular switches can be described as a molecule that possesses the ability to switch between two stable states

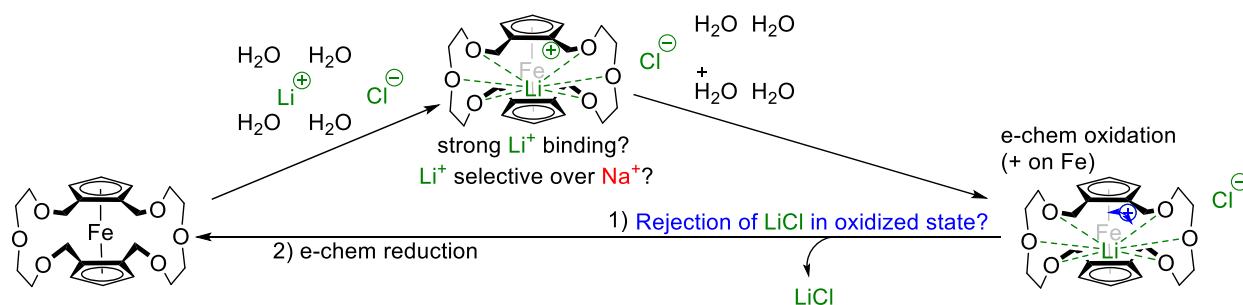
through changes in the environment surrounding it (Scheme 2.6).⁵⁴



Scheme 2.6: Molecular switch illustrating the photoisomerization of dithienylethene.⁵⁵

They typically have applications in pH indicators, photochromic switches for UV-VIS spectroscopy, and are more recently being used for host-guest applications, similar to our plans. The utility of a molecular switch relies heavily on the fact that the process is reversible, and the ability to have complete control over which state the molecule resides in, usually by controlling parameters such as temperature, pH, light, or electrical current.⁵⁵ An idea similar to this was conceived to be applicable to ferrocene and would be a major part of the process in retrieving lithium once it has been bound. In 1952, when ferrocene was first characterized, Woodward et al. discovered that although the molecule is air-stable, it undergoes oxidations fairly easily under the presence of most mild oxidizing agents.⁵⁶ Upon oxidation, ferrocene loses one electron to form a quite stable cation called ferrocenium. Wanting to avoid adding extra oxidants to the system, it was discovered that ferrocene can also be oxidized to ferrocenium by applying a small voltage (0.4 V vs. SCE). The same can be said about the reduction of ferrocenium.⁵⁶ By applying the same potential in the opposite direction, the system will regain one electron and revert back to

ferrocene which can be reused in an endlessly reversible process. This ferrocene redox process works so efficiently that it is commonly used as a standard for many electrochemical measurements. We plan to use this process as a way to expel the lithium once it's been collected. Lithium can be described as being a hard positive charge, hence why it holds such a strong affinity for common heteroatoms, most commonly oxygen. When ferrocene is oxidized to ferrocenium, the molecule goes from neutral to positively charged. Theoretically, this molecule will want to electrostatically repel other positive charges. We hope this process will eject the positively charged lithium ion out into solution along with its counterion, allowing us to collect it. Outlined below, the proposed mechanism of action for our ferrocene-based ligand involves the introduction of lithium-containing solution to the ligand, lithium binding, oxidation of ferrocene to ferrocenium to repel ions back into solution, lithium collection, and lastly reduction of ferrocenium to recover our original ligand and repeat the process (Scheme 2.7).

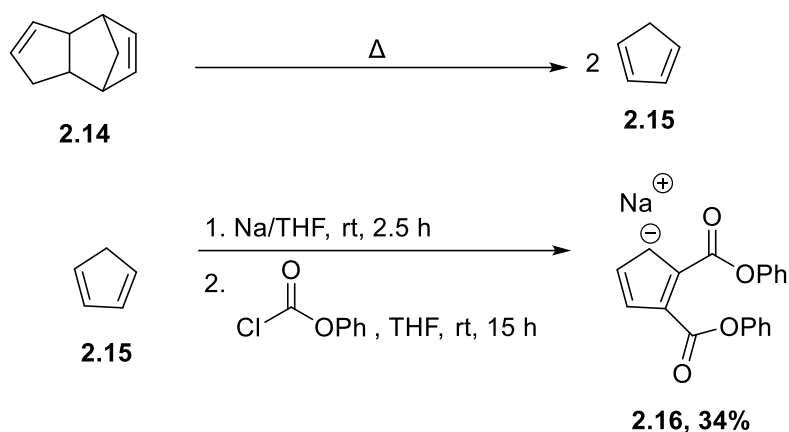


Scheme 2.7: Proposed mechanism of action for ferrocene-based lithium chelator.

2.3 Early Synthesis

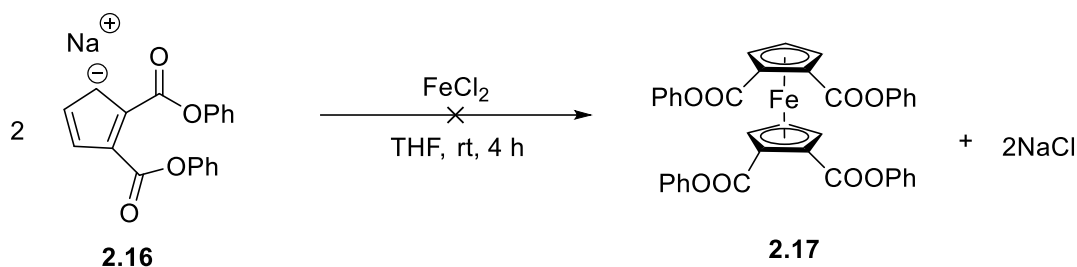
With a design and mechanism of action in mind, we began the early synthesis of

our binding motif. The first step involved the cracking of dicyclopentadiene **2.14** through a retro Diels-Alder reaction to form cyclopentadiene **2.15**. Cp was then deprotonated using sodium wire, occurring readily due to the aromaticity developed when Cp is deprotonated giving the molecule its 6 π electrons. Upon deprotonation, a double nucleophilic acyl substitution occurs using phenyl chloroformate to afford **2.16** in a 34% yield.



Scheme 2.8: Synthesis of molecule **2.16**.⁵⁷

Upon isolation of **2.16** we then attempted to form the ferrocene complex. Multiple attempts were made using various literature procedures, most commonly using FeCl_2 as the iron source. The last attempt on this reaction was the addition of 2 equivalents of **2.16**, along with FeCl_2 in THF at room temperature for 4 h.⁵⁸ TLC results showed that a new product was made which we suspected was our desired compound, however several isolation attempts of **2.17** were unsuccessful and the reaction was put to a halt in favour of other experiments.



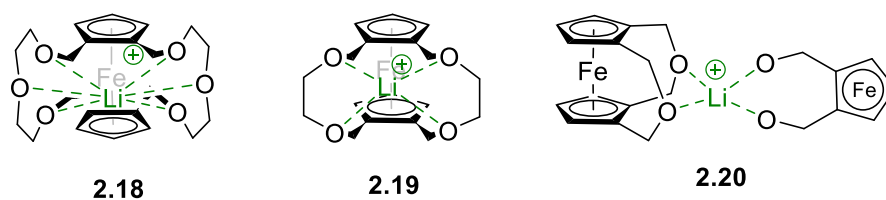
Scheme 2.9: Synthesis of molecule **2.17**.⁵⁸

2.4 Computational Experiments

As shown above in Scheme 2.7, the ferrocene was drawn with two 9-crown-3 bridges as opposed to the original 12-crown-4 bridges in Fig 2.4. Lithium is smaller than sodium so it is reasonable to assume that there is a cavity size that may be small enough to exclude sodium based off size alone. Since there are two crown ethers working together to bind the cation, we skipped 12-crown-4 as it seemed that the vast coordination sites along with the seemingly large cavity size would already make this unlikely to be selective towards lithium. Before physical experimentation was started, it seemed beneficial to gather some computational data on a few of our proposed ligand designs to try and simulate selectivity when exposed to the natural environments we plan to apply this to. Dr. Christian Ieritano from the Hopkins Lab at the University of Waterloo so generously performed a few computational experiments to test lithium vs. sodium selectivity with various proposed ligand designs using seawater as the theoretical lithium source. Seawater, which is widely known to contain copious amounts of sodium, was thought to be a good sample matrix as the Na:Li composition ratio is roughly 60 000:1. If a design proved to be selective towards lithium in these conditions, then it is only reasonable to assume it will perform even better when exposed to richer lithium sources.

Dr. Ieritano performed two different calculations to determine the viability of each of our binding motifs. Firstly, a Gibb's Free Energy (ΔG) value which we associated to as the theoretical binding energy was calculated. Similar to the typical thermodynamic use of Gibb's Free Energy, the more negative a value is, the more favourable that interaction is. The second calculation included a population calculation, which was described by calculating the equilibrium constant using the ΔG values found computationally. The equation $\Delta G = -RT \ln K$ was employed to determine the population (K), with the Na value multiplied by 60 000 due to the naturally occurring ratio of 60 000:1 Na:Li in seawater. These calculated populations were then normalized as a ratio relative to each other and displayed as a percentage to illustrate the amount of lithium or sodium bound from seawater comparatively. Lastly, a difference in the calculated ΔG values between lithium and sodium was calculated and shown, better illustrating the cation preferences for each molecule tested. We first examined the original ferrocene ligand design, molecule **2.18**. This complex proved to have a more negative ΔG when complexed with Na, so naturally once normalized using the concentrations it had a population of 100% Na. We hypothesized that this was due to the six coordination sites this molecule provided, as well as a large cavity size still. Next, molecule **2.19** with smaller crown ether bridges containing 2 oxygens in each. The decision behind this was the increasingly smaller cavity size, as well as the first introduction of the desired amount of coordination sites for Li.⁵⁹ This new design actually had a lower ΔG value for coordination with Li, however the difference between the ΔG value for Na was only about 5 kJ/mol, providing too small of a difference when normalized with the exceedingly high amounts of sodium giving a population of 100% Na. Even though Li ideally desires four coordination sites, Warnock

et al. did confirm that Na still has the ability to bind to four sites, especially if the cavity size is big enough to accommodate it.⁴⁷ We hypothesized this is why the binding energy doesn't greatly favour lithium, and designed another calculation in which there were bridges with only one oxygen in each, similar to compound **2.4** synthesized by Petter et al. We received promising results upon orientation of two of these molecules perpendicular to each other as shown in **2.20** to provide a tighter cavity size as well as ideal coordination sites. This orientation provided a ΔG value that favoured Li by 31 kJ/mol over Na, which was enough of a difference to overcome the massive concentration difference and afford a population of 82% Li.



		Li	Na
2.18	ΔG (kJ/mol)	-109.16	-131.09
	Population (%)	0	100
2.19	ΔG (kJ/mol)	-93.14	-88.3
	Population (%)	0	100
2.20	ΔG (kJ/mol)	-68.42	-37.37
	Population (%)	82.1	17.9

Table 2.1: Computationally calculated binding energies and populations for molecules **2.18**, **2.19**, and **2.20**.

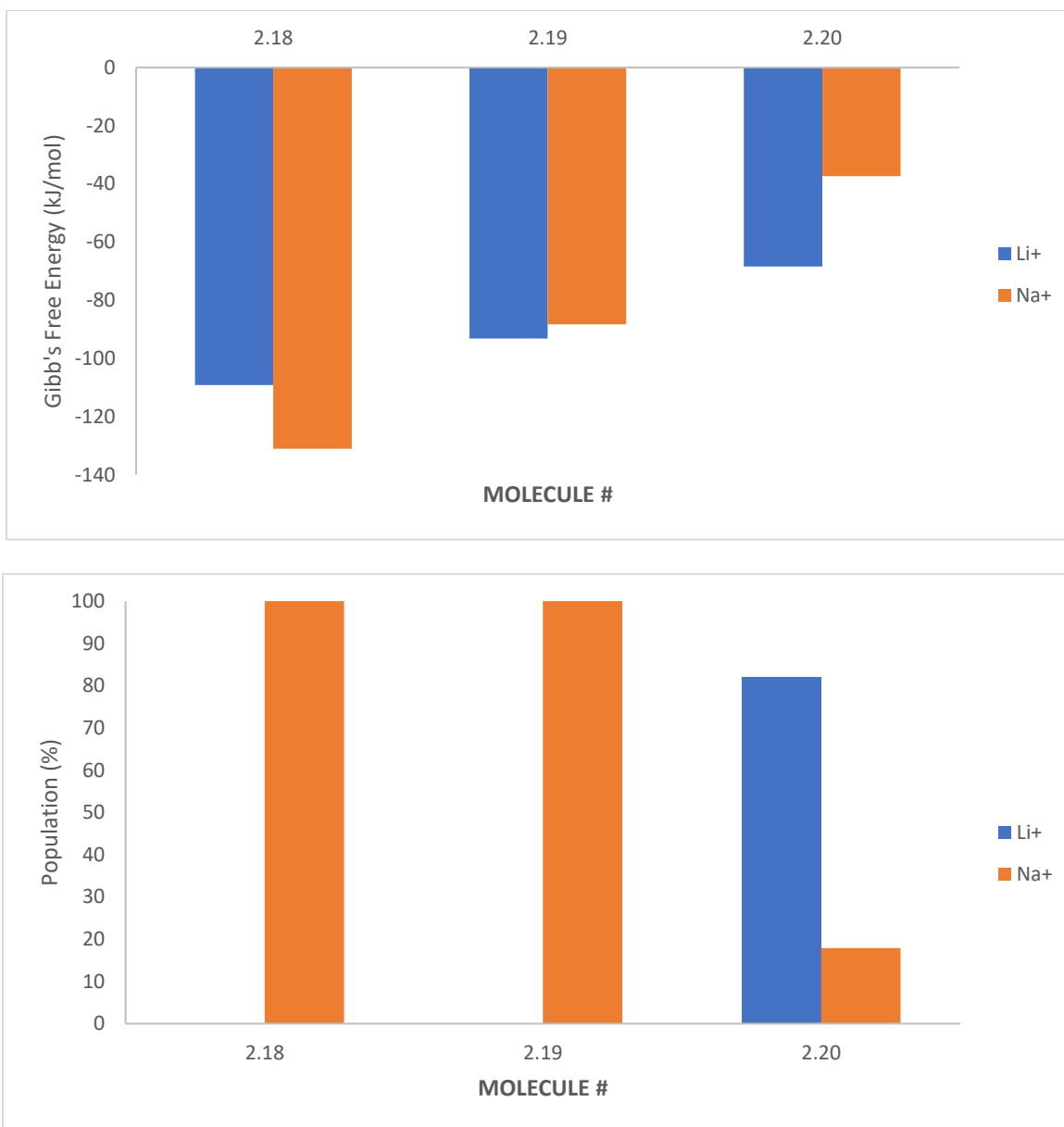


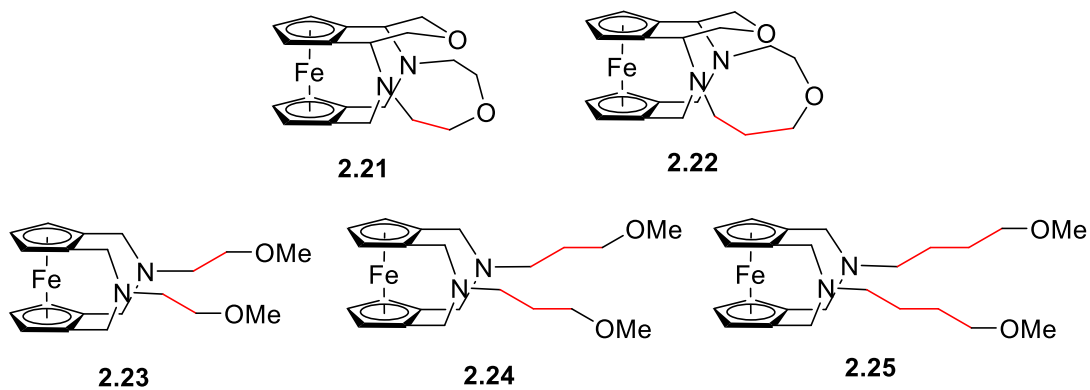
Figure 2.5: a) ΔG values for complexation of Li & Na with **2.18, 2.19, and 2.20**, b) adjusted binding populations for complexation of Li & Na with **2.18, 2.19, and 2.20**.

Although this binding motif would be entropically unfeasible requiring two molecules to come together and orient themselves this way in solution, it did provide some valuable insight onto the binding geometry that might be needed. This alignment

provided a tight tetrahedral geometry around the Li atom that may be a necessary incorporation into the design. With this insight, we began thinking about ferrocene motif designs with four coordination sites that could force a tetrahedral geometry around the binding cation. To test this hypothesis, we first started designing cage-like molecules that were exaggerated and impossible to synthesize to confirm our suspicions. These designs include amine bridges with only one amine in each instead of oxygen bridges. This allows another bond to come off the nitrogen to form an ether bridge connecting it with the other amine. We tested two very similar molecules **2.21** and **2.22**, both differing from only one carbon in the amine-amine bridge. Upon these same calculations, we were able to confirm two of our previous hypotheses. The first being the incorporation of a tetrahedral geometry being of utmost importance, and the second being the ability to exclude sodium based on cavity size alone. Molecule **2.21** had an extremely negative ΔG when complexed with Li and it actually had a positive ΔG when complexed with Na. Due to the extremely large $\Delta\Delta G$ of 105.28 kJ/mol in favour of Li shown below, the translation to populations it afforded a population of 100% Li. Molecule **2.22** which contained an extra carbon in one of its bridges making the cavity one atom larger, had a slightly less negative ΔG when complexed with Li, and a slightly less positive ΔG when complexed with Na. Again, the $\Delta\Delta G$ was -37 kJ/mol in favour of Li, so when translated to populations, the normalized population was 97% Li. This 3% change can likely be attributed to the slight increase in cavity size.

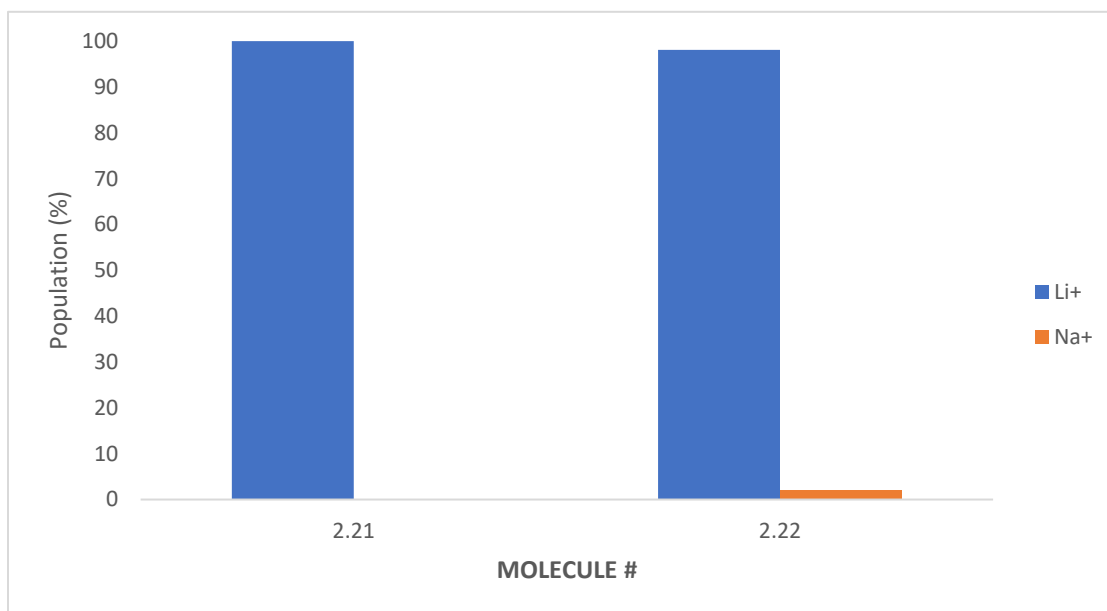
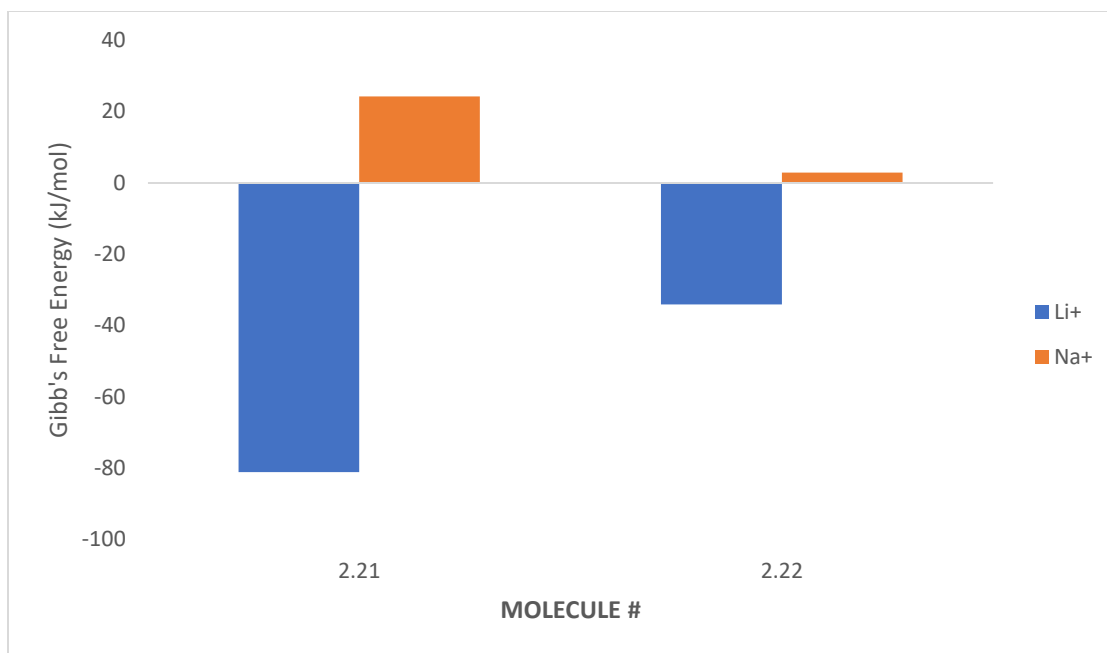
With this knowledge, we pivoted to a design that could be synthetically possible. Amine bridges with flexible methoxy arms instead of a rigid cage structure could allow for tetrahedral coordination as well. Calculations for this design were made with varying

carbon lengths in the methoxy arms ranging from two to four carbons. Most important to note from these calculations was the difference in values between the different alkyl chain lengths. The 2-carbon chain **2.23** had a very negative ΔG for both Li and Na, coming out to -110.6 kJ/mol and -81.75 kJ/mol respectively. This afforded a $\Delta\Delta G$ of 28.85 kJ/mol favouring Li which was large enough to achieve a majority Li population of about 65%. The 3-carbon chain **2.24** also had a very negative ΔG for both metals, that being -115.43 kJ/mol for Li, and -84.56 kJ/mol for Na. This slight 2 kJ/mol favourable change in $\Delta\Delta G$ between **2.24** and **2.23** gave a slightly larger Li population of about 81%. Moving onto the 4-carbon chain **2.25**, the ΔG values dropped significantly for both metals, being -71.86 kJ/mol for Li and -64.24 kJ/mol for Na. This small favourable $\Delta\Delta G$ difference of 7.62 kJ/mol for Li wasn't enough to overcome the concentration difference so this translated to a population of virtually 100% Na. Most interestingly from these results, we see that the 3-carbon chain **2.24** gave the greatest $\Delta\Delta G$ difference in favour of Li, as well as the most favourable population. This can be attributed to the balance of both having the proper tetrahedral geometry as well as the correct cavity size. Although uninvestigated, it can probably be assumed that **2.24** gives a more accurate tetrahedral geometry than **2.23**, while also having a smaller cavity than **2.25** to allow less Na to complex.



		Li	Na
2.21	ΔG (kJ/mol)	-81.04	24.24
	Population (%)	100	0
2.22	ΔG (kJ/mol)	-34.06	2.94
	Population (%)	98.06	1.94
2.23	ΔG (kJ/mol)	-110.6	-81.75
	Population (%)	65.37	34.63
2.24	ΔG (kJ/mol)	-115.43	-84.56
	Population (%)	81.01	18.99
2.25	ΔG (kJ/mol)	-71.86	-64.24
	Population (%)	0.04	99.96

Table 2.2: Computationally calculated binding energies and populations for molecules **2.21**, **2.22**, **2.23**, **2.24**, and **2.25**.



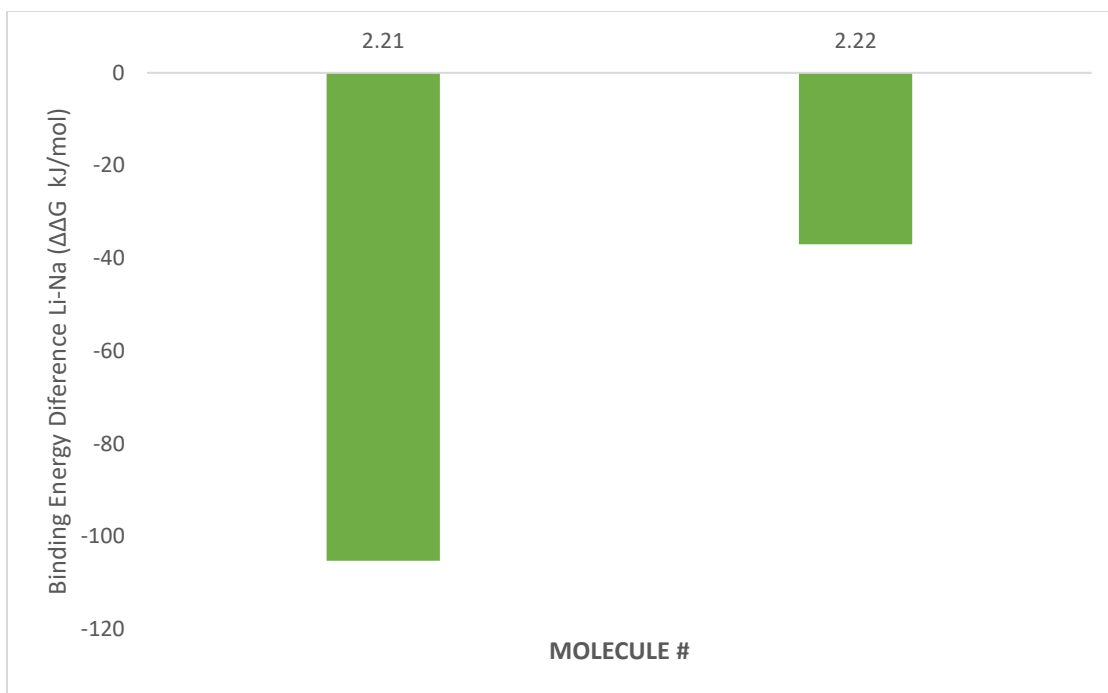
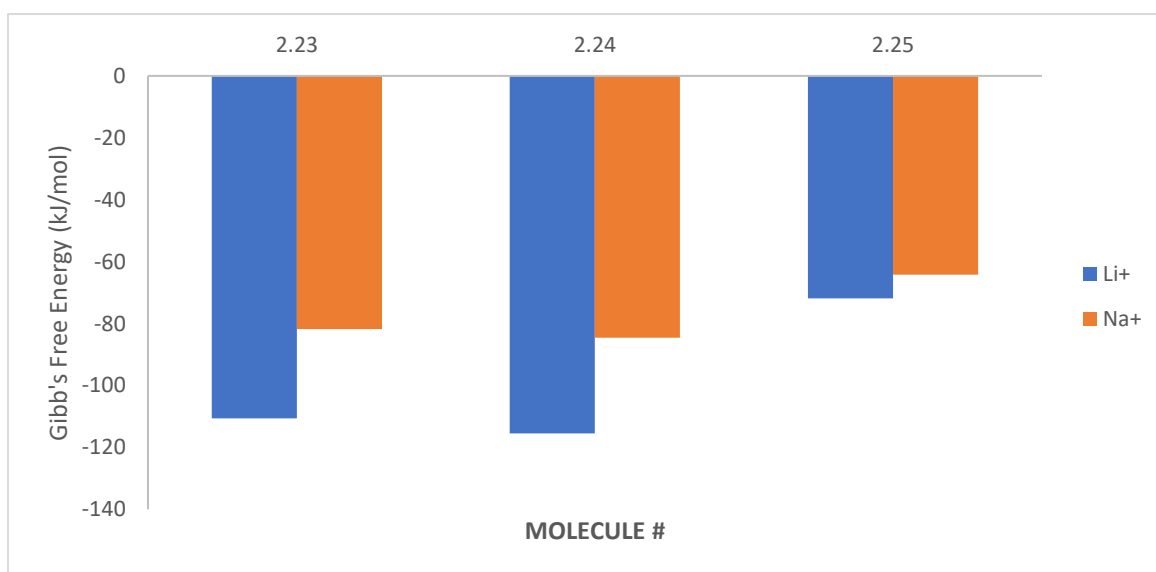


Figure 2.6: a) ΔG values for complexation of Li & Na with **2.21** and **2.22**, b) adjusted binding populations for complexation of Li & Na with **2.21** and **2.22**, c) $\Delta\Delta G$ values for Li-Na for **2.21** and **2.22**.



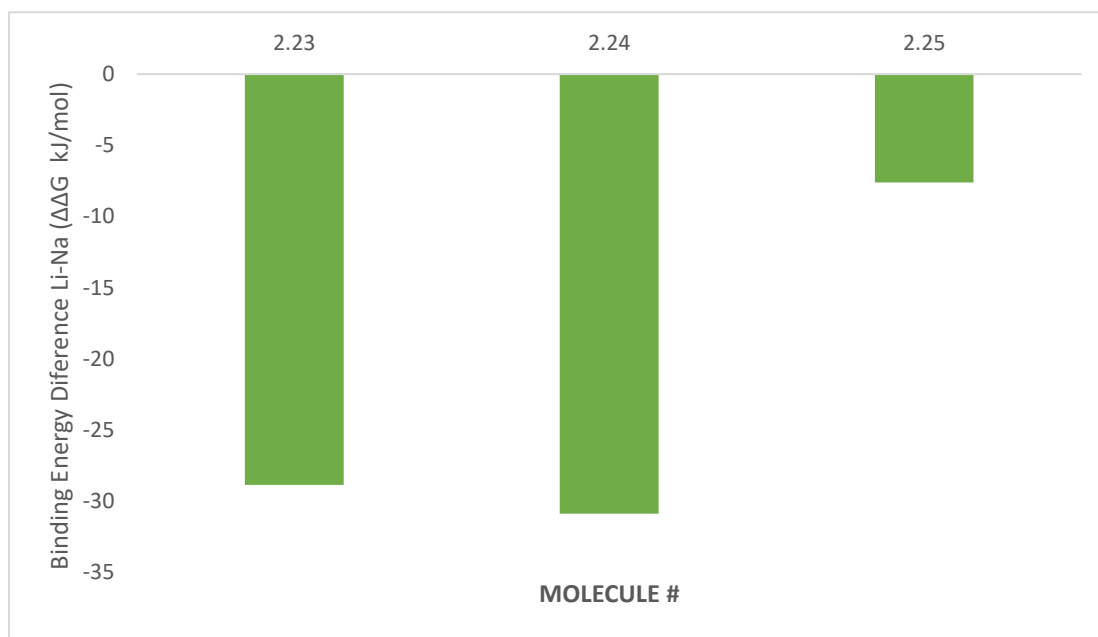
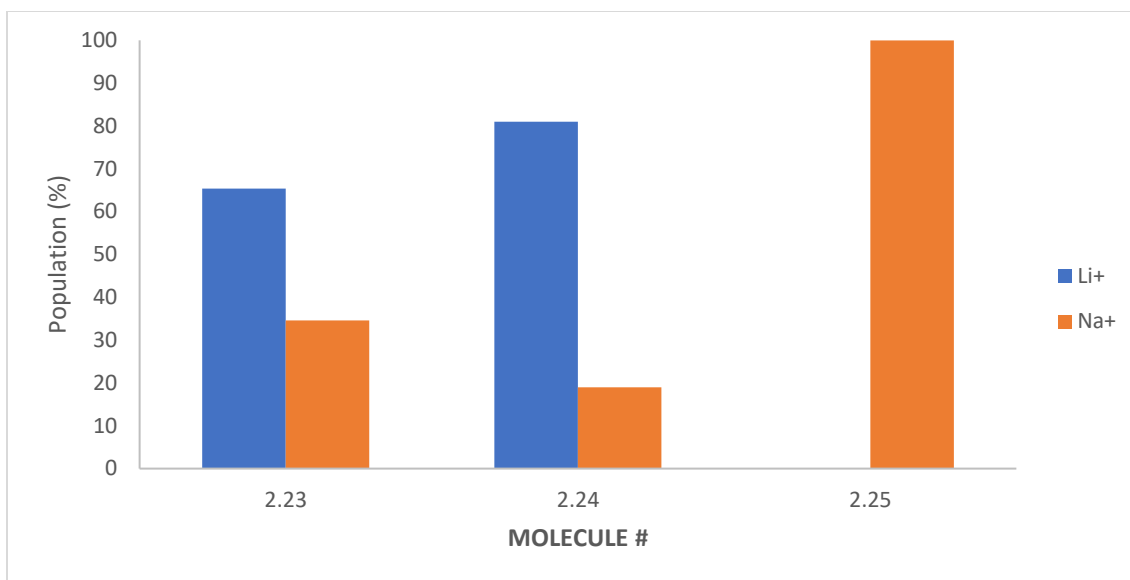
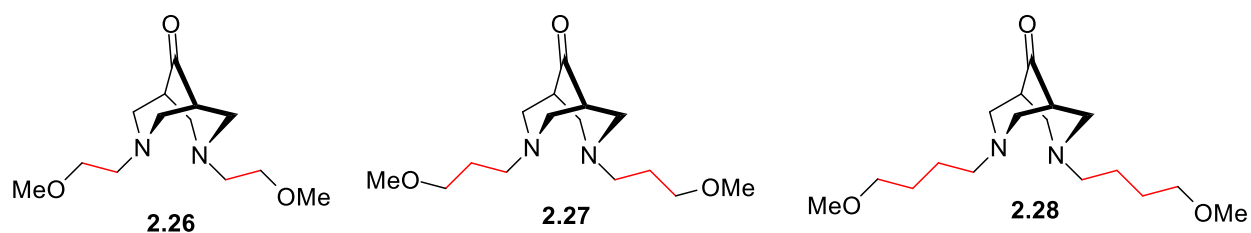


Figure 2.7: a) ΔG values for complexation of Li & Na with **2.23**, **2.24**, and **2.25**, b) adjusted binding populations for complexation of Li & Na with **2.23**, **2.24**, and **2.25**, c) $\Delta\Delta G$ values for Li-Na for **2.23**, **2.24** and **2.25**.

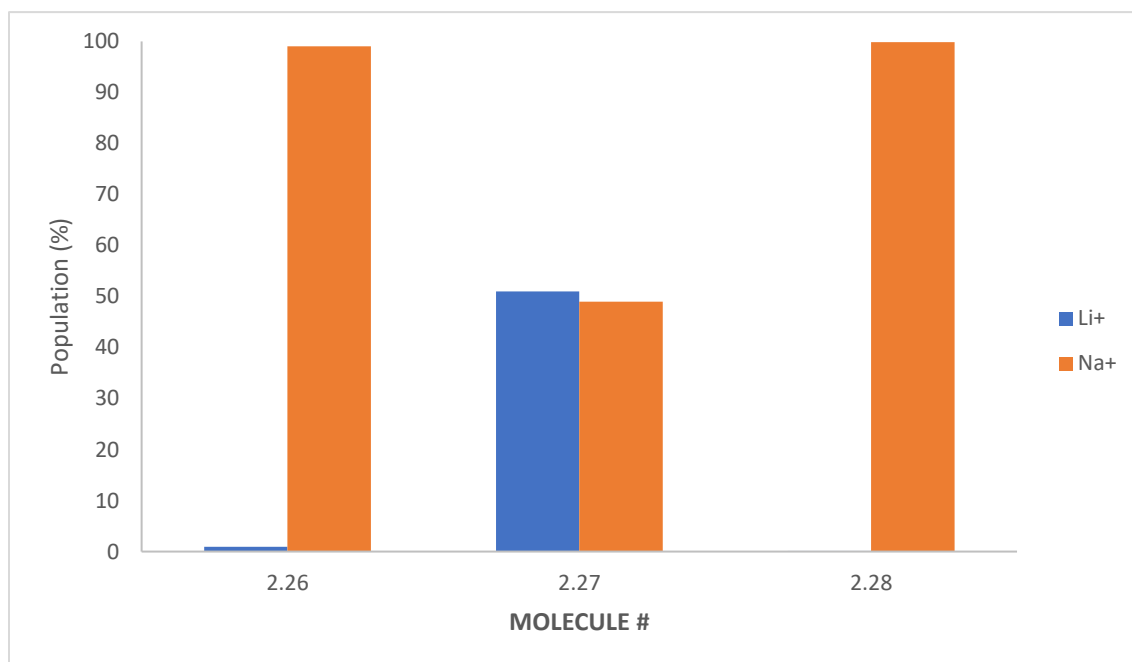
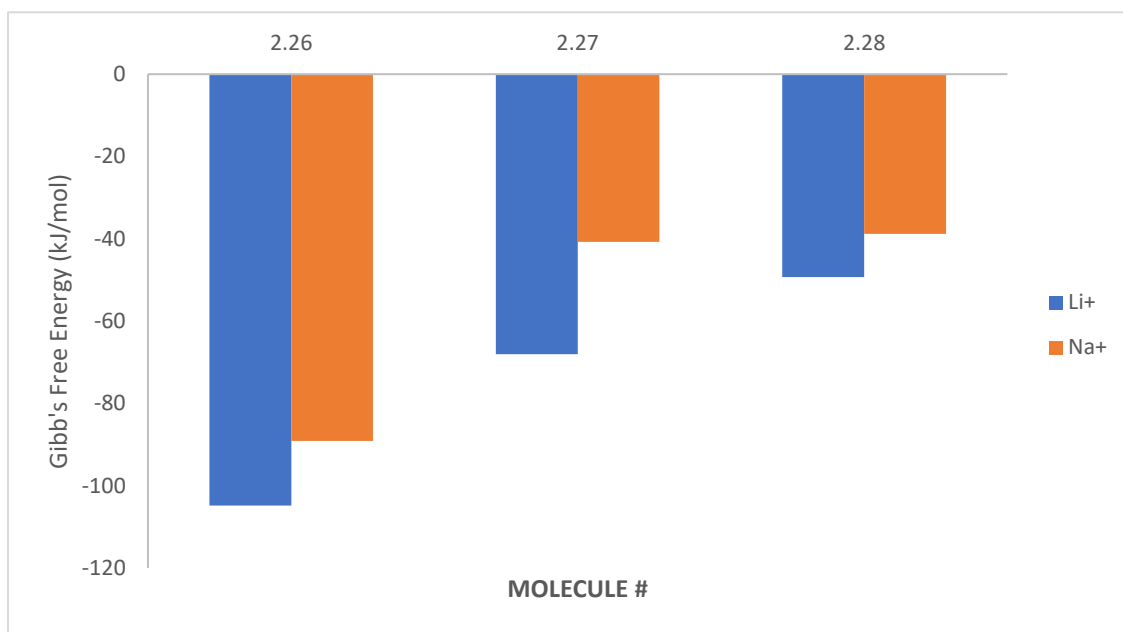
Reflecting on earlier synthetic attempts to synthesize the original crown ether design, we began modelling molecules that contained a tertiary amine with a 3-carbon

alkyl chain, without the ferrocene background. Although the redox molecular switch seemed enticing, synthetic achievability is also important if this is needed to be scaled up. There are more traditional decomplexation techniques such as simple acid-base chemistry that we can employ to try and decomplex Li. With this, we explored another class of molecules known as bispidinones, which we predict might be equipped with all the necessary properties we need to be Li-selective. The same computational calculations were performed on bispidinones with varying alkyl chain lengths, again from 2-4 carbons long with methoxy groups on the end. Very similar results were seen when compared to compounds **2.23-2.25** where the 3-carbon alkyl chain **2.27** provided the greatest favourable $\Delta\Delta G$ of 27.28 kJ/mol towards Li. A similar value, although not as great, of 15.74 kJ/mol was seen for the 2-carbon chain **2.26**, while the 4-carbon chain **2.28** provided the smallest $\Delta\Delta G$ value. The same trend was observed upon translation to populations, with the order of Li favourability being **2.27** > **2.26** > **2.28**.



		Li	Na
2.26	ΔG (kJ/mol)	-104.82	-89.08
	Population (%)	0.95	99.05
2.27	ΔG (kJ/mol)	-68.05	-40.77
	Population (%)	51	49
2.28	ΔG (kJ/mol)	-49.3	-38.78
	Population (%)	0.12	99.88

Table 2.3: Computationally calculated binding energies and populations for molecules **2.26**, **2.27**, and **2.28**.



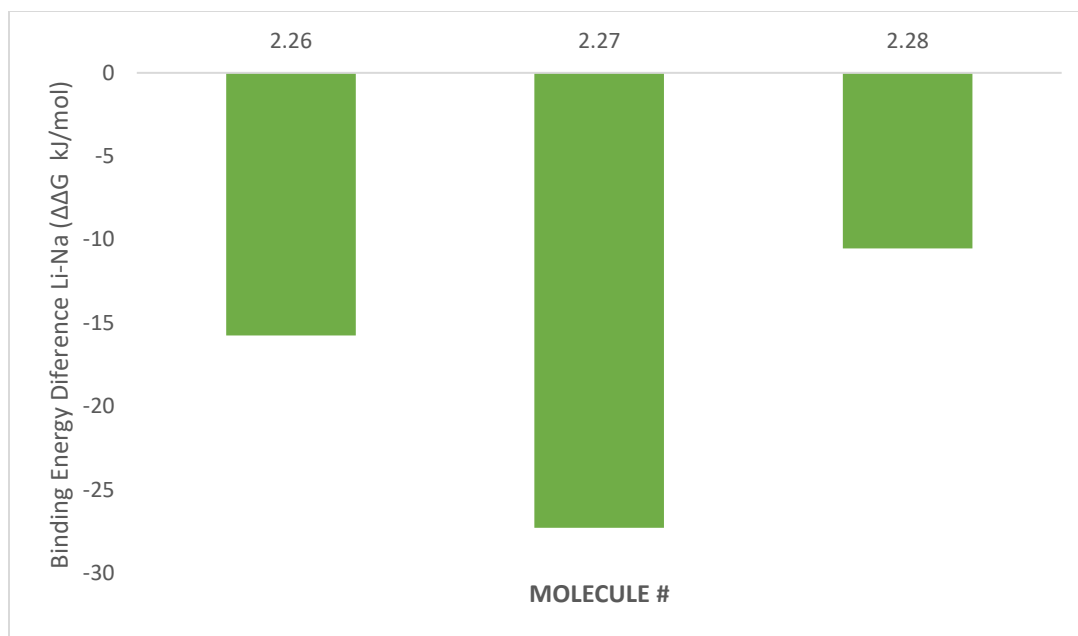


Figure 2.8: a) ΔG values for complexation of Li & Na with **2.26**, **2.27**, and **2.28**, b) adjusted binding populations for complexation of Li & Na with **2.26**, **2.27**, and **2.28**, c) $\Delta\Delta G$ values for Li-Na for **2.26**, **2.27** and **2.28**.

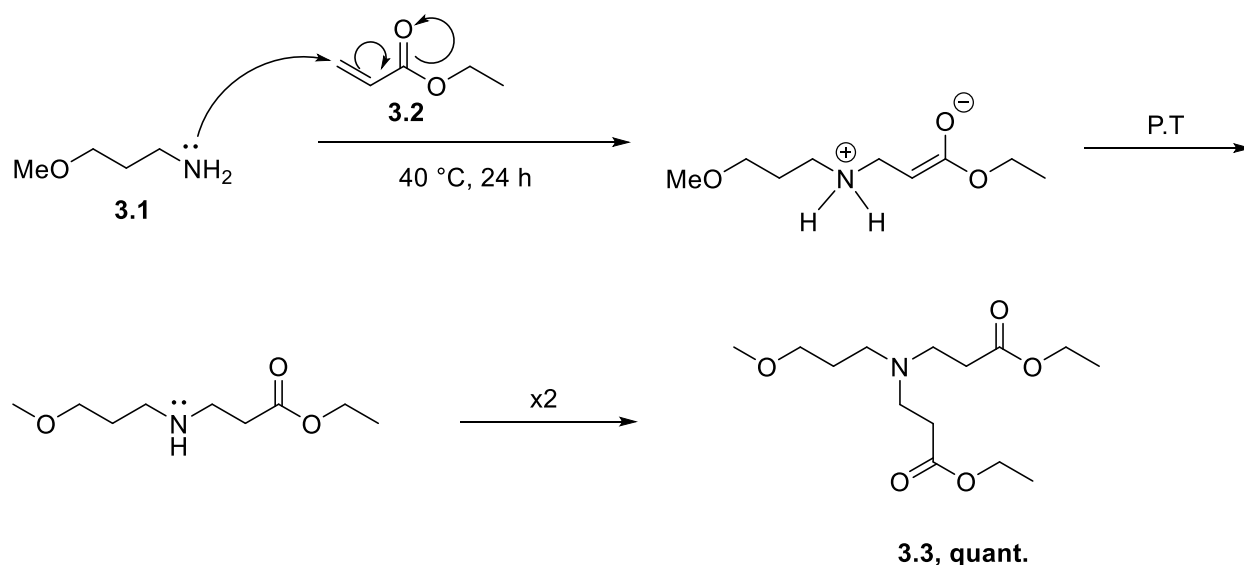
2.5 Concluding Remarks

Our motif, **2.27**, offers three attractive features, the first being the unused ketone on the other end of the molecule. This functional group will not participate in the binding of Li and could be used as a synthetic handle for further functionalization in more applications later on. The second and third important features were mentioned earlier, these being the use of amines to allow three bonds while still including a lone pair for binding, and the use of flexible arms to allow for the optimal tetrahedral coordination. Due to these features as well as its synthetic feasibility, this new class of molecules intrigued us and **2.27** is the primary molecule we chose to synthesize and study for this project.

Chapter 3: Synthesis and Study

3.1 Ligand Synthesis

After conclusion of our ligand design, it became time to begin the second attempt at synthesis. The first step involved a double conjugate addition using 3-methoxypropylamine **3.1** as the nucleophile and ethyl acrylate **3.2** as the electrophile. Nucleophilic addition of the neutral amine eventually performs 1,4-addition instead of the reversible 1,2-addition on the α,β -unsaturated carbonyl. 2.6 equivalents of ethyl acrylate were used for the reaction as a slight excess. This reaction was performed in MeOH and heated gently to 40 °C while stirring for 24 h to afford **3.3** in a quantitative yield.⁶⁰

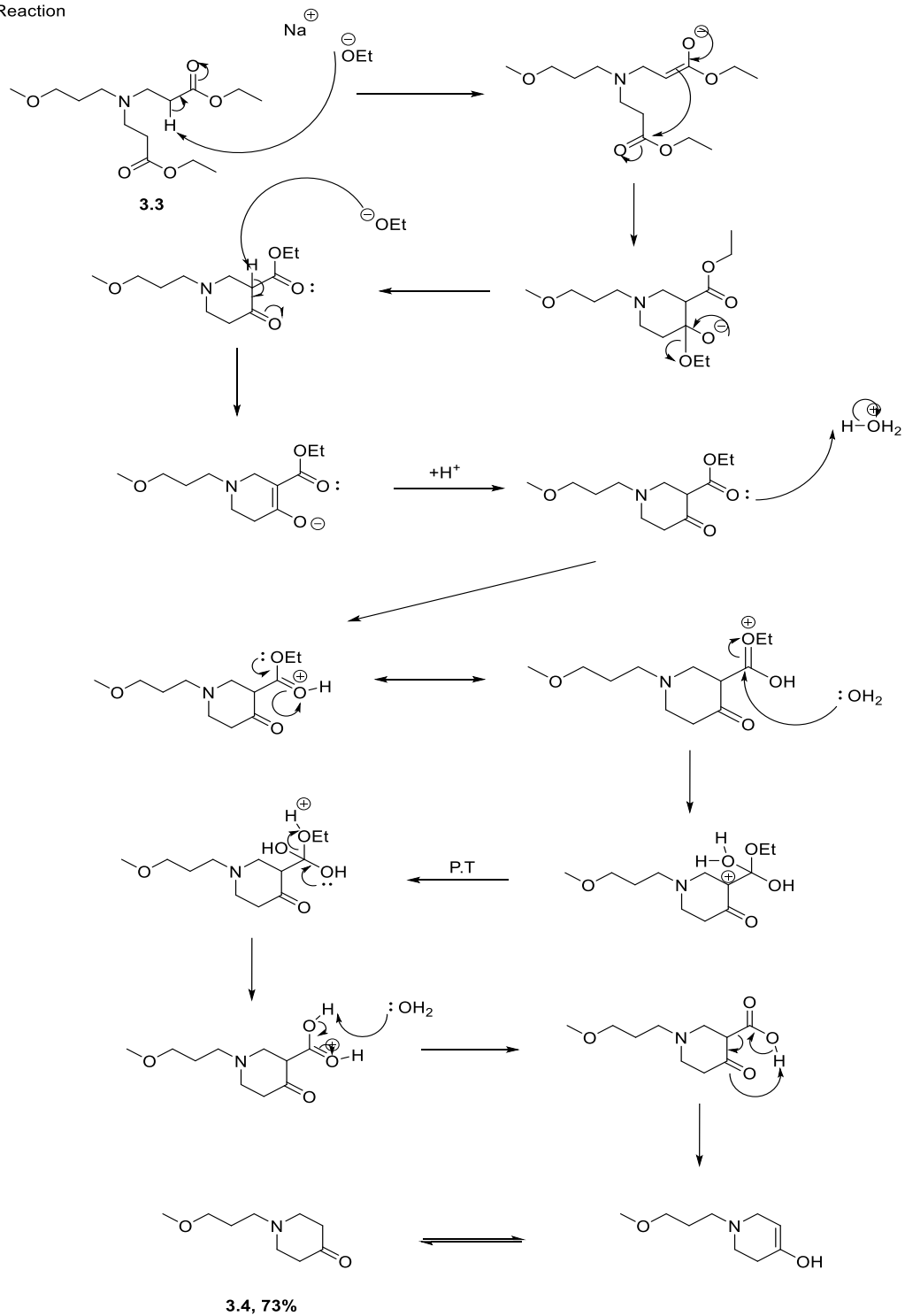


Scheme 3.1: Double conjugate addition reaction mechanism to form **3.3**.⁶⁰

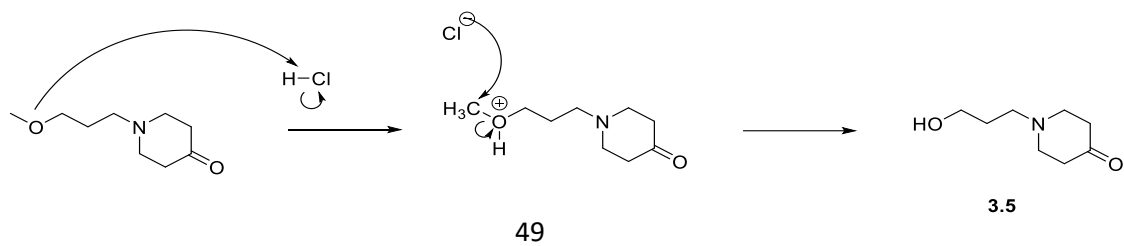
Next, a Dieckmann intramolecular condensation was performed to cyclize **3.3**, followed by a decarboxylation to form piperidinone **3.4**. To form the base needed to

deprotonate the α -carbon, NaOEt was generated by reacting EtOH and an excess of NaH (60% dispersed in mineral oil) in toluene. When H₂ evolution ceased, the mixture was refluxed to ensure complete conversion. Compound **3.3** was then added to the refluxing solution and allowed to reflux for 4 h to complete the cyclization. Upon cyclization, the compound was extracted with 6 M HCl and the aqueous layer was refluxed overnight to afford the decarboxylated product **3.4** in a 73% yield. TLC showed one side product higher in polarity relative to the desired product. Upon NMR analysis it was determined that this was the alcohol product produced after an S_N2 reaction with HCl to cleave the methyl ether and form **3.5**.⁶¹ This yield was considered sufficient to move on to the next step, so no further optimization was completed.

a) Main Reaction

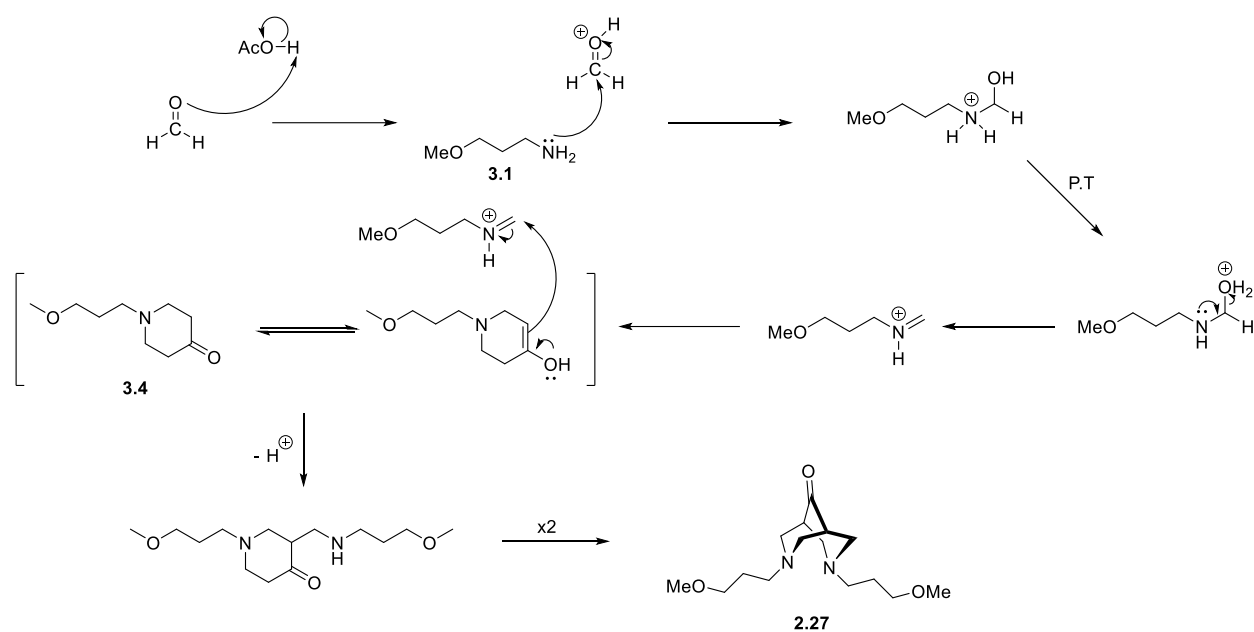


b) Side Reaction



Scheme 3.2: a) Dieckmann condensation/decarboxylation mechanism to form **3.4**; b) Side methyl ether cleavage mechanism to form **3.5**.⁶¹

The last step in the synthesis was the formation of desired molecule **2.27**. This was to be done by a Mannich reaction, involving the original 3-methoxypropylamine **3.1** reacting with paraformaldehyde under acidic conditions (AcOH) to form an iminium intermediate. Enolization of piperidinone **3.4** creates a nucleophile which will allow the α -carbon to attack the electrophilic iminium structure, forming a new C-C bond with an amine arm attached. This same process is done one more time with a second equivalent of paraformaldehyde to form another iminium intermediate. This time, the other α -carbon is used to form the enol, which then comes in to attack the iminium again, forming another C-C bond and cyclizing the molecule to form bispidinone **2.27**. This reaction is heated gently to 60 °C and typically takes around 24 h to complete, however each run is monitored by TLC. This reaction gave moderate yields, the highest being 42%, with material loss likely attributed to the purification.⁶¹ Another characteristic of this reaction was the drastic colour change, with **3.4** being clear/pale yellow and **2.27** being wine red. TLC shows no other products except for excess 3-methoxypropylamine. Purification by flash chromatography was spotty, with reproducibility serving to be quite an issue. The elution only worked when 90% DCM/9% MeOH/1% NH₄OH was used as the mobile phase. With all other mobile phases, including the use of different bases like triethylamine, co-elution was observed. Settling on these conditions proved lengthy, but once discovered the reproducibility increased. With material collection being the main focus of this synthesis, not much optimization was done for this reaction, and it stands to reason the yield could improve significantly upon optimization of purification.

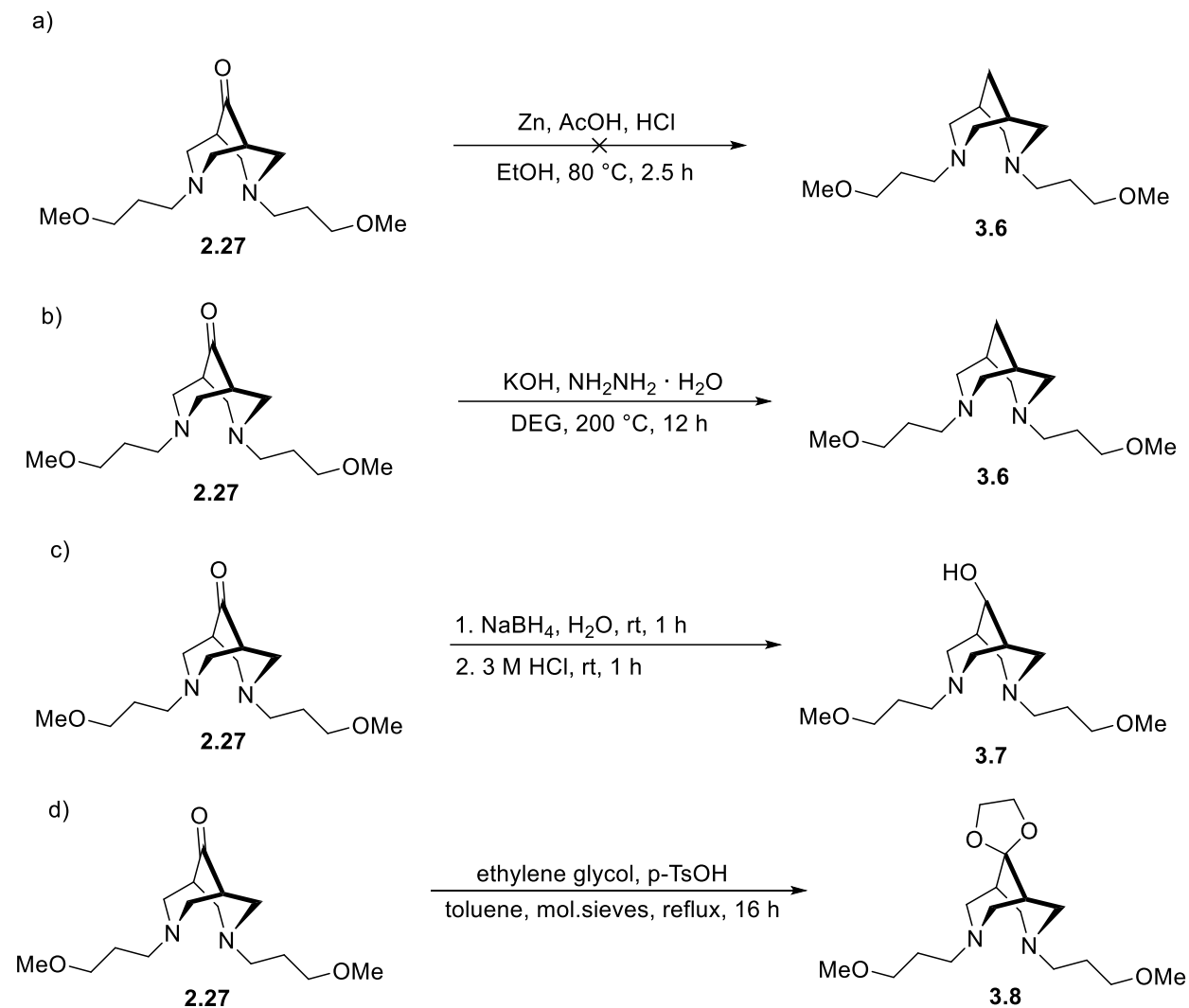


Scheme 3.3: Mannich reaction mechanism to form bispidinone **2.27**.⁶¹

3.1.1 Manipulations of Carbonyl

Although our proposed ligand was now synthesized, there were also a few derivatives similar to it that were interesting. Diving into reasons later, we wanted to try modifying the ketone by either protecting it with a cyclic acetal or by reducing it to either the alcohol or methylene derivative. Early attempts were made at the decarbonylation, either through a Wolff-Kishner reduction or a Clemmensen reduction. First the Clemmensen was attempted using zinc powder and HCl, stirring at room temp for a couple hours.⁶² No product **3.6** ever appeared by TLC and after work-up, only starting material was recovered (Scheme 3.4a). Next, the Wolff-Kishner reduction was attempted, first using hydrazine monohydrate and KOH and KOAc in diethylene glycol.⁶³ This reaction was refluxed in a pressure vial overnight, and after 12 hours all starting material was consumed and a new spot appeared on TLC. NMR of the crude reaction mixture

showed a new methylene peak with the correct integration, however purification became a common issue with this reaction and the product **3.6** was unable to be isolated. Four more attempts were made at this reaction, slightly altering conditions or reagents, all providing similar outcomes with isolation difficulty (Scheme 3.4b). The next alteration to **2.27** is the reduction to the alcohol, however we originally wanted to avoid this due to the asymmetry it imposed on the molecule, a feature thought to be important later on. This reduction was attempted multiple times using NaBH₄ in an H₂O/EtOH solvent mixture. Upon work-up, all starting material had been consumed by TLC, and an NMR of the crude reaction mixture showed a new peak integrating to one proton. Purification of **3.7** was achieved through flash chromatography, however a few small impurities still remained by NMR so a yield wasn't calculated (Scheme 3.4c).⁶³ Unfortunately, the asymmetry imposed by the new alcohol made the NMR slightly harder to follow so we didn't move forward with this compound in our future tests. The next manipulation was a simple acetal protection of the carbonyl using ethylene glycol and p-TsOH. Since the reaction scale was so small, a Dean Stark trap was not used to remove the water by-product and drive equilibrium. Instead, molecular sieves were added to the reaction mixture to trap the water as it was produced. This reaction was stirred overnight and all starting material was consumed according to TLC. Crude NMR showed one new downfield singlet that integrated to four protons indicating that the reaction was successful (Scheme 3.4d).⁶⁴ The purification of **3.8** was never attempted, and the manipulations of the original carbonyl group were put to rest.



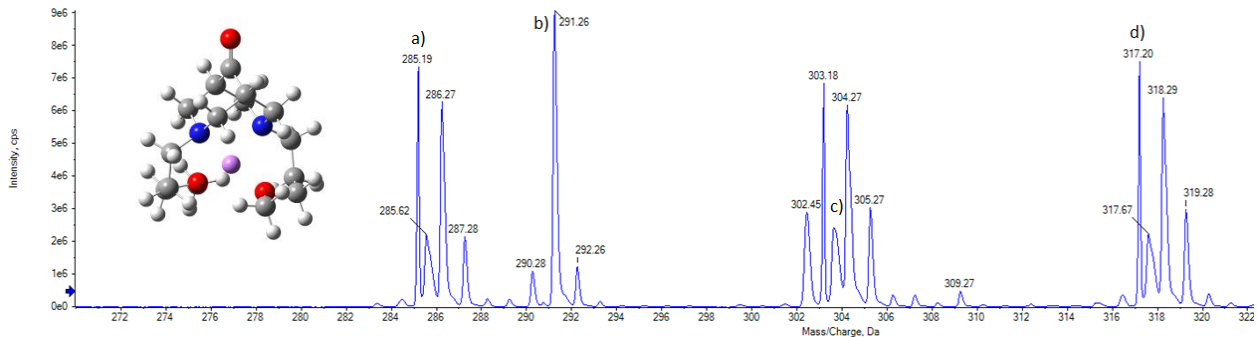
Scheme 3.4: a) Clemmensen reduction attempt conditions; b) Wolff-Kishner reduction attempt conditions; c) Sodium borohydride reduction attempt conditions; d) Cyclic acetal protection attempt conditions.^{62–64}

3.2 Preliminary Binding Characterization

3.2.1 Mass Spectrometry

After completion of the ligand synthesis, the first step in characterizing the binding was to simply determine if there was any evidence of lithium binding at all. To do

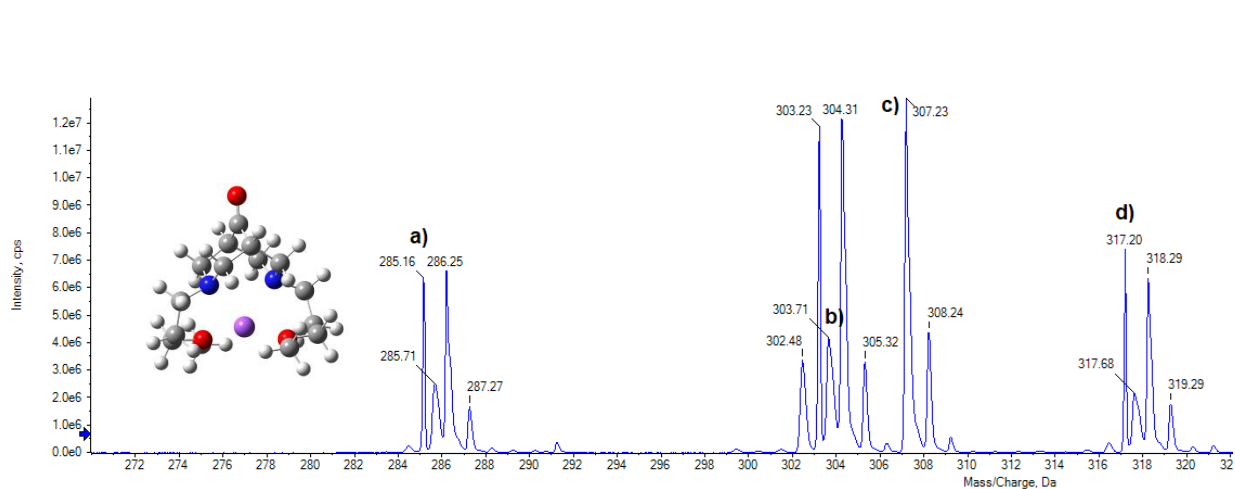
this, mass spectrometry was performed with our ligand in solution with a Li salt such as lithium acetate. The goal of this experiment was to retrieve an $[M + Li]^+$ peak at an m/z of around 291. Observation of this peak would show enough preliminary evidence that our ligand binds Li, allowing us to move forward with more binding studies. Since our primary focus is the selectivity of Li over other 1st group cations, the same experiment was performed using sodium acetate to confirm potential Na binding as well. There were a few notable peaks in both experiments summarized below, showing evidence of both Li and Na binding, unsurprisingly given the computational results described in Fig 2.8. Both experiments also showed evidence of an $[M + H_2O]^+$ peak, and an $[M + MeOH]^+$, which again was unsurprising for reasons suggested later. The carbonyl in our ligand is susceptible to attack in aqueous conditions so these peaks can be ascribed to the hydrate formed from attack by water, and the hemiacetal formed when attacked by MeOH. Nonetheless, these preliminary mass spec experiments provided us with enough reassurance to continue forward with the characterization of the binding.



Peak Label	Peak	Value (m/z)
a)	$[M+H]^+$	285.16

b)	$[M+Li]^+$	291.26
c)	$[M+H_2O]^+$	303.71
d)	$[M+MeOH]^+$	317.20

Figure 3.1; Table 3.1: Mass spectrum produced in MeOH/H₂O/FA solution when introduced with lithium acetate; Summary of important values and their peak assignments.



Peak Label	Peak	Value (m/z)
a)	$[M+H]^+$	285.16
b)	$[M+H_2O]^+$	303.71
c)	$[M+Na]^+$	307.23
d)	$[M+MeOH]^+$	317.20

Figure 3.2; Table 3.2: Mass spectrum produced in MeOH/H₂O/FA solution when introduced with sodium acetate; Summary of important values and their peak assignment.

3.2.2 NMR Experiments

After binding was confirmed by mass spectrometry, we attempted further characterization of the binding interaction and selectivity. To do this, we did an experiment similar to an NMR titration. Known amounts of ligand were measured out, and the idea was that the bound complex should theoretically be in a different chemical environment. With a new chemical environment comes new potential chemical shifts and splitting, hopefully allowing us to pick a characteristic, distinct peak that was attributed to the bound complex. With different concentrations of Li introduced to the molecule, we hypothesized that we would see a gradual disappearance in the unbound NMR peak, and a gradual appearance in the new bound peak. Using the known concentrations, we planned to use the relative integrations between the unbound and bound peaks to try and pull out some physical characteristics. To test if this experiment was feasible, we decided to take an NMR of our unbound ligand in D₂O, as well as one with our ligand in the presence of a fully saturated solution of LiCl in D₂O in hopes of seeing a new, identifiable peak to attribute to our bound ligand. Unfortunately, the fully saturated NMR did not inform us of much at first glance, however upon further analysis of the spectrum, it appears to be a duplicate of the original spectrum with most peaks being double. This informed us of potential reactivity issues of the ketone in our molecule when in water. The mass spectra shown earlier in Fig 3.1/3.2 show ligand + H₂O and ligand + MeOH adducts. These occur upon attack of the ketone from either H₂O or MeOH to form the hydrate or hemiacetal

respectively.

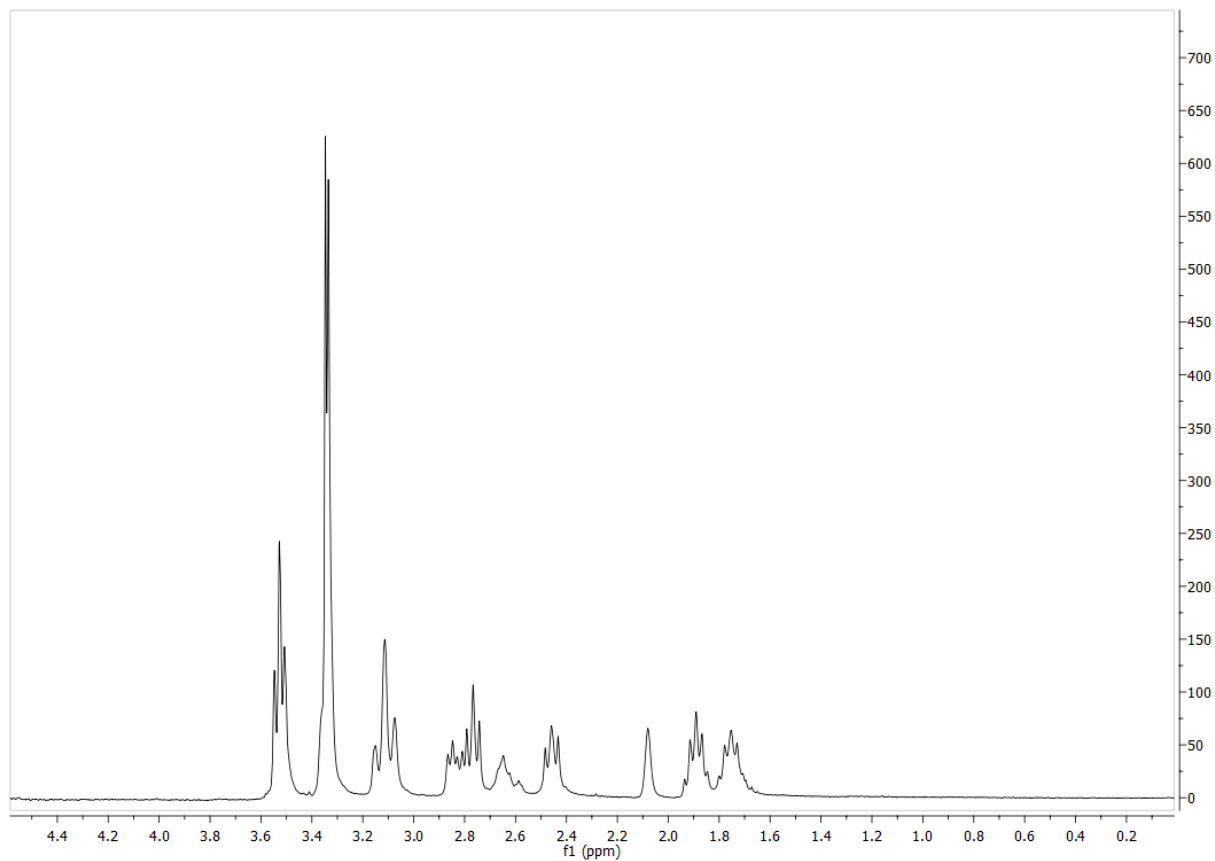
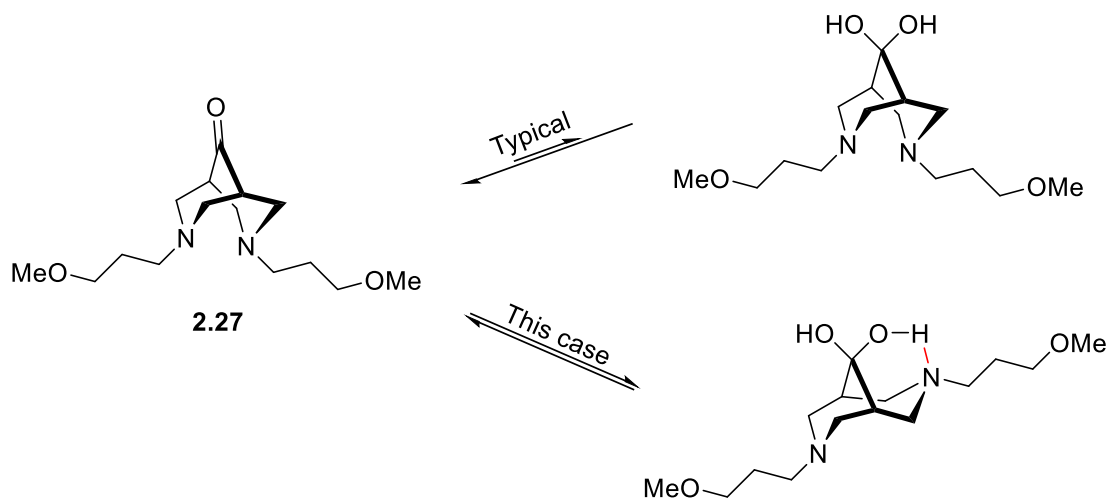


Figure 3.3: ¹H NMR spectrum of **2.27** in D₂O illustrating the equilibrium between diol and ketone forms; see Fig. S3-5 for comparison to original ligand in CDCl₃.

In aqueous environments, the ketone in our ligand tends to hydrate and be in equilibrium with the diol form of our ligand. However, whenever this duplication effect is seen in other NMR spectra with the same phenomenon, the duplicate peaks are not usually of similar intensity. It is commonly known in carbonyl equilibrium that the equilibrium heavily favours the carbonyl intermediate versus the hydrated product. With this rationale, the peak ratios between these two products should be very different, with the peaks assigned to the carbonyl product being much larger in comparison to the

hydrated product's peaks. We see however, that the duplicate peaks are almost identical in peak area to each other, contradicting the previous statement. An explanation for this may be due to a new bonding interaction with the alcohols in the hydrated product. Pyramidal inversion of amines is a swift process in which the amine nitrogen inverts by passing through a planar transition state. In this case, either amine can invert from the chair conformation to a boat-like conformation, with incentive to do so now due to the new alcohol formed. The proton in the alcohol is a suitable hydrogen bond donor, so upon nitrogen inversion the lone pair in the amine is able to hydrogen bond. This H-bonding creates a more stable intermediate than normal, making the species slightly longer lasting. The strained nature of the carbonyl also makes it more prone to hydration. Both reasons help even out the equilibrium between these two intermediates and explains why the peak sizes are the same when averaged in an NMR experiment (Scheme 3.5).



Scheme 3.5: Typical equilibrium for hydration of ketone vs. H-bonding incentivized equilibrium observed.

With this new discovery, we determined that NMR studies done in D₂O would not

be feasible with this ketone functional group. With plans of altering this functionality, we tried several different manipulations outlined in Section 3.1.1. All were relatively unsuccessful, except for the reduction to the alcohol shown in Scheme 3.4c. The small amount of pure compound we were able to isolate allowed us to try a sequential NMR titration using a basic Li salt to try and push the equilibrium to one side, potentially eliminating the duplicate effect. This did help eliminate some duplication making the NMR spectrum easier to interpret, however upon sequential additions of LiOH we did not notice any disappearance/reappearance of peaks like we had hoped. Instead, all peaks had just shifted slightly upfield with increasing concentration (Fig 3.4).

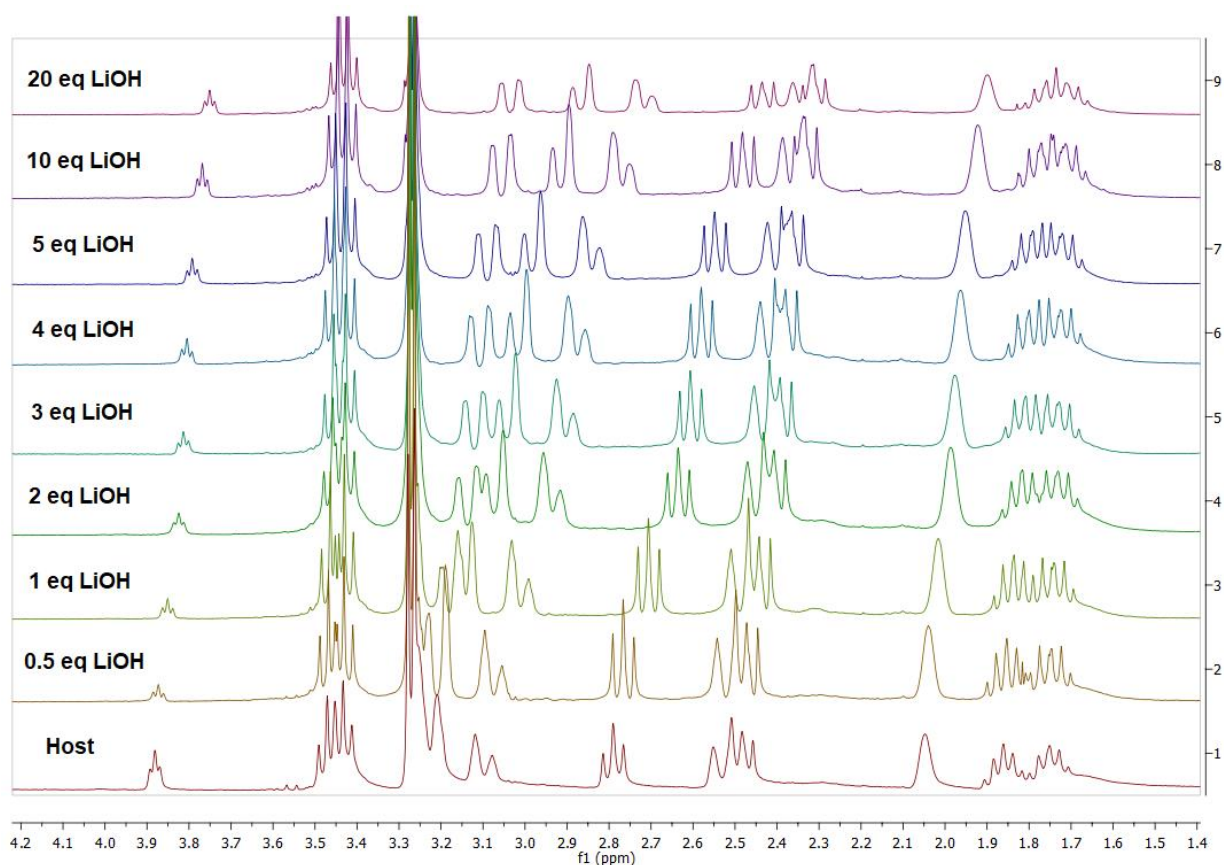
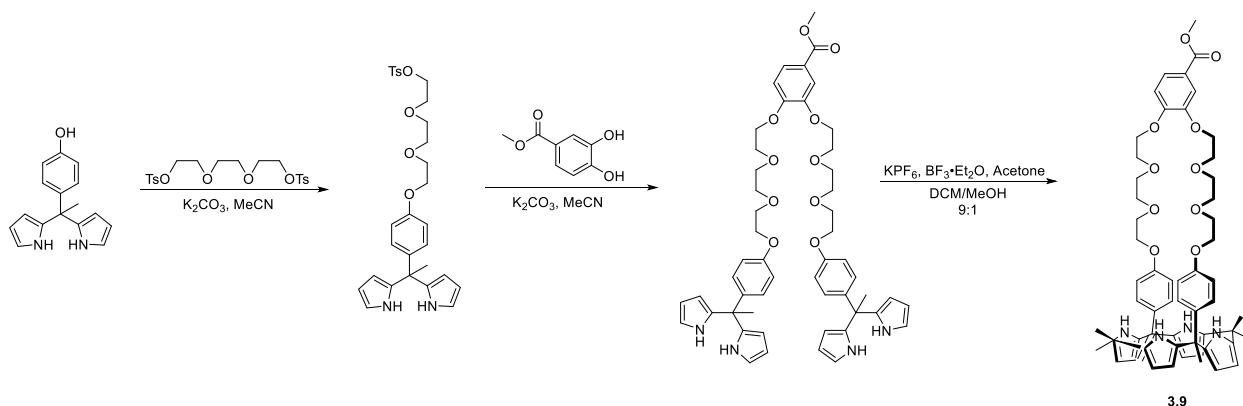


Figure 3.4: ¹H-NMR spectra (300 MHz, D₂O, 298 K) of Host, **3.7** solutions in D₂O and mixed with 0-20 eq LiOH.

After this realization, we took a step back to re-evaluate our approach to these NMR experiments. We assumed at the beginning that NMR would be able to show a strict disappearance/reappearance of peaks, allowing us to compare integrations. This assumption could only be true if the complexation-decomplexation process was slow enough to be measured on the NMR time scale. If both species existed for long enough, this would allow us to see two signals from two 'different' molecules. In most cases, the complexation-decomplexation process is very quick, only providing one peak to describe both systems. Since NMR takes an average of all of the scans, it stands to reason that there are two different chemical environments between the bound and unbound ligand, but only one peak is shown because they switch between each other so quickly. If the complexation-decomplexation happens too quick for the NMR timescale, the spectrum will produce an average of the two peaks which is what we observe. With this new insight and the desire to stray away from using D₂O for these experiments due to the complexity of the duplicated spectrum, we began looking for a new way to help quantify binding and selectivity.

3.3 Qualitative NMR Experiments

Although computational calculations outlined in Chapter 2 were used to prove Li selectivity, we looked for another confirmation of selectivity. Figure 2.8 shows that our ligand is slightly selective towards Li over Na when heavily outnumbered, similar to concentrations in seawater (1:60 000). If the Li concentration was increased to anything more concentrated than this, we may be able to see even more desired selectivity.



Scheme 3.6: Synthesis of a LiCl-selective organogel **3.9** developed by Sessler.⁶⁵

Sessler et al. developed an organogel **3.9** that was completely selective to binding LiCl. To probe the selectivity of their ligand, they designed an experiment in which they exposed their ligand to excess alkali chloride salts in MeCN and nitrobenzene. After contact, they took an NMR of each sample alone and in combination to see any changes in the spectrum. They noticed no changes in the spectrum for all chloride salts relative to the free **3.9** spectrum, except for the solution contacted with LiCl. This spectrum had discernible changes when compared to the **3.9** spectrum. The sample with all chloride salts combined also saw changes in the spectrum, however the changes were identical to the LiCl sample, thus confirming selectivity. In inspiration, we decided to perform a similar experiment with our ligand. To accomplish this, 10 mM solutions of **2.27** were made up in CD₃CN and mixed with excess LiCl, NaCl, and KCl alone and in combination to determine any discernible changes in the NMR spectra indicating binding (Fig 3.5). Compound **2.27** when contacted with LiCl produced discernible changes in the spectrum, most notably the peak ~2.75 ppm splitting into two separate peaks, as well as the appearance of a new doublet ~3.70 ppm. When contacted with the other salts (NaCl and

KCl), there were no changes in the spectrum and looked relatively identical to the host spectrum with no salt presence. In the combination sample, identical changes in the spectrum were seen compared to the spectrum with only LiCl, indicating Li selectivity using chloride salts.

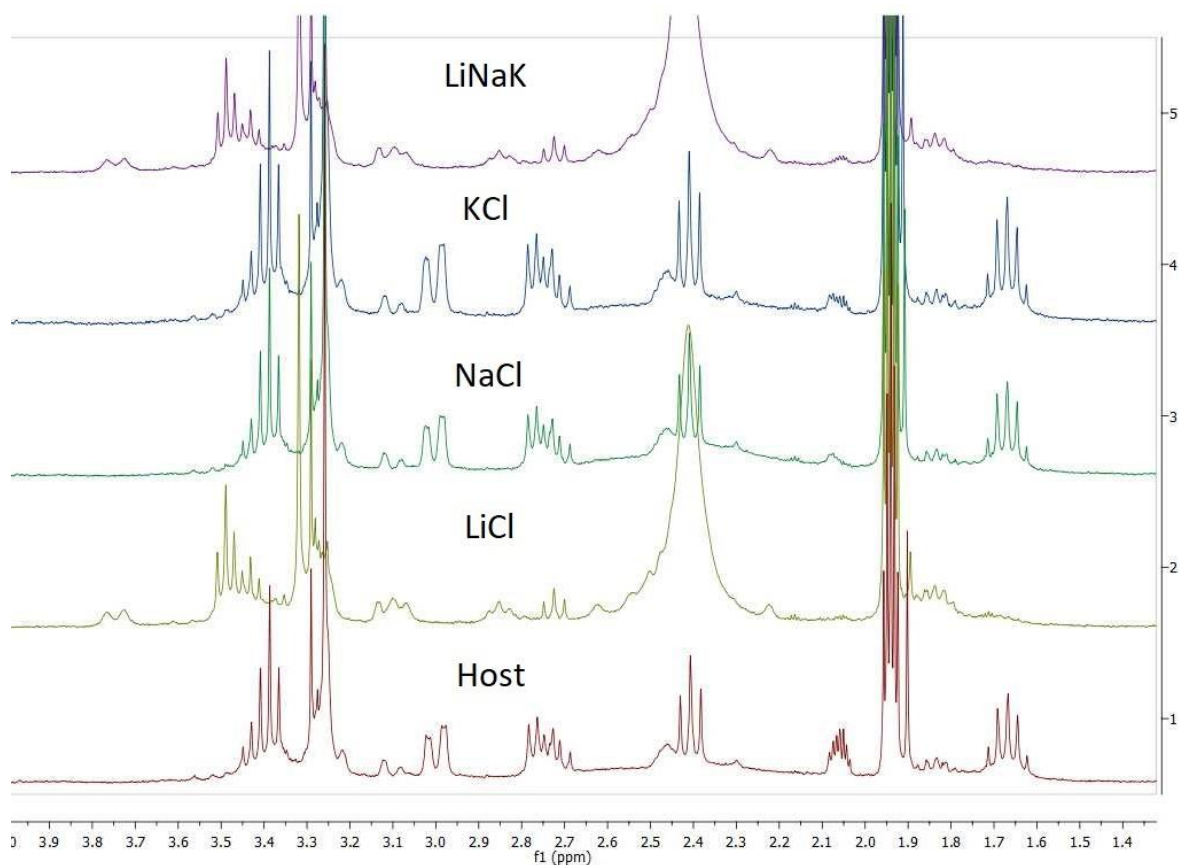


Figure 3.5. ¹H NMR spectra (300 MHz, CD₃CN, 298 K) of 10 mM (Host, **2.27**) solutions in CD₃CN and mixed with excess LiCl, NaCl, and KCl alone and in combination.

Compound **3.9** that Sessler developed in Scheme 3.6 was only selective towards LiCl as an ion pair, and not just Li alone. The Li⁺ portion would bind to the crown ether portion in the 'north' part of the molecule, and the Cl⁻ would be bound to the cyclic pyrrole structure in the 'south' region. However, after they completed the same experiments using

LiPF₆ and NaPF₆, selectivity was seen exclusively towards Na and not the desired Li.⁶⁵ This informed them that their ligand isn't selective towards Li alone, and only selective towards Li when paired with the correct Cl⁻ counterion. To test if the paired counterion had any affect on Li selectivity in our case, we carried out an identical experiment using lithium bis(trifluoromethanesulfonyl)imide (LiTFSI) and NaTFSI as our ion pairs. Also worth noting is that LiCl is inherently more soluble in acetonitrile than its other Cl⁻ counterparts, so this other experiment will be useful seeing as LiTFSI and NaTFSI are both quite soluble in acetonitrile (Fig 3.6). Both spectra have notable changes relative to the host spectrum, however the sample contacted with LiTFSI is almost identical to the combined sample indicating the preference favoring LiTFSI over NaTFSI. Slight differences between the LiTFSI spectrum and the combined spectrum can be attributed to a percentage of **2.27** binding Na (as predicted in Fig. 2.8), thus reducing the amount of **2.27** available to bind Li.

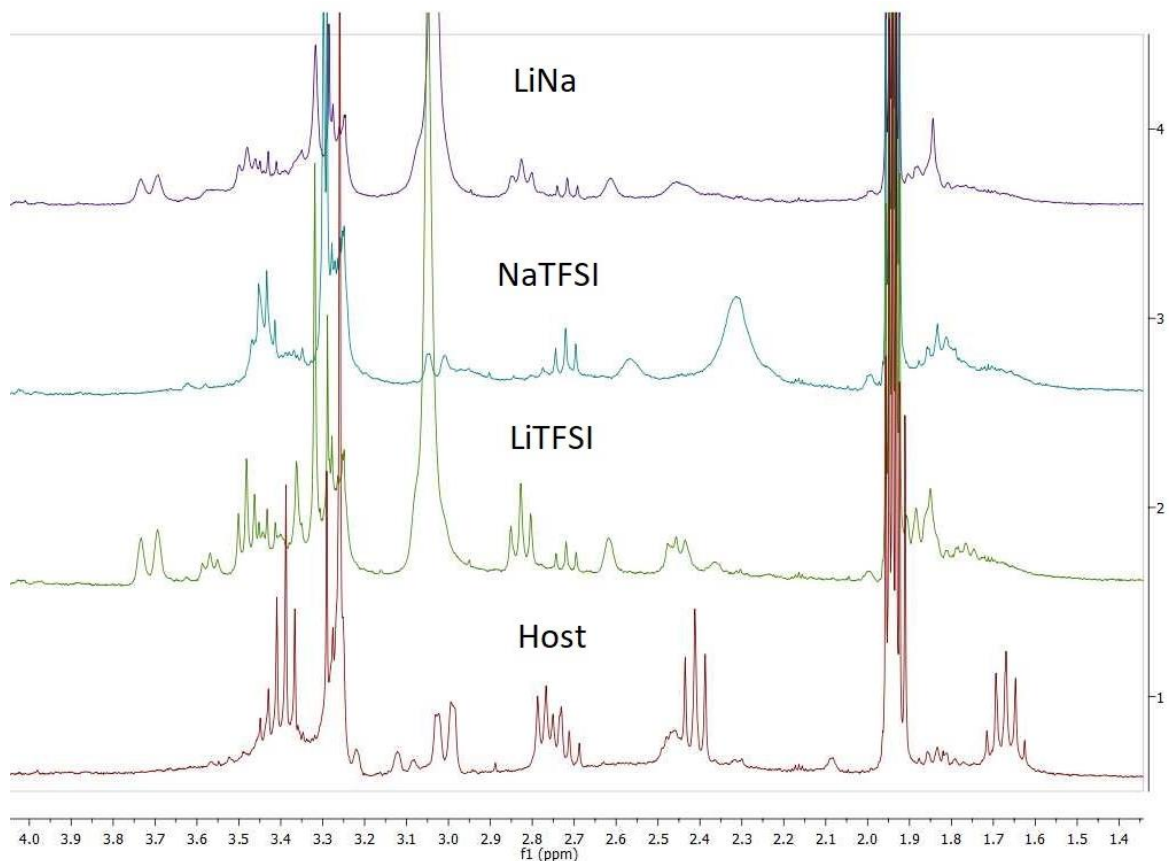


Figure 3.6: ^1H -NMR spectra (300 MHz, CD_3CN , 298 K) of 10 mM (Host, **2.27**) solutions in CD_3CN and mixed with excess LiTFSI and NaTFSI alone and in combination.

These qualitative NMR experiments illustrate that our ligand is selective towards Li over all the other 1^{st} group cationic contaminants in MeCN. Some Na-binding was expected and observed, however when in competition with Li-binding, Li selectivity was ultimately observed. The counter-anion associated with Li has relatively major effects on its solubility in the extraction solvent, however these experiments indicate that in our case, **2.27** is Li-selective regardless of counterion. Between our computational calculations and these qualitative NMR studies, we have confidently determined Li-selectivity over all other 1^{st} group cations. Knowing this, we began to re-explore ways to attempt to quantify this

binding interaction between **2.27** and Li^+ .

3.4 Quantitative Binding Characterization

To characterize the binding interaction between **2.27** and Li^+ , we looked to calculate an association constant. Association constants are essentially an equilibrium constant between states of unbound partners and bound partners.⁶⁶ They are the measure of how strongly a host and guest interact, with larger association constants favouring the bound together form. In Section 3.2, we attempted to calculate an association constant through an NMR titration. We hypothesized that we would be able to track an unbound peak's disappearance as well as a bound peak's reappearance to try and quantify this interaction. Unfortunately, we only noticed a shift in the peaks when titrating compound **3.7** with various equivalents of LiOH . We then realized that the complexation and decomplexation of Li^+ to **2.27** may be occurring too fast for the NMR to scan both intermediates. Since NMR takes an average of the signals it detects, we only see a shift of the original peak. The possible range the peak can be in will be somewhere between the unbound peak, and the point at which all ligand is complexed.^{66,67} As more equivalents of Li^+ salt is added, the average peak signal will shift further towards the fully complexed peak until it reaches that value or close to it.

Similar NMR titrations for this application are typically done in MeCN and not D_2O , so knowing this we are able to do our titration on our ligand with no modifications due to no potential hydration of the ketone. To perform this experiment 14 samples were prepared with **2.27** at a concentration of 10 mM in CD_3CN . Each sample was then contacted with varying amounts of LiTFSI and made up to 0.5 mL total volume.

Concentrations of Li salt ranged from 0 mM to 30 mM, the maximum containing about 1:3 L:M. The shift of the most downfield methylene peak was monitored upon concentration increase, and the chemical shift of the triplet was reported at each concentration (Fig 3.7).

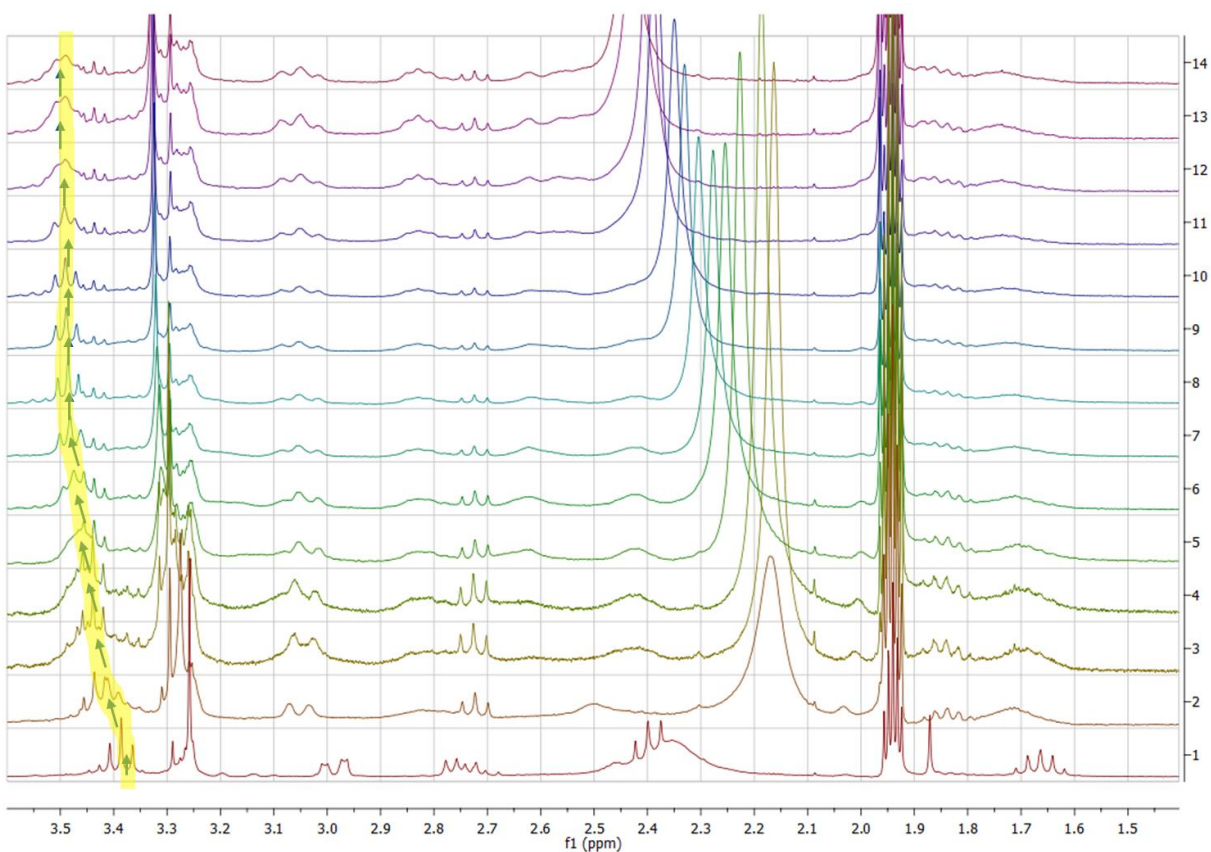


Figure 3.7: ^1H -NMR spectra (300 MHz, CD_3CN , 298 K) of **2.27 (Host)** recorded at a concentration of 10 mM in the presence of different concentrations of LiTFSI (**Guest**): (a) 0 mM; (b) 2 mM; (c) 5 mM; (d) 7 mM; (e) 9 mM; (f) 12 mM; (g) 14 mM; (h) 16 mM; (i) 18 mM; (j) 21 mM; (k) 23 mM; (l) 25 mM; (m) 28 mM; (n) 30 mM.

Upon recording the change in chemical shift per concentration of host, we can then fit the data using the equation below where $\Delta\delta$ is the chemical shift change of

(proton) at $[G]_0$, $\Delta\delta_\infty$ is the chemical shift change of (proton) when the host is completely complexed, $[H]_0$ is the fixed initial concentration of Host, and $[G]_0$ is the varying concentration of Li, an association constant was estimated (Fig 3.8):

$$\Delta\delta = (\Delta\delta_\infty/[H]_0) \left(0.5[G]_0 + 0.5([H]_0 + 1/K_a) - \left(0.5([G]_0^2 + (2[G]_0(1/K_a - [H]_0)) + (1/K_a + [H]_0)^2) \right)^{0.5} \right)$$

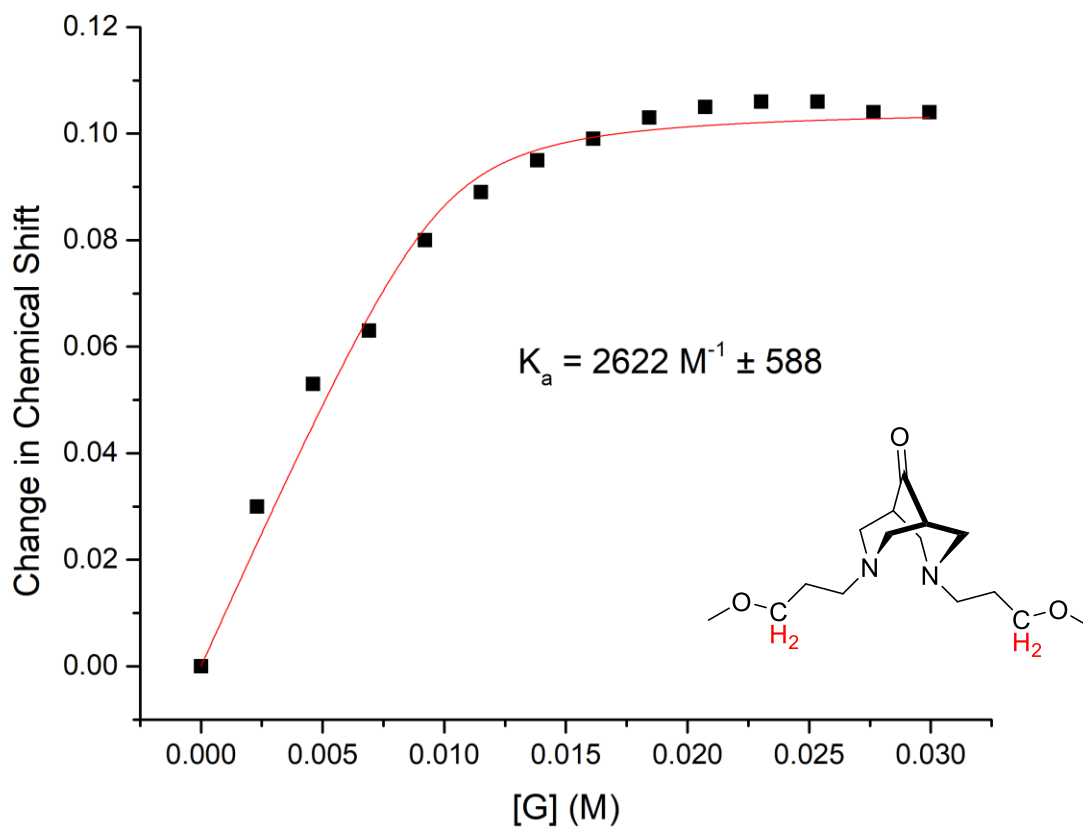


Figure 3.8: Changes in the chemical shift of (proton) on **2.27** (Host) as a function of added LiTFSI (Guest). The red solid line was obtained from a non-linear curve fitting using the equation above.

This association constant estimation tells us roughly how strong our binding interaction between our ligand and Li^+ is. A value of 2622 M^{-1} ensures us that our

interaction is similar to or improves on many examples found in literature.⁶⁸⁻⁷⁰ A few examples in literature such as the organogel **3.9** produced by Sessler in Scheme 3.6 can have quite large K_a values, with this particular one having a value of about $20\,000\text{ M}^{-1}$.⁶⁵ However, ligands with very high association constants usually come with a caveat such as only being selective towards a specific ion pair, or issues with decomplexation due to the binding affinity being too great. We feel that this K_a estimation for our system falls into a good area in terms of strong binding affinity as well as strong selectivity.

3.5 Future Work

Given our current results, we can say with confidence that our ligand is one that is Li-selective, one that can conform to an optimal tetrahedral lithium coordination environment, and one that has a moderate-good binding affinity towards Li^+ . There is still more binding characterization that would be useful. The same association constant could be calculated for the interaction with Na^+ since we are aware that our ligand does bind sodium as well, although not preferentially. This comparison in values between lithium and sodium could give us even more insight into how or why our ligand is more Li-selective. Other crucial experiments that could be done to further probe the selectivity towards Li^+ could be some SLE experiments.^{71,72} We could have a pre-made solid mixture of metals which is then exposed to a solution of our ligand in some known concentration. We could then quantify the amount of each metal that is pulled into solution by our ligand via ICP-MS to verify that we pull in more lithium than any other metal.^{71,72} These two experiments would be very useful to fully confirm Li-selectivity before potentially scaling up to more industrial applications.

Once selectivity was completely characterized, we would like to explore industrial applications for this ligand. We could try functionalizing the ketone to form a polymer that can potentially bind to a resin and be applicable in large-scale lithium isolation. We had also started some preliminary collaboration on this project with the Nazar Group at the University of Waterloo where our ligand could potentially be used as an additive to an electrolyte to help better solubilize LiS_2 for use in batteries. Modifications would have to be made to the functionality of the ligand to make it more electrochemically stable in these applications, but it is an interesting field that could be explored in the future.

Conclusion

The design and synthesis of a Li-selective ligand was attempted. With deep economical and environmental importance, lithium recovery seemed like an exciting area to explore. Improvement on current lithium isolation methods is absolutely necessary to keep up with expected demands in the electric vehicle industry. The project began with ferrocene as a potential candidate due to previous crown ether modifications seen in literature, with crown ethers being a known cation binder. The potential to act as an electrochemical molecular switch also added to the enticing nature of ferrocene. After some computational experiments we determined that our ferrocene idea would not be feasible synthetically or selectivity-wise. Deeper thought enlightened us to try and design structures that will put lithium into its ideal tetrahedral coordination environment to help selectivity. More computational experiments with these new designs led us to a new proposed bispidinone ligand. This ligand contained four heteroatoms to bind lithium, flexible arms to conform to the tetrahedral environment, and lastly a non-participating ketone to allow for further functionalization in applications. Computationally, this ligand was selective towards lithium in even the most dilute natural matrix so synthesis of this ligand was attempted. After a smooth 3-step synthesis we retrieved our ligand in which we began testing.

Preliminary binding characterization saw evidence of both lithium and sodium binding through mass spectrometry. NMR titrations in D₂O were attempted next, leading to the discovery of our ketone's susceptibility towards hydration. To continue doing NMR studies in water, manipulations of the carbonyl in our ligand were attempted with limited

success. Once we realized the new bound peak and old unbound peak were not going to disappear/reappear on the NMR timescale, we discovered you could titrate in an aprotic solvent and use the change in chemical shift to determine an association constant. These titrations gave us a moderate-good estimated association constant for the interaction between our ligand and lithium. Qualitative NMR competition experiments were conducted with other 1st group alkali metals to probe the selectivity towards lithium. These experiments further validated lithium selectivity and leave us confident with the ligand we have developed. Further work in this project should focus on further probing the selectivity through SLE, as well as work on the application of this process upon scale-up to industrial use.

References

- (1) Nitta, N.; Wu, F.; Lee, J. T.; Yushin, G. Li-Ion Battery Materials: Present and Future. *Materials Today* **2015**, *18* (5), 252–264. <https://doi.org/10.1016/j.mattod.2014.10.040>.
- (2) Thomas G. Goonan. Lithium Use in Batteries. *US Geological Survey* **2012**.
- (3) Winter, M.; Barnett, B.; Xu, K. Before Li Ion Batteries. *Chem Rev* **2018**, *118* (23), 11433–11456. <https://doi.org/10.1021/acs.chemrev.8b00422>.
- (4) National Minerals Information Center. *Mineral Commodity Summaries 2024*; **2024**. <https://doi.org/10.3133/mcs2024>.
- (5) *Ultra Lithium Inc. Lithium Uses: Glass and Ceramics*. <https://ultralithium.com/lithium-uses-glass-ceramics/> (accessed 2024-08-12).
- (6) *Grease Monkey Direct. Grease Guide: What is Lithium Grease Used For?* <https://www.greasemonkeydirect.com/blogs/news/grease-guide-what-is-lithium-grease-used-for#:~:text=Lithium%20grease%20is%20the%20most,wheel%20bearing%20and%20chassis%20applications>. (accessed 2024-08-12).
- (7) Larcher, D.; Tarascon, J.-M. Towards Greener and More Sustainable Batteries for Electrical Energy Storage. *Nat Chem* **2015**, *7* (1), 19–29. <https://doi.org/10.1038/nchem.2085>.
- (8) *Government of Canada. Lithium facts*. <https://natural-resources.canada.ca/our-natural-resources/minerals-mining/mining-data-statistics-and-analysis/minerals-metals-facts/lithium-facts/24009> (accessed 2024-08-12).
- (9) United States Environmental Protection Agency. *Greenhouse Gas Emissions from a Typical Passenger Vehicle*. <https://www.epa.gov/greenvehicles/greenhouse-gas-emissions-typical-passenger-vehicle> (accessed 2024-08-12).
- (10) Dunn, J. B.; Gaines, L.; Sullivan, J.; Wang, M. Q. Impact of Recycling on Cradle-to-Gate Energy Consumption and Greenhouse Gas Emissions of Automotive Lithium-Ion Batteries. *Environ Sci Technol* **2012**, *46* (22), 12704–12710. <https://doi.org/10.1021/es302420z>.
- (11) Kavanagh, L.; Keohane, J.; Garcia Cabellos, G.; Lloyd, A.; Cleary, J. Global Lithium Sources—Industrial Use and Future in the Electric Vehicle Industry: A Review. *Resources* **2018**, *7* (3), 57. <https://doi.org/10.3390/resources7030057>.
- (12) Benchmark Mineral Intelligence. *Benchmark Q4 2019*. <https://source.benchmarkminerals.com/downloads/magazine> (accessed 2024-08-12).
- (13) Government of Canada. *Canada’s Electric Vehicle Availability Standard (regulated targets for zero-emission vehicles)*. <https://www.canada.ca/en/environment-climate->

change/news/2023/12/canadas-electric-vehicle-availability-standard-regulated-targets-for-zero-emission-vehicles.html (accessed 2024-08-12).

- (14) Swain, B. Recovery and Recycling of Lithium: A Review. *Sep Purif Technol* **2017**, *172*, 388–403. <https://doi.org/10.1016/j.seppur.2016.08.031>.
- (15) Yan, Q.; Li, X.; Wang, Z.; Wu, X.; Wang, J.; Guo, H.; Hu, Q.; Peng, W. Extraction of Lithium from Lepidolite by Sulfation Roasting and Water Leaching. *Int J Miner Process* **2012**, *110–111*, 1–5. <https://doi.org/10.1016/j.minpro.2012.03.005>.
- (16) Meng, F.; McNeice, J.; Zadeh, S. S.; Ghahreman, A. Review of Lithium Production and Recovery from Minerals, Brines, and Lithium-Ion Batteries. *Miner. Process. Extr. Metall. Rev.* **2021**, *42* (2), 123–141. <https://doi.org/10.1080/08827508.2019.1668387>.
- (17) Meshram, P.; Pandey, B. D.; Mankhand, T. R. Extraction of Lithium from Primary and Secondary Sources by Pre-Treatment, Leaching and Separation: A Comprehensive Review. *Hydrometallurgy* **2014**, *150*, 192–208. <https://doi.org/10.1016/j.hydromet.2014.10.012>.
- (18) Christie, T.; Brathwaite, R. *Mineral Commodity Report 19 - Beryllium, Gallium, Lithium, Magnesium, Uranium and Zirconium*; **2008**. <https://www.nzpam.govt.nz/assets/Uploads/doing-business/mineralpotential/beryllium.pdf> (accessed 2024-08-12).
- (19) Grosjean, C.; Miranda, P. H.; Perrin, M.; Poggi, P. Assessment of World Lithium Resources and Consequences of Their Geographic Distribution on the Expected Development of the Electric Vehicle Industry. *Renew. Sustain. Energy Rev.* **2012**, *16* (3), 1735–1744. <https://doi.org/10.1016/j.rser.2011.11.023>.
- (20) Clark, G. M. Lithium-Ion Batteries: Raw Material Considerations. *Chem Eng Prog* **2013**, *109* (10), 44–52.
- (21) Talens Peiró, L.; Villalba Méndez, G.; Ayres, R. U. Lithium: Sources, Production, Uses, and Recovery Outlook. *JOM* **2013**, *65* (8), 986–996. <https://doi.org/10.1007/s11837-013-0666-4>.
- (22) Xu, Z.; Zhang, H.; Wang, R.; Gui, W.; Liu, G.; Yang, Y. Systemic and Direct Production of Battery-Grade Lithium Carbonate from a Saline Lake. *Ind Eng Chem Res* **2014**, *53* (42), 16502–16507. <https://doi.org/10.1021/ie502749n>.
- (23) Tran, T.; Luong, V. T. Lithium Production Processes. In *Lithium Process Chemistry*; Elsevier, **2015**; pp 81–124. <https://doi.org/10.1016/B978-0-12-801417-2.00003-7>.
- (24) Chen, Y.; Tian, Q.; Chen, B.; Shi, X.; Liao, T. Preparation of Lithium Carbonate from Spodumene by a Sodium Carbonate Autoclave Process. *Hydrometallurgy* **2011**, *109* (1–2), 43–46. <https://doi.org/10.1016/j.hydromet.2011.05.006>.

- (25) Del Rose, T.; Li, Y.; Qi, L.; Hlova, I. Z. Mechanochemical Extraction of Lithium from α -Spodumene at Low Temperatures. *Rare Metal Tech* **2024**; pp 141–149. https://doi.org/10.1007/978-3-031-50236-1_15.
- (26) Laferriere, A.; Dessureault, Y.; Skiadas, N.; Pearse, G. H. K.; Lamontagne, A.; Larouche, I.; Michaud, A.; Bilodeau, M.; Charbonneau, C. *NI 43-101 Technical Report Preliminary Economic Assessment of the Whabouchi Lithium Deposit and Hydromet Plant*. Nemaska Lithium.; Quebec, **2012**. <https://gq.mines.gouv.qc.ca/documents/examine/GM66008/GM66008.pdf> (accessed 2024-08-12)
- (27) Guo, H.; Kuang, G.; Wang, H.; Yu, H.; Zhao, X. Investigation of Enhanced Leaching of Lithium from α -Spodumene Using Hydrofluoric and Sulfuric Acid. *Minerals* **2017**, *7* (11), 205. <https://doi.org/10.3390/min7110205>.
- (28) Archambault, M.; Olivier, C. A. Carbonatizing Roast of Lithiumbearing Ores. US3380802A, April 30, 1968.
- (29) Kuang, G.; Liu, Y.; Li, H.; Xing, S.; Li, F.; Guo, H. Extraction of Lithium from β -Spodumene Using Sodium Sulfate Solution. *Hydrometallurgy* **2018**, *177*, 49–56. <https://doi.org/10.1016/j.hydromet.2018.02.015>.
- (30) Barbosa, L. I.; Valente, G.; Orosco, R. P.; González, J. A. Lithium Extraction from β -Spodumene through Chlorination with Chlorine Gas. *Miner Eng* **2014**, *56*, 29–34. <https://doi.org/10.1016/j.mineng.2013.10.026>.
- (31) Barbosa, L. I.; González, J. A.; Ruiz, M. del C. Extraction of Lithium from β -Spodumene Using Chlorination Roasting with Calcium Chloride. *Thermochim Acta* **2015**, *605*, 63–67. <https://doi.org/10.1016/j.tca.2015.02.009>.
- (32) Vyas, M. H.; Sanghavi, J. R.; Seshadri, K. Lithium Extraction from Indian Lepidolite Ores. *Research and Industry* **1975**, *20.2* (2), 68–70.
- (33) Yan, Q.; Li, X.; Wang, Z.; Wang, J.; Guo, H.; Hu, Q.; Peng, W.; Wu, X. Extraction of Lithium from Lepidolite Using Chlorination Roasting–Water Leaching Process. *Transactions of Nonferrous Metals Society of China* **2012**, *22* (7), 1753–1759. [https://doi.org/10.1016/S1003-6326\(11\)61383-6](https://doi.org/10.1016/S1003-6326(11)61383-6).
- (34) Löf, G. O. G.; Lewis, W. K. Lithium Chloride from Lepidolite. *Ind Eng Chem* **1942**, *34* (2), 209–216. <https://doi.org/10.1021/ie50386a014>.
- (35) Choubey, P. K.; Chung, K.-S.; Kim, M.; Lee, J.; Srivastava, R. R. Advance Review on the Exploitation of the Prominent Energy-Storage Element Lithium. Part II: From Sea Water and Spent Lithium Ion Batteries (LIBs). *Miner Eng* **2017**, *110*, 104–121. <https://doi.org/10.1016/j.mineng.2017.04.008>.

- (36) An, J. W.; Kang, D. J.; Tran, K. T.; Kim, M. J.; Lim, T.; Tran, T. Recovery of Lithium from Uyuni Salar Brine. *Hydrometallurgy* **2012**, *117–118*, 64–70. <https://doi.org/10.1016/j.hydromet.2012.02.008>.
- (37) Xu, P.; Hong, J.; Qian, X.; Xu, Z.; Xia, H.; Tao, X.; Xu, Z.; Ni, Q.-Q. Materials for Lithium Recovery from Salt Lake Brine. *J Mater Sci* **2021**, *56*, 16–63. <https://doi.org/10.1007/s10853-020-05019-1>.
- (38) Chen, J.; Lin, S.; Yu, J. Quantitative Effects of Fe₃O₄ Nanoparticle Content on Li⁺ Adsorption and Magnetic Recovery Performances of Magnetic Lithium-Aluminum Layered Double Hydroxides in Ultrahigh Mg/Li Ratio Brines. *J Hazard Mater* **2020**, *388*, 122101. <https://doi.org/10.1016/j.jhazmat.2020.122101>.
- (39) Jiang, H.; Yang, Y.; Sun, S.; Yu, J. Adsorption of Lithium Ions on Lithium-aluminum Hydroxides: Equilibrium and Kinetics. *Can J Chem Eng* **2020**, *98* (2), 544–555. <https://doi.org/10.1002/cjce.23640>.
- (40) Liu, G.; Zhao, Z.; Ghahreman, A. Novel Approaches for Lithium Extraction from Salt-Lake Brines: A Review. *Hydrometallurgy* **2019**, *187*, 81–100. <https://doi.org/10.1016/j.hydromet.2019.05.005>.
- (41) Xu, X.; Chen, Y.; Wan, P.; Gasem, K.; Wang, K.; He, T.; Adidharma, H.; Fan, M. Extraction of Lithium with Functionalized Lithium Ion-Sieves. *Prog Mater Sci* **2016**, *84*, 276–313. <https://doi.org/10.1016/j.pmatsci.2016.09.004>.
- (42) Feng, Q.; Kanoh, H.; Ooi, K. Manganese Oxide Porous Crystals. *J Mater Chem* **1999**, *9* (2), 319–333. <https://doi.org/10.1039/a805369c>.
- (43) Frensdorff, H. K. Stability Constants of Cyclic Polyether Complexes with Univalent Cations. *J Am Chem Soc* **1971**, *93* (3), 600–606. <https://doi.org/10.1021/ja00732a007>.
- (44) McLaughlin, W.; Adams, T. S. Li Reclamation Process. US5888463A, March 30, 1998.
- (45) Sojka, R. Innovative Recycling Technologies for Rechargeable Batteries. In Fourth International Battery Recycling Congress; Hamburg, Germany, 1998.
- (46) De Vries, T. S.; Bruneau, A. M.; Liou, L. R.; Subramanian, H.; Collum, D. B. Azaaldol Condensation of a Lithium Enolate Solvated by N,N,N',N' -Tetramethylethylenediamine: Dimer-Based 1,2-Addition to Imines. *J. Am. Chem. Soc.* **2013**, *135* (10), 4103–4109. <https://doi.org/10.1021/ja400345c>.
- (47) Warnock, S. J.; Sujanani, R.; Zofchak, E. S.; Zhao, S.; Dilenschneider, T. J.; Hanson, K. G.; Mukherjee, S.; Ganesan, V.; Freeman, B. D.; Abu-Omar, M. M.; Bates, C. M. Engineering Li/Na Selectivity in 12-Crown-4-Functionalized Polymer Membranes. *Proc. Natl. Acad. Sci. U.S.A.* **2021**, *118* (37). <https://doi.org/10.1073/pnas.2022197118>.
- (48) Zofchak, E. S.; Zhang, Z.; Wheatle, B. K.; Sujanani, R.; Warnock, S. J.; Dilenschneider, T. J.; Hanson, K. G.; Zhao, S.; Mukherjee, S.; Abu-Omar, M. M.; Bates, C. M.; Freeman, B. D.; Ganesan, V. Origins of Lithium/Sodium Reverse Permeability Selectivity in 12-

- Crown-4-Functionalized Polymer Membranes. *ACS Macro Lett* **2021**, *10* (9), 1167–1173. <https://doi.org/10.1021/acsmacrolett.1c00243>.
- (49) Kobiros, K. New Class of Lithium Ion Selective Crown Ethers with Bulky Decalin Subunits. *Coord Chem Rev* **1996**, *148*, 135–149. [https://doi.org/10.1016/0010-8545\(96\)01209-X](https://doi.org/10.1016/0010-8545(96)01209-X).
- (50) Pedersen, C. J. Crystalline Salt Complexes of Macrocyclic Polyethers. *J Am Chem Soc* **1970**, *92* (2), 386–391. <https://doi.org/10.1021/ja00705a605>.
- (51) Petter, R. C.; Milberg, C. I.; Jagadishwar Rao, S. Cooperative Dehydration of 1,1',2,2'-Ferrocenetetramethanol. *Tetrahedron Lett* **1990**, *31* (43), 6117–6120. [https://doi.org/10.1016/S0040-4039\(00\)97002-3](https://doi.org/10.1016/S0040-4039(00)97002-3).
- (52) Rao, S. J.; Milberg, C. I.; Russell, C., P. Heteroannular Ferrocene-Crown Ether Conjugates via Acid-Catalyzed Macrocyclization. *Tetrahedron Lett* **1991**, *32* (31), 3775–3778. [https://doi.org/10.1016/S0040-4039\(00\)79373-7](https://doi.org/10.1016/S0040-4039(00)79373-7).
- (53) Czech, B.; Ratajczak, A.; Nagraha, K. Diastomeric Oxathia[n](1,1')ferrocenophanes. *Chem. Monthly* **1982**, *113* (8-9), 965-972. <https://doi.org/10.1007/BF00799237>.
- (54) Zhang, J. L.; Zhong, J. Q.; Lin, J. D.; Hu, W. P.; Wu, K.; Xu, G. Q.; Wee, A. T. S.; Chen, W. Towards Single Molecule Switches. *Chem Soc Rev* **2015**, *44* (10), 2998–3022. <https://doi.org/10.1039/C4CS00377B>.
- (55) Pan, Y.; Zhang, C.; Liu, S. H.; Tan, Y.; Yin, J. Fluorescent Switch Based on Dithienylethene with Dansulfonamide in Multimediu. *Dyes and Pigments* **2020**, *181*, 108546. <https://doi.org/10.1016/j.dyepig.2020.108546>.
- (56) Fabbrizzi, L. The Ferrocenium/Ferrocene Couple: A Versatile Redox Switch. *ChemTexts* **2020**, *6* (4), 22. <https://doi.org/10.1007/s40828-020-00119-6>.
- (57) Pokharel, U. R.; Selegue, J. P.; Parkin, S. Ruthenocene 1,2-Dicarboxylic Acid, Carboxylic Anhydride, and Acid Chloride: A Facile Route to Metallocene-Fused Acenequinones. *Organometallics* **2011**, *30* (12), 3254–3256. <https://doi.org/10.1021/om2003915>.
- (58) Busetto, L.; Cassani, M. C.; Zanotti, V.; Albano, V. G.; Sabatino, P. Coordination Chemistry of Cyclopentadienyl Ester-Disubstituted Ligands. Synthesis and Solid State Structures of [Na([18]-Crown-6)][C₅H₃(CO₂Et)₂-1,2] and [Mn{C₅H₃(CO₂Ph)₂-1,2}(CO)₃]. *Organometallics* **2001**, *20* (2), 282–288. <https://doi.org/10.1021/om000662x>.
- (59) Nadeem, M.; Bhatti, M. H.; Yunus, U.; Mehmood, M.; Asif, H. M.; Mehboob, S.; Flörke, U. Synthesis and Characterization of Unique New Lithium, Sodium and Potassium Coordination Polymers. *Inorganica Chim Acta* **2018**, *479*, 179–188. <https://doi.org/10.1016/j.ica.2018.04.045>.

- (60) Wang, Z.; Shi, X.; Zhang, H.; Yu, L.; Cheng, Y.; Zhang, H.; Zhang, H.; Zhou, J.; Chen, J.; Shen, X.; Duan, W. Discovery of Cycloalkyl-Fused N-Thiazol-2-yl-Benzamides as Tissue Non-Specific Glucokinase Activators: Design, Synthesis, and Biological Evaluation. *Eur J Med Chem* **2017**, *139*, 128–152. <https://doi.org/10.1016/j.ejmech.2017.07.051>.
- (61) Miyahara, Y.; Goto, K.; Inazu, T. Convenient Synthesis of 3,7-Diazabicyclo[3.3.1]Nonane (Bispidine). *Synthesis (Stuttg)* **2001**, *2001* (03), 0364–0366. <https://doi.org/10.1055/s-2001-11427>.
- (62) Bonjoch, J.; Casamitjana, N.; Bosch, J. A New Synthesis of 5-Phenylmorphans 1,2. *Tetrahedron* **1988**, *44* (6), 1735–1741. [https://doi.org/10.1016/S0040-4020\(01\)86738-7](https://doi.org/10.1016/S0040-4020(01)86738-7).
- (63) Barker, G.; O'Brien, P.; Campos, K. R. Investigation of Bispidines as the Stoichiometric Ligand in the Two-Ligand Catalytic Asymmetric Deprotonation of N-Boc Pyrrolidine. *Arkivoc* **2011**, *2011* (5), 217–229. <https://doi.org/10.3998/ark.5550190.0012.519>.
- (64) Cui, H.; Goddard, R.; Pörschke, K.-R.; Hamacher, A.; Kassack, M. U. Bispidin-9,9-Diol Analogues of Cisplatin, Carboplatin, and Oxaliplatin: Synthesis, Structures, and Cytotoxicity. *Inorg Chem* **2016**, *55* (6), 2986–2997. <https://doi.org/10.1021/acs.inorgchem.5b02855>.
- (65) Wang, H.; Jones, L. O.; Hwang, I.; Allen, M. J.; Tao, D.; Lynch, V. M.; Freeman, B. D.; Khashab, N. M.; Schatz, G. C.; Page, Z. A.; Sessler, J. L. Selective Separation of Lithium Chloride by Organogels Containing Strapped Calix[4]Pyrroles. *J Am Chem Soc* **2021**, *143* (48), 20403–20410. <https://doi.org/10.1021/jacs.1c10255>.
- (66) Thordarson, P. Determining Association Constants from Titration Experiments in Supramolecular Chemistry. *Chem. Soc. Rev.* **2011**, *40* (3), 1305–1323. <https://doi.org/10.1039/C0CS00062K>.
- (67) Kleckner, I. R.; Foster, M. P. An Introduction to NMR-Based Approaches for Measuring Protein Dynamics. *Biochimica et Biophysica Acta (BBA) - Proteins and Proteomics* **2011**, *1814* (8), 942–968. <https://doi.org/10.1016/j.bbapap.2010.10.012>.
- (68) Luo, Y.; Marets, N.; Kato, T. Selective Lithium Ion Recognition in Self-Assembled Columnar Liquid Crystals Based on a Lithium Receptor. *Chem Sci* **2018**, *9* (3), 608–616. <https://doi.org/10.1039/C7SC03652C>.
- (69) Tai, O.; Hopson, R.; Williard, P. G. Ligand Binding Constants to Lithium Hexamethyldisilazide Determined by Diffusion-Ordered NMR Spectroscopy. *J Org Chem* **2017**, *82* (12), 6223–6231. <https://doi.org/10.1021/acs.joc.7b00800>.
- (70) Brachvogel, R.-C.; Maid, H.; Von Delius, M. NMR Studies on Li⁺, Na⁺ and K⁺ Complexes of Orthoester Cryptand o-Me₂-1.1.1. *Int J Mol Sci* **2015**, *16* (9), 20641–20656. <https://doi.org/10.3390/ijms160920641>.

- (71) Szliszka, E.; Czuba, Z. P.; Domino, M.; Mazur, B.; Zydowicz, G.; Krol, W. Ethanollic Extract of Propolis (EEP) Enhances the Apoptosis- Inducing Potential of TRAIL in Cancer Cells. *Molecules* **2009**, *14* (2), 738–754. <https://doi.org/10.3390/molecules>.
- (72) Zhang, J.; Wenzel, M.; Steup, J.; Schaper, G.; Hennersdorf, F.; Du, H.; Zheng, S.; Lindoy, L. F.; Weigand, J. J. 4-Phosphoryl Pyrazolones for Highly Selective Lithium Separation from Alkali Metal Ions. *Chemistry – A European Journal* **2022**, *28* (1). <https://doi.org/10.1002/chem.202103640>.

Appendix

A General Considerations

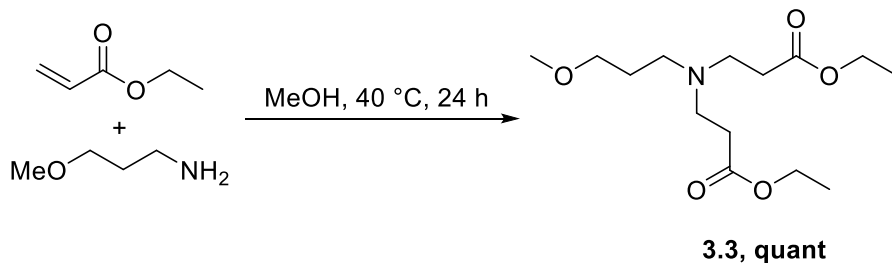
Materials & Instrumentation

All chemicals were purchased from either Sigma-Aldrich Ltd. or Oakwood Products, Inc. and were used without further purification unless otherwise stated. Reactions were performed under an argon atmosphere with flame-dried glassware, unless otherwise specified. Toluene was dried and purified using a JC Meyer solvent purification system (SPS), all other reaction solvents were analytical grade and used without purification. Thin layer chromatography (TLC) was performed on alumina-backed silica plates (Kieselgel 60 F₂₅₄, Merck) and developed plates were stained with KMnO₄ and heated before examination. Flash chromatography was performed on a Teledyne Isco CombiFlash Rf+ and packed with 230-400 mesh silica gel (SiliCycle).

¹H-NMR spectra were recorded on a Bruker AVANCE300 (300 MHz) δ or Bruker AC300 (300 MHz) δ NMR spectrometers. ¹³C-NMR spectra were broadband proton decoupled and recorded on a Bruker AVANCE300 (75 MHz) δ or Bruker AC300 (75.5 MHz) δ NMR spectrometers. Chemical shifts are reported in parts per million (ppm) relative to either chloroform ($\delta = 7.26$), or acetonitrile ($\delta = 1.94$) for ¹H-NMR, and relative to chloroform ($\delta = 77.16$) for ¹³C-NMR. All coupling constants (J) are reported in hertz (Hz). Singlet = s, doublet = d, triplet = t, quartet = q, quintet = qu, multiplet = m. High-resolution mass spectra were obtained via electrospray ionization, which was measured on a Thermo Scientific Q Exactive Plus Hybrid Quadrupole-Orbitrap at the University of Waterloo Mass Spectrometry Facility.

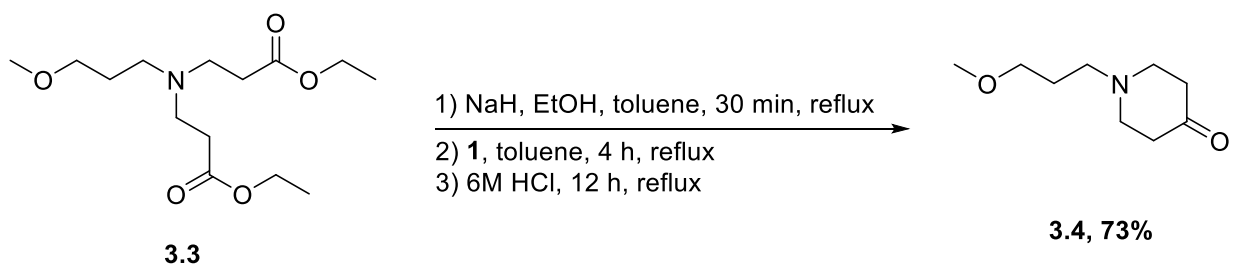
B Reaction Procedures

Synthesis of bisester (**3.3**)



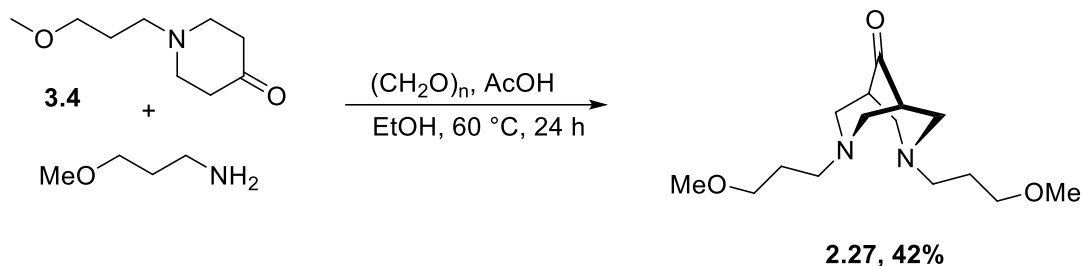
To a solution of 3-methoxypropylamine (7.68 g, 86.2 mmol, 1 eq) in 85 mL of methanol was added ethyl acrylate (22 g, 220 mmol, 2.6 eq) dropwise at room temperature. The solution was stirred for 24 h at 40 °C, then the solvent was removed through distillation to produce a clear oil **3.3** that was used without further purification (24.77g, 85.6 mmol, 99%). ¹H-NMR (300 MHz; CDCl₃): δ 4.12 (q, *J* = 7.1 Hz, 4H), 3.37 (t, *J* = 6.3 Hz, 2H), 3.31 (s, 3H), 2.75 (t, *J* = 7.1 Hz, 4H), 2.48 (t, *J* = 7.1 Hz, 2H), 2.42 (t, *J* = 7.1 Hz, 4H), 1.74 – 1.60 (m, 2H), 1.25 (t, *J* = 7.1 Hz, 6H). ¹³C-NMR (75 MHz, CDCl₃): 172.1, 70.7, 60.5, 58.7, 51.7, 50.6, 49.5, 32.8, 14.4. HRMS-ESI: *m/z* [M + H]⁺ calcd for C₁₅H₂₉N₂O₃, 290.1962; found, 290.1965.

Synthesis of piperidinone (**3.4**)



To a suspension of NaH (789 mg of 60% dispersion in mineral oil, 19.7 mmol, 1.1 eq) in 21 mL of dry toluene was added a solution of EtOH (2.5 mL, 42.8 mmol) in 13 mL of dry toluene dropwise. When H₂ evolution stopped, the mixture was refluxed under an argon atmosphere to ensure complete conversion of NaH to NaOEt. A solution of **3.3** (5.15 g, 17.8 mmol, 1 eq) in 13 mL of dry toluene was added to the mixture after 15 minutes under an argon atmosphere and the mixture was refluxed for 4 h. Then, approx. 90% of the toluene was removed via rotary evaporation. 20 mL 6 M HCl was added to the oily solution and the organic layer was extracted with 6 M HCl (2 × 10 mL). The aqueous layers were combined and refluxed for 12 h. Once cooled, the reaction mixture was made pH = 12 using NaOH pellets. The aqueous layer was then extracted with dichloromethane (3 × 40 mL), and the combined extracts were dried with MgSO₄. The solvent was removed via rotary evaporation to afford a faint yellow crude oil. The crude oil was purified by flash chromatography (5% methanol in dichloromethane) to afford piperidinone **3.4** (2.2 g, 12.9 mmol, 73%) as a yellow oil. R_f = 0.31 (5% methanol in dichloromethane). ¹H-NMR (300 MHz; CDCl₃): δ 3.45 (t, *J* = 6.3 Hz, 2H), 3.34 (s, 3H), 2.75 (t, *J* = 6.1 Hz, 4H), 2.54 (d, *J* = 6.3 Hz, 2H), 2.45 (t, *J* = 6.1 Hz, 4H), 1.87 – 1.73 (m, 2H). ¹³C-NMR (75 MHz, CDCl₃): 209.3, 71.0, 58.7, 54.4, 53.2, 41.2, 27.7. HRMS-ESI: *m/z* [M + H]⁺ calcd for C₉H₁₈NO₂, 172.1333; found, 172.1336.

Synthesis of bispidinone (**2.27**)



To a solution of paraformaldehyde (76 mg, 2.53 mmol, 2.1 eq) in 12 mL EtOH was added piperidinone **3.4** (206 mg, 1.20 mmol, 1 eq), 3-methoxypropylamine (117.9 mg, 1.32 mmol, 1.1 eq) under an inert argon atmosphere. AcOH (0.15 mL, 2.53 mmol, 2.1 eq) was then added to this solution in an ice bath under magnetic stirring. The solution was stirred for 24 h at 60 °C under argon and the progress of the reaction was monitored by TLC (silica gel, 90%:9%:1% CH_2Cl_2 :MeOH: NH_4OH). Once full conversion was observed, the solvent was removed via rotary evaporation to afford a viscous, amber crude oil. The crude oil was purified by flash chromatography (90%:9%:1% CH_2Cl_2 :MeOH: NH_4OH) to afford bispidinone **2.27** (143.7 mg, 0.505 mmol, 42%) as an amber oil. $R_f = 0.20$ (90%:9%:1% CH_2Cl_2 :MeOH: NH_4OH). $^1\text{H-NMR}$ (300 MHz; CDCl_3): δ 3.43 (t, $J = 6.4$ Hz, 4H), 3.33 (s, 6H), 3.01 (d, $J = 9.9$ Hz, 4H), 2.82 (dd, $J = 10.7, 6.1$ Hz, 4H), 2.65 – 2.51 (m, 2H), 2.46 (t, $J = 7.1$ Hz, 4H), 1.81 – 1.65 (m, 4H). $^{13}\text{C-NMR}$ (75 MHz, CDCl_3): 215.0, 70.9, 58.8, 58.6, 53.6, 46.7, 27.5. HRMS-ESI: m/z $[\text{M} + \text{H}]^+$ calcd for $\text{C}_{15}\text{H}_{29}\text{N}_2\text{O}_3$, 285.2173; found, 285.2167.

C Spectral Data

Figure S3-1. ¹H-NMR (300 MHz, CDCl₃) of **3.3**:

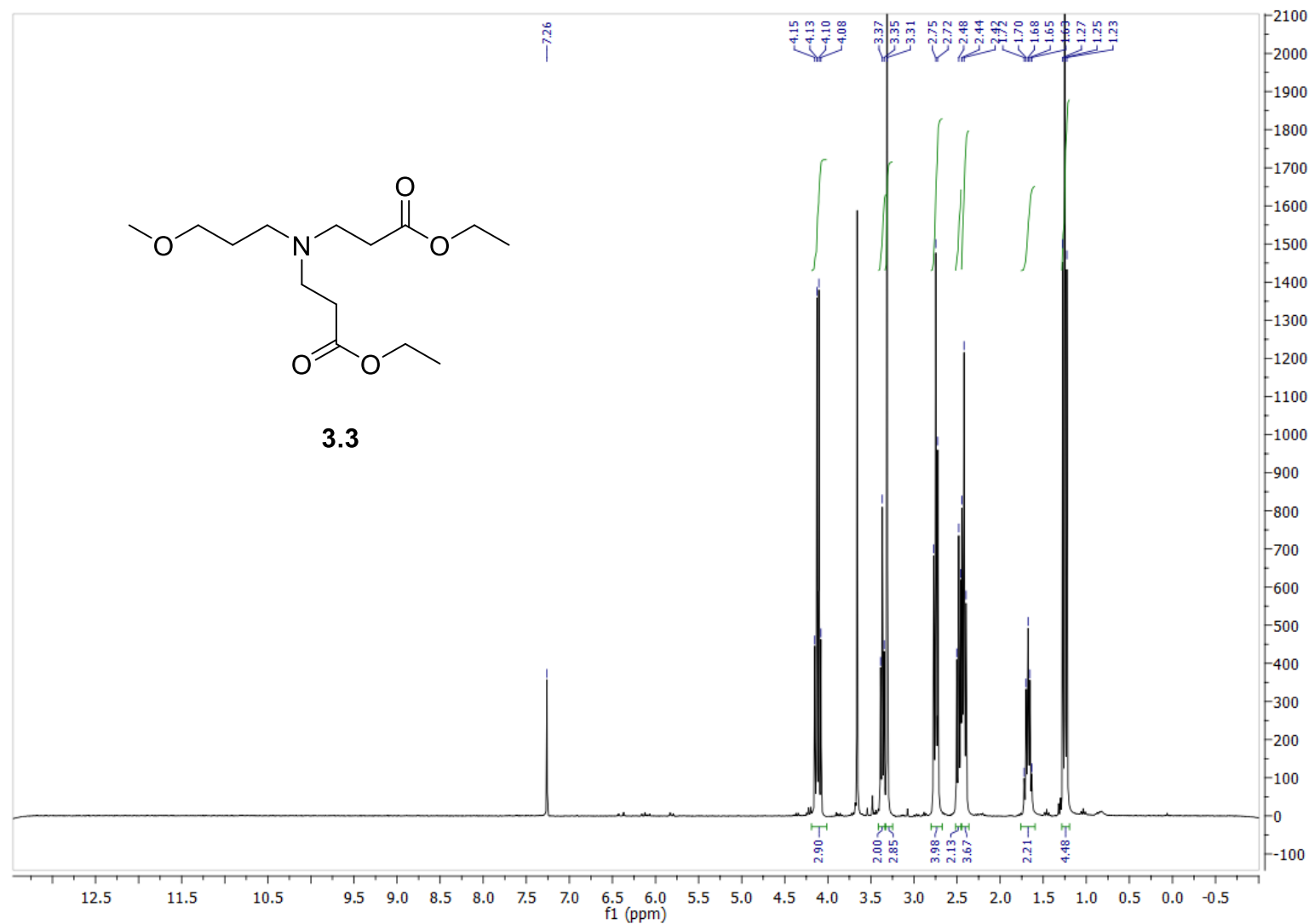


Figure S3-2. ^{13}C -NMR (75 MHz, CDCl_3) of **3.3**:

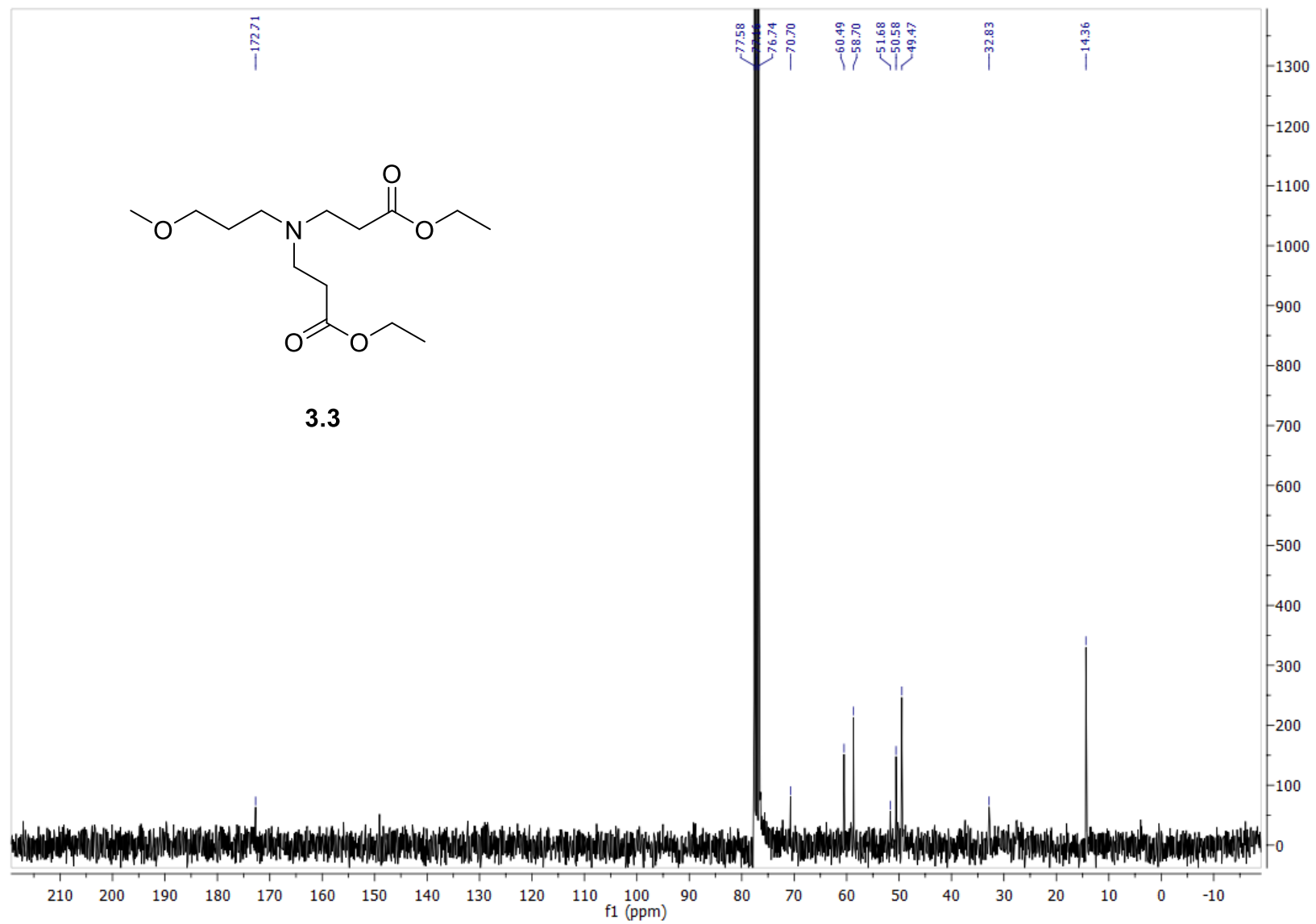


Figure S3-3. $^1\text{H-NMR}$ (300 MHz, CDCl_3) of **3.4**:

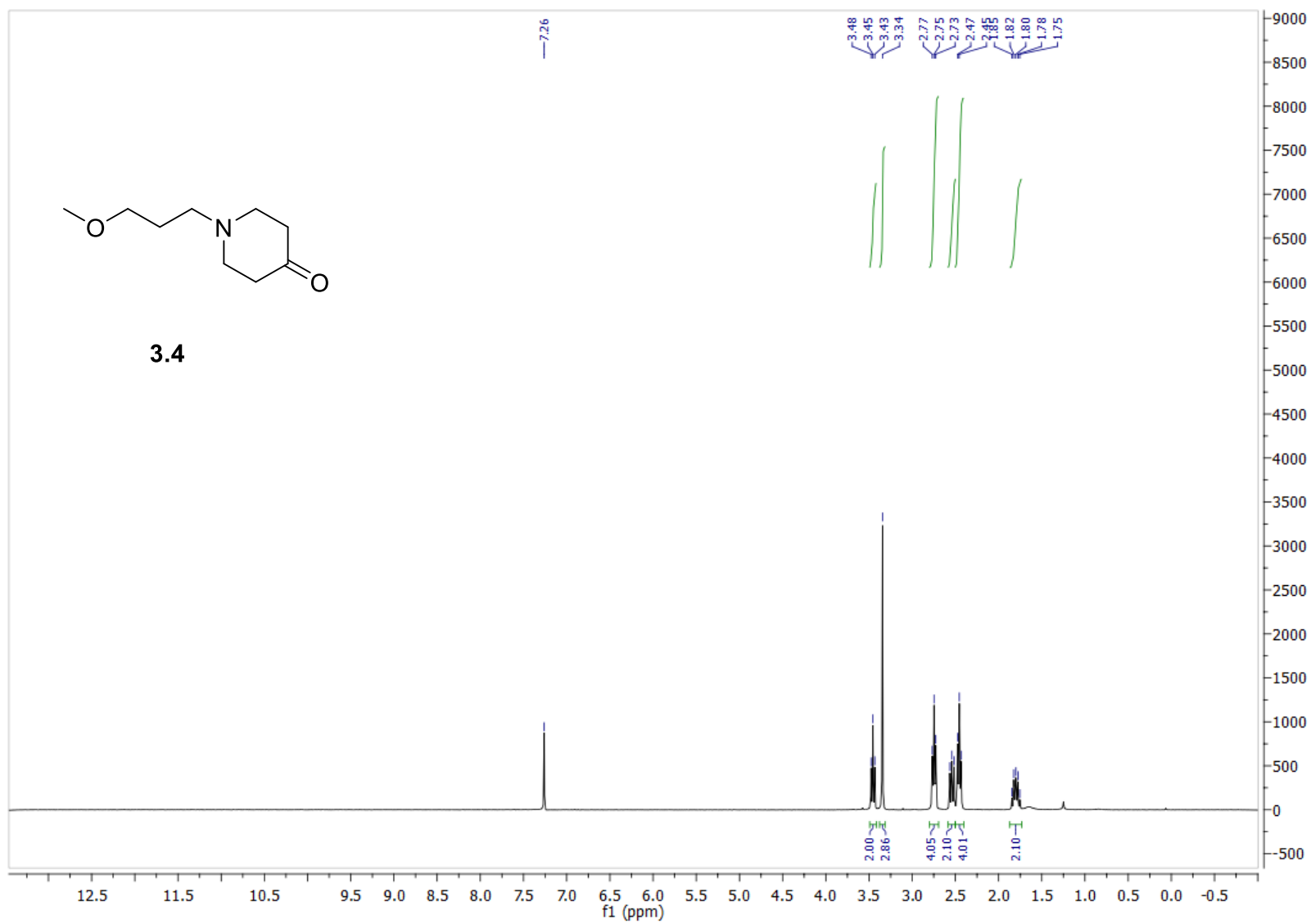


Figure S3-4. ^{13}C -NMR (75 MHz, CDCl_3) of **3.4**:

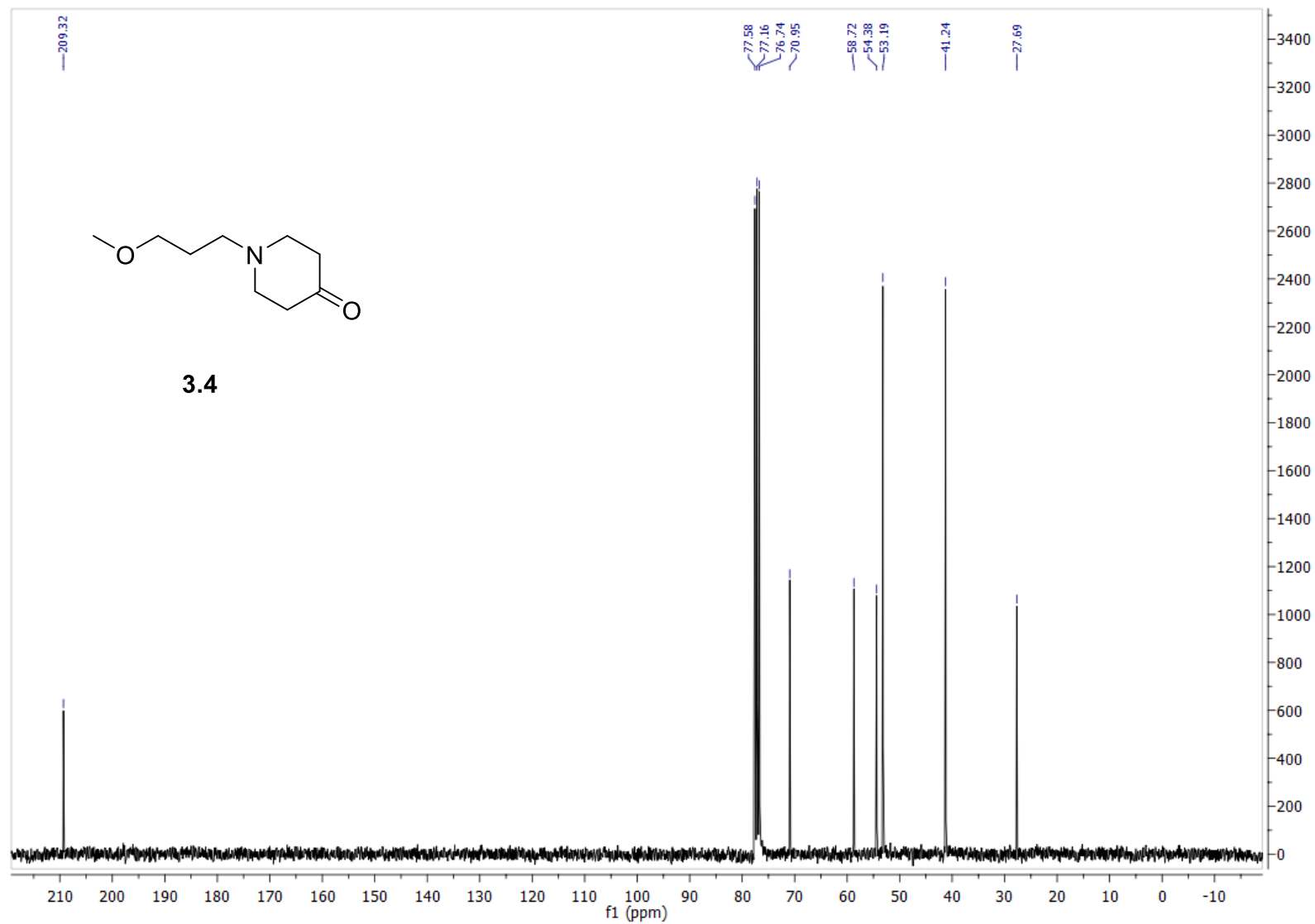


Figure S3-5. $^1\text{H-NMR}$ (300 MHz, CDCl_3) of **2.27**:

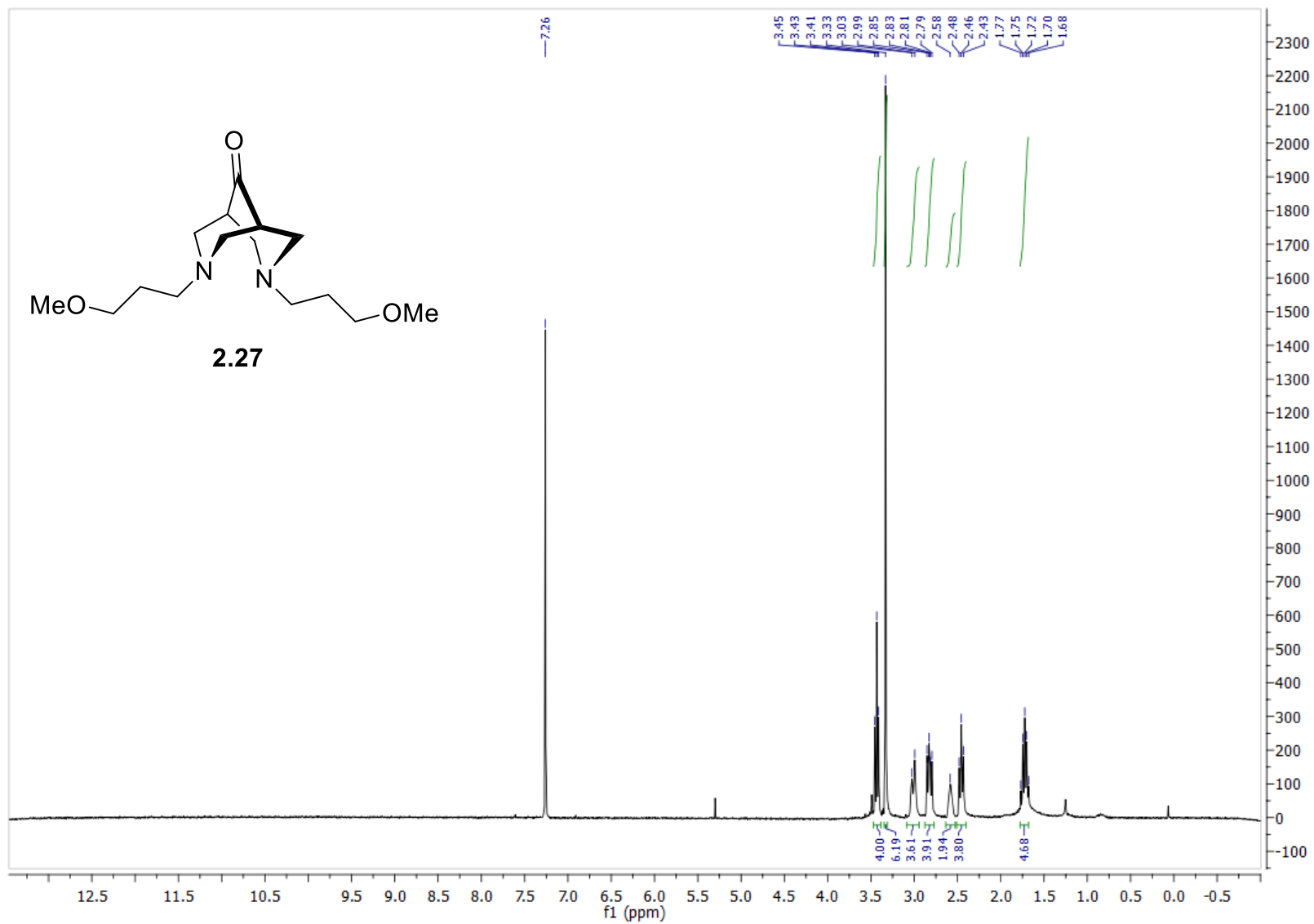
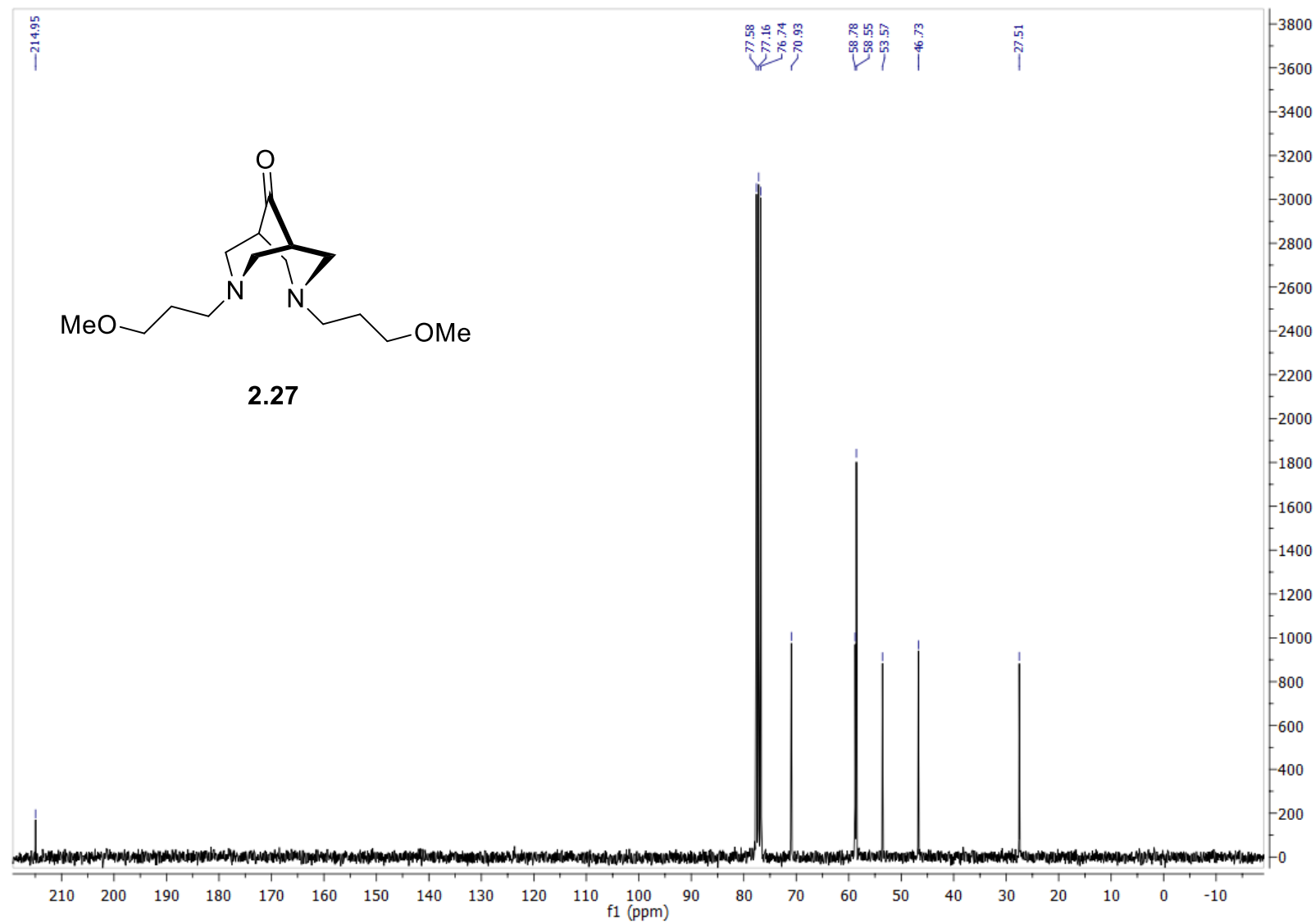


Figure S3-6. ^{13}C -NMR (75 MHz, CDCl_3) of **2.27**:



D Quantitative NMR Data

Figure S4-1: (0.5 mL, CD₃CN, LiTFSI); (a) 0 mM; (b) 2 mM; (c) 5 mM; (d) 7 mM; (e) 9 mM; (f) 12 mM; (g) 14 mM; (h) 16 mM; (i) 18 mM; (j) 21 mM; (k) 23 mM; (l) 25 mM; (m) 28 mM; (n) 30 mM; (in order, not labelled).

